CHEMTAX determination of Southern Ocean phytoplankton distribution and adaption

An observational and experimental study assessing the co-limitation of Light, Iron and other Trace Metals on phytoplankton productivity and community composition.

by

Johannes Jacobus Viljoen

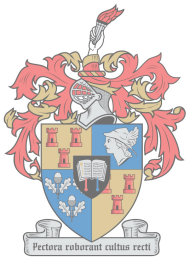

Thesis presented in fulfilment of the requirements for the degree of Master of Science in the Faculty of Science at Stellenbosch University

Supervisor: Dr. Susanne Fietz

December 2018

Declaration

By submitting this thesis electronically, I declare that the entirety of the work contained therein is my own, original work, that I am the sole author thereof (save to the extent explicitly otherwise stated for the different manuscripts contained in this thesis), that the reproduction and publication thereof by Stellenbosch University will not infringe any third party rights and that I have not previously in its entirety or in part submitted it for obtaining any qualification. In the case of manuscripts formulated into chapters, there are clear statements of my significant contribution to them in the **List of Manuscripts and Contribution** section on page **3**.

December 2018

Johannes Jacobus Viljoen

Abstract

This multi-manuscript study reports an elucidated understanding of the consequences key environmental changes has on phytoplankton community structure, productivity and their acclimation abilities for the Atlantic Sector of the Southern Ocean. All three manuscripts are based on data gathered on board the RV SA Agulhas II on a north-south transect along the Good Hope monitoring between Cape Town and the Antarctic Fimbul ice shelf (0° longitude). This transect crossed multiple oceanic fronts and zones from which a multi-parameter in-situ observational study of the links between trace metals and phytoplankton dynamics could be carried out. In addition, two stations were used to conduct bulk-community bottle incubation experiments to assess the response of phytoplankton in growth, photophysiology and community structure to iron and light variability in the Polar Frontal Zone and Antarctic waters. The results from the incubation studies revealed that the response of phytoplankton to changes in iron and light availability are very region-specific. In the Polar Frontal Zone irradiance is limiting significant phytoplankton growth and in the Antarctic Zone, iron addition resulted in growth stimulation even at low light levels. By combining data from the surface and the un-amended incubation bottles sampled from the respective depth of fluorescence maximum an assessment of how representative the surface and chla-max communities are of their region and, considering logistical constraints, if we can only use one to understand phytoplankton dynamics. Due to additional changes in irradiance and availability of iron with vertical depth, which is region specific, the acclimation of phytoplankton, which affects their photochemical efficiency (Fv/Fm) and productivity, can vary with depth which is exemplified by regional differences in water column structure and dynamics. The possibility of sampling a niche community when only one depth is sampled, which could lead to results of a very depth-specific acclimated phytoplankton community and not that of a regional representative one, was also investigated. The multi-parameter in-situ observational study that includes parallel trace metal and phytoplankton community structure data showed that there are certain changes in phytoplankton community structure that can only be explained by the addition of a suite of trace metals as additional variables. This led to the observation that when these essential micronutrients are incorporated into studies, the timing of phytoplankton sampling relative to the time of an event like the release of trace metals from hydrothermal vents or melting ice can be very important. For the Atlantic Southern Ocean, it can be shown that the present and future state of phytoplankton

dynamics greatly depends on key environmental changes such as irradiance, varying degrees of iron-light co-limitation and the proven strong influence of trace metal availability.

Keywords: pigments; acclimation; multi-parameter; incubation; GEOTRACES

Opsomming

Hierdie studie bestaan uit veelvoudige manuskripte wat lig werp op die gevolge wat kern omgewingsveranderinge het op fitoplankton se gemeenskapstrukture, produktiwiteit en hul vermoë om te akklimatiseer in die Atlantiese Sektor van die Suidelike Oseaan. Al drie manuskripte wat hierin vervat is, is gebaseer op data wat ingesamel is aan boord die RV SA Agulhas II op ’n noord-suid transek, al langs die Goeie Hoop moniteringslyn tussen Kaapstad en die Antarktiese Fimbul-ysbank (0° lengtegraad). Aangesien hierdie transek verskeie oseanies fronte en sones gekruis het, was dit moontlik om ’n multi-parameter, in situ waarnemingstudie uit te voer wat die verhouding tussen spoormetale en fitoplankton dinamika ondersoek. Daarbenewens is daar by twee monsternemingstasies inkubasiebottel eksperimente uitgevoer op omvangryke fitoplankton gemeenskappe om hul reaksie in groei, fotofisiologie en gemeenskapstrukture tot die veranderlikheid van yster en lig in die Polêre Frontsone en die Antarktiese seegebied te bepaal. Die uitslae van die inkubasiestudies het onthul dat die reaksie van fitoplankton tot veranderinge in die beskikbaarheid van yster en lig baie streekspesifiek is. In die Polêre Frontsone beperk uitstraling opmerklike fitoplankton groei en in die Antarktiese sone het die toevoeging van yster die groei van fitoplankton gestimuleer ten spyte van die lae ligvlakke. Deur die data te kombineer van die watermonsters wat op die oppervlak geneem is en die ongewysigde inkubasiebottels wat op die respektiewe dieptes van die maksimum fluoressensie geneem is, kan ‘n waardebepaling gedoen word van hoe verteenwoordigend die fitoplanktongemeenskappe op die oppervlakte en die gemeenskappe by die chlorofil maksimum van die streek is. Dit kan ook ‘n aanduiding gee van die moontlikheid om net een datastel (oppervlak/diepte) te gebruik, veral wanneer logistieke uitdagings in ag geneem moet word. Die akklimatisering van fitoplankton, wat hul fotochemiese doeltreffendheid (Fv/Fm) en produktiwiteit beïnvloed, kan verskil met diepte as gevolg van die bykomende veranderinge in uitstraling en beskikbaarheid van yster. Hierdie veranderinge is streekspesifiek en kan verduidelik word deur streeksverskille in die waterkolomstruktuur en –dinamika. Daar is ook ondersoek ingestel na die moontlikheid om ’n nisgemeenskap te toets wanneer monsters slegs op een diepte geneem word. Dit kan daarna toe lei dat resultate slegs verteenwoordigend is van ’n baie spesifieke fitoplankton gemeenskap wat op ’n spesifieke diepte geakklimatiseer het en dus nie ’n streeksvoorstelling is nie. Die multi-parameter, in situ waarnemingstudie, wat parallelle spoormetaaldata en fitoplankton gemeenskapstruktuurdata insluit, het getoon dat daar sekere veranderinge in die fitoplanktongemeenskapstruktuur is wat

slegs deur die toevoeging van ‘n spoormetaaldatastel as addisionele veranderlikes verduidelik kan word. Wanneer hierdie noodsaaklike mikrovoedingstowwe in ‘n studie ingesluit word, speel tydsberekening ‘n baie belangerike rol. Die inagneming van die vrystelling van spoormetale deur hidrotermiese openinge of smeltende ys ten tye van fitoplankton-monsterneming is baie belangrik. Die huidige en toekomstige toestand van fitoplankton dinamika in die Atlantiese Suidelike Oseaan is grootliks onderhewig aan kern omgewingsveranderinge soos uitstraling, wisselende vlakke van die gelyktydige beperkinge van yster en lig en die bevestigde sterk invloed van die beskikbaarheid van spoormetale.

Sleutelwoorde: pigmente; akklimatisering; multi-parameter; inkubasie; GEOTRACES

Acknowledgements

It is with utmost gratitude that I thank my research supervisor, Dr Susanne Fietz, for the opportunity you gave to me to undertake such a project and for your patience, guidance and the constant faith you put in me. Thank you for improving my abilities as an academic researcher, scientific writer and for sharing your scientific knowledge and experience throughout my undergraduate and postgraduate studies. Also, to Prof Alakendra Roychoudhury for your guidance and encouragement of critical thinking.

I thank the rest of the TracEx team (Jean Loock, Ryan Cloete, Ismael Kangueehi and Ian Weir) for the constant support during research cruises, assistance and discussion meetings. Also, a great thanks to all the co-authors of the manuscripts, especially to Dr. Raissa Philibert for her support during the writing of manuscripts and data interpretation through emails and Skype meetings. To Ian Weir, my cabinmate, co-author and lab partner, for his constant advice, laughs, input and discussion about all things science and not. I also extend my thanks to the SANAE 54 team for the sampling of the data used in this project as well as the conduction of the incubation experiments.

I thank the Captain and crew of the SA Agulhas II during the SANAE 56 and Winter 2017 cruises, for their professionalism and high standard of maritime expertise. I would like to express my gratitude to the NRF for financial support through a Masters Innovation Scholarship which without this project would not have been possible.

To my parents, Johann and Elmarie Viljoen, and my brother, Thinus: thank you for your encouragement, emotional support, interest in my studies and reminding me of all the important things in life. A special thanks to my grandfather and namesake, Johannes Jacobus Viljoen, for your constant interest in my life and endeavours and for teaching me the importance of religion, family and my heritage. I would also like to express my gratitude to the rest of my extended family, in-laws and friends for their support and encouragement in my pursuit to further advance my education. Special mention to my mother-in-law, Cecilia, and oom Jimmy, also for making sure I got to the ship on time!

Finally, I would like to thank my wife and best friend, Alecia, for always supporting me in my pursuit of knowledge and a scientific career. You started me on this amazing path of academic research on which I have learned so much with you at my side. I will be forever grateful. *Baie dankie*. Always.

Table of Contents

1 General Introduction

Phytoplankton form the base of the marine food web, play a critical role in biogeochemical cycles which mediate the global climate (Deppeler and Davidson 2017) and are of particular significance in the Southern Ocean due to its vastness. The Southern Ocean, in particular, accounts for ~4% of global carbon fluxes (Takahashi et al. 2009) and 40% of anthropogenic CO_2 taken up by oceans (Deppeler and Davidson 2017). Given phytoplankton's role associated with impacts on climate, it is important that we understand the factors regulating their growth, photosynthetic performance, community structure and acclimation strategies (Strzepek et al. 2012). The varying drivers of phytoplankton dynamics within different water masses are projected to vary considerably across oceanic regions within the future due to climate change (Howes et al. 2015; e.g., Deppeler and Davidson 2017) and as a consequence phytoplankton dynamics across varying water masses are likely to be different.

Two of the main factors is iron and light, especially in the Southern Ocean where they are often co-limiting (Saito et al. 2008), as they are vital for phytoplankton functionality in which both are essential for photosynthesis and photochemical efficiency (Raven 1990; Strzepek and Harrison 2004; Petrou et al. 2014). In addition to the latitudinal changes of multiple driver of phytoplankton dynamics between water masses, variations in the vertical structure of the water column results in depth gradients of certain parameters, like irradiance, which may lead to variability in phytoplankton community structure and photo-acclimation with depth (Alderkamp et al. 2011; Cheah et al. 2013). However, very often, studies conducted on bulk communities are collected from one water depth due to logistical sampling constraints that also hinders the understanding of phytoplankton acclimations. Our understanding of the relationship between trace metals and phytoplankton is traditionally hindered by a lack of parallel trace metal and community composition data. Accordingly, current initiatives aim at providing multi-parameter data sets focussed that includes a suite of trace metals, as more than just iron is essential for an array of photosynthetic and metabolic functions in marine phytoplankton.

This thesis expands on our current understanding of phytoplankton dynamics and their driving factors through three studies, from a cruise within the Atlantic Southern Ocean, separated into three manuscripts, each allocated to its own chapter (3, 4 & 5). Manuscript I compare the response of bulk communities to iron enrichment and exposure to higher light with the hypothesis that the response is regionally different in the Southern Ocean and dependent on the

co-limitation of iron and light. Manuscript II aims to assess the relationship between micro- to macronutrient concentrations and phytoplankton community distribution along a latitudinal transect. Further, manuscript III postulates that over and above the community structure, the photophysiology also changes with depth even within deep mixed layers and that it might not be suitable to only sample one depth within a region. Hence manuscript III will discuss the change in phytoplankton community structure with depth within the two distinctly different regions and how they change their various acclimation strategies to changes in light and iron availability.

Therefore, overall this thesis aims to expand our understanding of iron-light co-limitation on phytoplankton and their links to trace metal availability as well as their different acclimation strategies regionally and vertically in the water column. Ultimately, this thesis aims to improve our understanding of the consequences of key environmental changes in the present and future ocean.

2 List of Manuscripts and Contributions

This thesis is comprised of a short introduction to the background, problem statement and aims of my MSc work accompanied three manuscripts.

2.1 Manuscripts

Viljoen, J. J.*, R. Philibert*, N. Van Horsten, T. Mtshali, A. N. Roychoudhury, S. Thomalla, and S. Fietz. 2018. Phytoplankton response in growth, photophysiology and community structure to iron and light in the Polar Frontal Zone and Antarctic waters. Deep. Res. Part I. doi:10.1016/J.DSR.2018.09.006

Viljoen, J. J.*, I. Weir*, S. Fietz, R. Cloete, J. Loock, R. Philibert, and A. N. Roychoudhury. Links between phytoplankton community composition and trace metal distribution in the surface waters of the Atlantic Southern Ocean. (in preparation).

Viljoen, J. J.*. and S. Fietz. How representative are surface and chla-max communities: can we use only one or do we need both to understand phytoplankton dynamics in the Southern Ocean? (in preparation).

2.2 Contribution

Manuscript I (Chapter-3): **J. J. Viljoen** shared first authorship with R. Philibert and **J. J. Viljoen** was the main contributor in terms of phytoplankton pigment concentration interpretation and determination of phytoplankton community composition with CHEMTAX software and interpretation and writing thereof. **J. J. Viljoen** completed the final version of the manuscript and was also responsible of response to the reviewers and incorporating reviewers' comments. R. Philibert was responsible of the macronutrients and Fv/Fm data in this manuscript. R. Philibert and N. Van Horsten conducted the setup of the incubation experiments with S. Fietz' and S. Thomalla's assistance. A.N. Roychoudhury and T. Mtshali provided dFe data and supported incubation experiments. S. Fietz designed the study and supervised on-board and experimental work as well as the writing. This manuscript has been accepted to the international peer review journal *Deep Sea Research Part I* (doi:10.1016/J.DSR.2018.09.006) and has been published online.

Manuscript II (Chapter-4): **J. J. Viljoen** shared first authorship with I. Weir. **J. J. Viljoen** was the main contributor in terms of phytoplankton pigment concentration interpretation and determination of phytoplankton community composition with CHEMTAX software and interpretation and writing thereof. I. Weir was responsible for the macronutrients. R. Cloete and J. Loock under A.N Roychoudhury's supervision sampled all trace metals with the assistance of the S54 team, processed and interpreted all trace metal data. R. Philibert supervised the sampling during the expedition on board SA Agulhas II in 2015. S. Fietz supported the production of some figures and tables and supervised manuscript writing. Intended for submission to the international peer review journal *Limnology & Oceanography*.

Manuscript III (Chapter-5): The idea was initiated by **J. J. Viljoen** and he was the main author and contributor in terms of interpretation, writing and production of figures and tables. S. Fietz assisted with interpretations and editing of the manuscript being prepared and the production of some preliminary figures. Intended for submission to the international peer review journal *Polar Biology*.

Note: Tables and Figures for each manuscript are at the end of each chapter with all supplemental information in the appendices. The reference style used within entire thesis are the style of the journal L&O. Each chapter has its own acknowledgements of funding and support.

The following papers are not included as a part of this thesis but J.J Viljoen contributed to as personal communication citation for the phytoplankton data referred to in these papers:

Cloete, R., J. C. Loock, T. N. Mtshali, S. Fietz, and A. N. Roychoudhury. Winter and summer distributions of Copper, Zinc and Nickel along the International GEOTRACES section GIPY05: Insights into deep winter mixing. Chem. Geol. (revisions submitted) (manuscript nr. CHEMGE-S-18-00174).

Loock, J., R. Cloete, T. Mtshali, S. Fietz, and A. Roychoudhury. The biogeochemistry of Co, Mn and Cd on a seasonal re-occupation of the Southern Ocean. Chem. Geol. (revisions submitted) (manuscript nr. CHEMGE-S-18-00176).

3 Chapter-3: S54 Incubations Manuscript 1

3.1 Title and Authors

Manuscript accepted to Deep Sea Research Part I. Published online September 2018.

Phytoplankton response in growth, photophysiology and community structure to iron and light in the Polar Frontal Zone and Antarctic waters

Johannes J. Viljoen[1*]

Raïssa Philibert[1*,¥]

Natasha Van Horsten[1,2]

Thato Mtshali[2]

Alakendra N. Roychoudhury[1]

Sandy Thomalla[2]

Susanne Fietz[1,£]

[1]Department of Earth Sciences, Stellenbosch University, 7600 Stellenbosch, South Africa

[2]Southern Ocean Carbon and Climate Observatory, CSIR, 7599 Stellenbosch, South Africa

[*]these authors contributed equally

[¥]Current address: Coastal Ocean Research Institute, Vancouver, British Columbia

[£]corresponding author: Department of Earth Sciences, Stellenbosch University, 7600 Stellenbosch, South Africa, sfietz@sun.ac.za, +27218083117

Running title: Southern Ocean phytoplankton response to iron, light

3.2 Abstract

Availability of dissolved iron and light are both regulating factors for primary productivity in high (macro)nutrient, low chlorophyll regions of the Southern Ocean. Here, using on-board iron/light incubation experiments conducted in 2015 in the Atlantic sector of the Southern Ocean, we show that irradiance is limiting significant phytoplankton growth (in chlorophyll-a and particulate organic carbon) north of the Polar Front (46 °S 08 °E), while iron addition resulted in growth stimulation even at low light levels in the Antarctic zone (65 °S 0 °E). The phytoplankton community in the Polar Frontal Zone showed a greater functional diversity than the one in the Antarctic Zone. The community structure changed over the course of the incubations in response to increased iron and light. The observed increase in chlorophyll-a under high light in the Polar Frontal Zone was driven predominantly by an increase in pico- (0.2-2 µm) and large (>5 µm) nanophytoplankton. Pigment fingerprinting indicated an increase in the contribution of diatoms, *Phaeocystis* and also pelagophytes over the course of the incubation. In contrast, in the Antarctic Zone, the increase in chlorophyll-a after iron enrichment was predominantly due to an increase in the contribution of diatoms and large nanophytoplankton. The photochemical efficiency (Fv/Fm) was low at both sites at the beginning of the incubations, but increased upon iron fertilization in both water masses, indicating stress relief, however, the acclimation strategies fundamentally differed between the two communities. The ratio of photoprotective versus light-harvesting pigments increased under high light in the Polar Frontal Zone independent of iron enrichment, whereas this ratio declined upon iron enrichment in the Antarctic Zone even under high light. At the same time, the functional cross section of photosystem II (σ_{PSII}) decreased upon iron enrichment in the Antarctic Zone, but not in the Polar Frontal Zone. Our experiments support the need to take biogeographical differences between Southern Ocean water masses into account when interpreting ecosystem dynamics.

Key index words: bioassay; GEOTRACES; iron fertilisation; pigments; CHEMTAX

Geographic bounding coordinates: 46.00 °S 08.00 °E; 65.00 °S 00.00 °E

3.3 Introduction[1]

The ocean plays a crucial role in controlling the concentration of atmospheric CO_2 and consequently the Earth's climate. The Southern Ocean in particular accounts for ~33% of the global organic carbon flux (Schlitzer 2002), which is largely driven by phytoplankton growth and the subsequent sinking and sequestration of organic matter. Given phytoplankton's role in carbon cycling and its associated impact on climate, it is important that we understand the factors regulating their growth, photosynthetic performance and community structure.

It is well-established that phytoplankton growth in the Southern Ocean is limited by iron and light availability (de Baar et al. 1990; Martin et al. 1990; Boyd et al. 2010), which leads to the occurrence of High (macro)Nutrients, Low Chlorophyll (HNLC) regions. Iron is a vital micronutrient for phytoplankton functionality. The main requirement for iron in phytoplankton is in photosynthesis (e.g. PSI, PSII, the Cyt b6/f complex) and not chlorophyll synthesis (Raven 1990; Strzepek and Harrison 2004). Subnanomolar iron concentrations are observed in HNLC regions due to limited external or continental iron inputs (e.g. from dust, rivers and shelf sediments), low solubility, internal recycling and/or access to deep iron rich reservoirs (Boyd and Ellwood 2010). Where there are no other limiting factors, sudden iron addition leads to enhanced phytoplankton growth in the Southern Ocean and artificial fertilization experiments conducted over the past two decades have unequivocally led to phytoplankton blooms in iron limited regions (e.g. Boyd et al., 2000; Coale et al., 2004; Lance et al., 2007; Moore et al., 2013).

However, phytoplankton growth is often limited by more than one factor (Moore et al. 2013). Limitation in the natural environment might happen in different ways, either one factor represents the primary limiting factor, e.g. iron, with the other one, e.g. light, being the next limiting factor if iron is relieved, or both are required simultaneously (Saito et al. 2008). In studies using in-situ assemblage or single phytoplankton species, artificial iron enrichment led not only to growth stimulation, but also to enhanced photochemical efficiency and structural changes in the photosystems (Strzepek et al. 2012; Petrou et al. 2014) due to the involvement of iron in major photosynthetic processes (Morel et al. 2003; Behrenfeld and Milligan 2013). The strong coupling between iron availability and photosynthetic physiology suggests that dependent co-limitation (Saito et al., 2008) between iron and light availability is likely to occur,

[1] **Non-standard abbreviations:**

AAZ – Antarctic Zone of the Southern Ocean; PFZ – Polar Frontal Zone of the Southern Ocean

where iron for example can only be utilized under sufficient light availability, or vice versa. This means that iron and light limitation can exacerbate each other (Sunda 1997). However, culture studies have also demonstrated that the phytoplankton response to iron and light limitation can be group and/or species specific and that some Southern Ocean phytoplankton are able to thrive under low iron and low light conditions (Timmermans et al. 2001, 2005; DiTullio et al. 2007). This could mean that the response of Southern Ocean phytoplankton to changes in iron and light conditions may occur at community level, instead of or in addition to cellular acclimation. Therefore, although uni-algal cultures can provide insights into the mechanisms controlling iron and light limitation, experiments with whole phytoplankton communities are desirable as they highlight changes at the community level.

Physical properties (e.g. temperature, salinity, light intensity, mixing regime, day length; Carter et al., 2008) and chemical properties (e.g. nitrate, silicate, iron availability; Klunder et al., 2011; Pollard et al., 2002) vary across oceanic regions. Furthermore, changes due to projected climate change are also likely to vary considerably across oceanic regions (e.g. Deppeler and Davidson, 2017; Howes et al., 2015). As a consequence, responses of phytoplankton communities to changes in light and iron are unlikely to be uniform across varying water masses. Experiments on in-situ communities have investigated iron and light co-regulation for phytoplankton growth in the South Indian Ocean (Moore et al. 2007; Cheah et al. 2013), south of Tasmania (Petrou et al. 2011; Cheah et al. 2013), in the South Pacific Ocean (Peloquin et al. 2011), the Ross Sea (Feng et al. 2010) and in other Antarctic regions (Alderkamp et al. 2012b; Mills et al. 2012), where the natural iron supply is temporarily enhanced due to land run-off or ice melt. However, there are very few studies in the open Atlantic Southern Ocean on iron and light co-regulation. Van Oijen et al. (2004) established that in autumn, phytoplankton in the Atlantic Southern Ocean was light rather than iron limited, while Boyd and Abraham (2001), in the Pacific Southern Ocean, observed iron limitation north of the Subantarctic Front at 47 °S but iron and light co-limitation south of the Subantarctic Front at 54 °S.

Here we expand on these studies by comparing the response of bulk communities to iron enrichment and exposure to higher light in the Atlantic Southern Ocean, at two stations; one north of the Polar Front at 46 °S and the other in Antarctic Waters at 65 °S, with a focus on changes in growth, community structure and photophysiology. We evaluate changes in the phytoplankton community composition using marker pigments and the CHEMTAX matrix factorisation programme (Mackey et al. 1996; Wright et al. 2010), along with size fractionated

chl-a measurements. To further investigate the photophysiological response to iron and light enrichment we use photosynthetic efficiency (Fv/Fm), and the absorption cross-section of photosystem II (σ_{PSII}) as well as changes in photoprotective pigments. Fv is the variable fluorescence and is equivalent to the difference between the maximum fluorescence (Fm; minimum absorption of photons) and the minimum fluorescence (Fo; maximum level of photon absorption). We aim to test that the Southern Ocean community response in growth, structure and physiology is regulated by dependent co-limitation of iron and light. We hypothesise that the type of response to iron or light is regionally different in the Southern Ocean. With this we aim to improve our understanding of the consequences of key environmental changes in the present and future ocean.

3.4 Methods

3.4.1 Sampling stations

The iron and light incubation experiments were conducted during the 54th South African National Antarctic Expedition (SANAE) from December 2014 to February 2015 (from here on referred to as S54). The cruise track mainly followed the Good Hope monitoring line (Figure 3.1) crossing the Subtropical Front, Subantarctic Front and Polar Front until the Antarctic ice shelf was reached. The Good Hope line generally crosses the Subantarctic Front and Polar Front at about 45 °S and 49 °S, respectively, with some seasonal and interannual variability (Billany et al. 2010). The frontal positions at the time of this study were identified based on temperature data from the eXpendable BathyThermographs (XBT) transects AX25 (NOAA 2015). During S54, the south-bound AX25 transect from December 2014 was used. The frontal detection criteria set by Orsi et al. (1995), from 4 to 5 °C at 400 m for the Subantarctic Front and 2 °C at 200 m for the Polar Front, were used. Following this approach, during S54, the Subtropical Front was situated at 40.4 °S, the Subantarctic Front at 44.1 °S and the Polar Front at 50.4 °S (Figure 3.1). Two stations were visited during this mid-summer cruise: S54-46 (46.00 °S 08.00 °E) within the Polar Frontal Zone (PFZ) and S54-65 (65.00 °S 00.00 °E) within the Antarctic zone (AAZ; Figure 3.1).

3.4.2 Sampling and incubation set-up

At both stations, temperature (Supplemental Information Figure S3.1; Appendix A) and salinity profiles were obtained from a Sea-Bird CTD (Sea-Bird Electronics, USA) mounted on the CTD rosette. The mixed layer depth (Table 3.1) was identified from the temperature profiles as the first depth where the temperature differs from the temperature at 10 m by more than 0.2 °C (de Boyer Montégut et al. 2004). A fluorescence sensor was also attached to the

rosette. The fluorescence signal (Figure S3.1) was corrected for quenching and calibrated against bottle measurements of chl-a. Seawater for incubation experiments was collected from the apparent depths of fluorescence maxima at the bottom of the mixed layer at both stations (ca. 85m at 46 °S, station S54-46, and ca. 30m at 65 °S, station S54-65; Figure S3.1). The seawater was sampled according to GEOTRACES trace metal clean protocols (Cutter et al., 2014; Cutter and Bruland., 2012) using an epoxy coated aluminium frame CTD rosette equipped with 24x12-L GoFlo sampling bottles. Sample preparation and manipulation were conducted inside a class 100 trace metal clean container. The seawater was filtered through a 200 µm pore size mesh into two acid-washed (details provided in Supplemental Information) 50-L low-density polyethylene (LDPE) carboys (Thermo Fisher Scientific, USA). The homogenised seawater was then redistributed equally into acid washed 2.4-L Nalgene™ polycarbonate bottles (Thermo Fisher Scientific, USA; Supplemental Information Figure S3.2).

To characterise initial conditions three sample bottles were analysed immediately (details follow below). A further 36 bottles were incubated under four different iron/light treatments (details follow below) in specifically designed incubators (Minus40 Specialised Refrigeration, South Africa). The incubators were equipped with adjustable light-emitting diode (LED) strips above each shelf and a cooling fan for temperature control. Temperatures were set to mimic the respective in-situ temperatures (Table 3.1) for both experiments using the incubators' built-in temperature control systems, which maintained the temperature within a range of ±0.5°C. Temperatures were monitored using a handheld thermometer probe (Penta Digital, USA). Light levels were set using a handheld 4π photosynthetically active radiation (PAR) sensor (Biosphere QSL 2100, Biospherical Instruments Inc., USA). Day:night cycles were adjusted according to in-situ day:night cycles at the time and site of sampling (Supplemental Information; Appendix A).

Briefly, treatments consisted of i) low light level, no iron addition (L1), ii) low light level and iron addition (L1 +Fe), iii) higher light intensities, no iron addition (L2), and iv) higher light intensities and iron addition (L2 +Fe). Each treatment was conducted in triplicate bottles (Figure S3.2). The low light level (L1) was set to the in-situ PAR (15 µE m^{-2} s^{-1}; Figure S3.1) measured at the time (early afternoon) and depth (chl-a maximum; ca. 85 m) of sampling for the station at 46 °S. For the station at 65 °S, the measured in-situ PAR at the sampling depth (chl-a maximum; ca. 30 m) and time (early morning) was 0 µE m^{-2} s^{-1} (Figure S3.1), which

represents an unsuitable light level for incubation studies. Therefore, low light level (L1) was set to PAR at 10 m depth (25 µE m^{-2} s^{-1}; Figure S3.1). The high light (L2) was set to 65 µE m^{-2} s^{-1} for both sites. Synthetic iron was added as 1 nM $FeCl_3$ to the +Fe treatments under the laminar flow hood inside the onboard class 100 trace metal clean laboratory using an 89.5 µM acidic $FeCl_3$ solution made from a 1000 mgL^{-1} stock solution (Iron Atomic Spectroscopy Standard, Sigma Aldrich). Additions of 1 nM dissolved iron (dFe) have previously been shown to noticeably alleviate iron limitation (Boyd and Abraham 2001) and were therefore considered to be appropriate for this set of experiments. Further details of the incubations are given in the Supplemental Information (Appendix A).

The dFe of the initial seawater was analysed in triplicate for both incubation experiments (S54-45 and S54-65; Table 3.1). Sample processing and analysis for dFe followed GEOTRACES guidelines (Cutter et al., 2014; Cutter and Bruland., 2012) inside the on-board class 100 clean container. The collected seawater was filtered for dFe determination from the GoFlo bottles into acid-washed 125mL LDPE bottles through 0.2µm pore size Acropak™ 500 Supor® membrane filters with filtered (Midisart 2000, 0.20 µm) nitrogen assistance (BIP Technology). All samples were immediately acidified using hydrochloric acid (Ultrapur, Merck) to a pH of 1.7 and stored. A SeaFAST-pico SC-4 DX (Elemental Scientific) module was used for offline pre-concentration (by a factor of 40 times) inside a class 100 trace metal clean laboratory, prior to injection into a quadrupole inductively coupled plasma mass spectrometer (ICP-MS; Agilent 7900) at Stellenbosch University, South Africa. Details on the acid-washing of material, the instrument configuration and chelating resin as well as intercalibration, within laboratory calibration and check standards are provided by Cloete et al. (under revision).

3.4.3 Measurements of growth and photophysiology

Concentrations of total chl-a, particulate organic carbon (POC) and dissolved nutrients (NO^-_3 + NO_2^- , PO_4^{3-} and $Si(OH)_4$) were measured to determine differences in growth and nutrient uptake between treatments. Samples for frequent (ca 48h) determination of total chl-a were filtered through glass fibre filters with nominal pore sizes of 0.2, 2 and 5 µm, frozen for 24 hours, extracted in 90 % acetone and analysed using a Turner fluorometer. Chl-a concentrations for pico- (0.2 – 2 µm), nano- (2 – 5 µm) and micro-phytoplankton (>5 µm) were measured to obtain information on the size structure of the phytoplankton community. Samples for POC were filtered through ashed glass fibre filters with a nominal pore size of 0.7 µm. The filters were acid fumed to remove any inorganic carbon and analysed using an elemental analyser. Nutrient concentrations were determined using a flow injection autoanalyser for NO^-_3 + NO_2^-

and $Si(OH)_4$ (Wolters 2002; Egan 2008), while PO_4^{3-} concentrations were determined manually according to the methods described by Grasshoff et al. (1983). Incubation bottles were sampled for all variables at four time-points, i.e., at the start and end of the incubation and at two intermediary time points. Photophysiology analysis (Fv/Fm and σ_{PSII}) was conducted every 24 hours using Fast Repetition Rate fluorometry (FRRf; Chelsea SMD Telecommunications (Pty) LTD, UK). Details on filters, instruments and calibration standards for chl-a, POC and macronutrients as well as on FRRf settings are provided in the Supplemental Information. All statistical analyses were performed in R Statistical Software (R Core Team 2015) and all graphs plotted with Ggplot2 (Wickham 2009).

3.4.4 Determination of accessory pigments and community composition

Samples were also taken for accessory pigment analysis. Amber sample bottles were used for subsampling from the incubation bottles and filtration carried out under dim light due to the sensitivity of accessory pigments to light. The water was filtered through glass fibre filters (0.7 µm nominal pore size) and filters immediately stored at -80°C until analysis. Analysis for phytoplankton pigments by High-Performance Liquid Chromatography (HPLC) was conducted at Laboratoire d'Océanographie de Villefranche-sur-Mer as described by Ras et al. (2008). Phytoplankton pigment samples were collected only at the start of the experiment and again at the final termination after five to six days of incubation to represent the community for the initial conditions and at the end of each treatment. Detailed pigment data are provided in Table S3.1. In this study we will focus on phytoplankton chemotaxonomic composition and specific pigment ratios indicative for photoacclimation.

The contribution of individual phytoplankton functional groups to total chl-a (used here as a proxy for biomass) was calculated using the CHEMTAX v1.95 chemical taxonomy software (Mackey et al. 1996; Wright et al. 2010). The CHEMTAX phytoplankton community composition estimates are based on the relative abundance of a suite of marker pigments to total chl-a in the water. Each group has a characteristic pool of accessory pigments, but all phytoplankton groups contribute to the total chl-a. However, the interpretation of pigment data for the assessment of community composition can be difficult due to marker pigments that are present in several groups. The CHEMTAX matrix factorisation is therefore based on the ratios between one or more accessory pigments and chl-a per group (Mackey et al. 1996; Wright et al. 2010). Below we briefly describe the approach of the CHEMTAX protocol for the identification of phytoplankton functional groups and determination of their relative abundances.

The main phytoplankton groups to be included into the CHEMTAX processing were selected based on literature data published for the Atlantic Southern Ocean and nearby regions (Wright et al. 2010; Schlüter et al. 2011; Gibberd et al. 2013; Mendes et al. 2015). Nine phytoplankton groups were chosen: cyanobacteria, prasinophytes, dinoflagellates, *Phaeocystis*-H (High iron-acclimated state of *Phaeocystis antarctica*), *Phaeocystis*-L (Low iron-acclimated state of *P. antarctica*), coccolithophores (haptophytes-6), pelagophytes (pelago-1), chlorophytes and diatoms. Cryptophytes were excluded from the CHEMTAX calculations, since alloxanthin, their marker pigment, was not detected. *Phaeocystis* here refer exclusively to *P. antarctica*, a species within the haptophytes-8 group (Wright et al. 2010) but are separated into functional forms acclimated to low and high iron concentrations, which together with coccolithophores represent the larger haptophyte phytoplankton group. These two functional forms were included because *P. antarctica* adjust their pigment ratios to the ambient iron concentrations as observed in cultures grown under iron enriched vs. iron depleted conditions (DiTullio et al. 2007; Wright et al. 2010). Further details regarding the choice of specific pigments and phytoplankton groups for the CHEMTAX processing as well as the optimised ratios after the CHEMTAX analyses can be found in the Supplemental Information and Table S3.2 (Appendix A). As outlined above (1.4.2 Sampling and incubation set-up), each experiment was conducted in triplicate and hence estimates of contributions of phytoplankton groups were obtained in triplicate. These triplicate contributions were averaged (Table S3.3) similarly to all other parameters presented in this study for each treatment.

3.5 Results

3.5.1 Sampling site characterisation

The observed in-situ conditions at both sites, at 46 °S (S54-46; PFZ) and at 65 °S (S54-65; AAZ) were characteristic of typical conditions of the respective water masses. Average surface temperatures between January and March generally range between 6 - 9 °C for PFZ and below 5 °C for the AAZ (Boyer et al. 2013). Average January to March nitrate concentrations typically increase southwards from about 10 µM in the SAZ to 20 µM in the PFZ and > 25 µM in the AAZ (Boyer et al. 2013). Typical surface silicic acid concentrations are generally low throughout the Subantarctic Zone and PFZ (< 10 µM) and increase sharply south of the Polar Front to > 50 µM (Boyer et al. 2013). Table 3.1 summarises the in-situ conditions for our experiments. At 46 °S, station S54-46 was characterised by a deep mixed layer (89 m). Low temperatures (~6 °C) and low chl-a concentrations (0.12 µg L^{-1}) were observed at the sampling depth (depth of chlorophyll maximum). The nitrate concentration at 46 °S was relatively high

(23 µM), while silicic acid concentrations were low (5.8 µM). Conditions at 65 °S in the AAZ were characterised by much lower temperatures (0 °C), relatively shallow mixed layer depths (31 m), and high chl-a (1 µg L^{-1}), nitrate (25 µM), and silicic acid (74 µM) concentrations. The molar Si:NO_3 ratio was ca. ten times higher in the AAZ (2.9) compared to the PFZ (0.25). The dFe concentrations were 0.37 nM at 46 °S and 0.19 nM at 65 °S (Table 3.1). The molar dFe:NO_3 ratios were thus $0.016x10^{-3}$ at 46 °S and $0.0075x10^{-3}$ at 65 °S.

The photosynthetic efficiency (Fv/Fm) and functional absorption cross-section of photosystem II (σ_{PSII}) further provide an indication of the nutrient limitation in phytoplankton. Under nutrient limitation, the photosynthetic efficiency (Fv/Fm) decreases. Such nutrient limitation can also cause a loss of reaction centres (where photochemical reactions leading to the evolution of O_2 occur) and may lead to an increase in the light absorption cross section (or light absorption coefficient) of PSII (σPSII; Suggett et al. 2004). The initial Fv/Fm values were around 0.25 at both stations (46 °S and 65 °S) indicating that the phytoplankton experienced stress and potential iron limitation prior to the incubation (Figures 1.2a, c). The initial effective rate of light absorption (σ_{PSII}) was much higher at 65 °S compared to 46 °S (Figures 1.2b, d).

In addition to the abiotic and physiological differences, the water masses studied here showed differences in the initial phytoplankton composition. At 46 °S, the largest cell fraction (>5 µm) dominated with a 48 % contribution to total chl-a (Figure 3.3a). The lowest chl-a contribution (14 %) was observed in the 2 - 5 µm size fraction. The smallest size fraction (0.2 – 2 µm) contributed 38 %. Pigment signatures indicated that the initial community in the PFZ was dominated by both *Phaeocystis* and diatoms with contributions of 45% and 43%, respectively and minor amounts of coccolithophores (Figure 3.4a). This initial PFZ community also contained noticeable pico-phytoplankton contributions of prasinophytes and pelagophytes (9% and 3%, respectively). In the AAZ, the largest cell fraction (>5 µm) in the initial seawater dominated with 71% (Figure 3.3b). Much lower chl-a contributions were observed in the 2 - 5 µm (16 %) and 0.2 – 2 µm (13 %) size fractions. The pigment composition suggests that those large cells were presumably diatoms and coccolithophores. Diatoms showed the largest contribution (62%) to chl-a in the AAZ, while coccolithophores contributed ca. 20% and *Phaeocystis* 17% (Figure 3.4b).

3.5.2 Responses to increasing iron and light in the PFZ (46 °S)

Indicators of growth: The growth rates derived from changes in chl-a were mostly similar to those derived from POC (Figure 3.3a, 1.5a) and the changes in POC and chl-a concentrations

were linearly correlated (Figure S3.3, $p < 0.01$). Chl-a derived growth is therefore considered to be a robust representation of the changes in phytoplankton growth. The chl-a concentration in the PFZ (0.12 µg L^{-1} under initial conditions) did not change significantly after incubation under the low light treatments with or without iron enrichment (Figure 3.4a). Under high light, the chl-a concentration doubled to 0.25 µg L^{-1} and 0.28 µg L^{-1}, respectively, in the treatments with or without added iron (Figure 3.4a) and the chl-a:POC ratio nearly doubled (from 0.007 to 0.013 µg µg; Table S3.4) with the addition of iron. The changes in the dissolved macronutrient concentrations in the medium generally corresponded to the changes in chl-a and POC, with stronger nutrient depletion observed where chl-a and POC increased (Table S3.5).

Phaeopigments (i.e. the sum of phaeophytin-a and phaeophorbide-a) are used in this study to estimate the extent of cell degradation over the course of the incubations. At 46 °S, the initial phaeopigment concentrations were below detection limit and remained below detection in the low light treatment with iron. Phaeopigment:chl-a ratios reached 0.007 µg:µg in the low light treatment without iron, together indicating that degradation was not a major process at low light (Table 3.2). In contrast, phaeopigment:chl-a ratios increased up to 0.022 µg:µg under high light, where only phaeophytin-a was detected; phaeophorbide-a was below detection (Table S3.8). While we cannot exclude the possibility of grazing in our incubations, these low and treatment-specific phaeopigment:chl-a ratios point to minor grazing impacts.

Shifts in the community composition: The largest cell fraction (>5 µm) showed strongest growth in all treatments from 48% to around 61-63% of total chl-a at the end of the incubations (Figure 3.3a). In contrast, the contribution of the 0 – 2 µm fraction decreased to 28 - 30 % and that of the 2 – 5 µm fraction decreased to 7 - 11 % (Figure 3.3a). These shifts in the community at 46 °S at the end of incubations were, however, almost the same across all treatments, independent of the light and iron availability implying that neither iron nor light induced particular shifts in the size fractions of the community at 46 °S (Figure 3.3a).

The initial composition in the PFZ incubation was dominated by contribution of diatoms along with *Phaeocystis*. Coccolithophore contribution to chl-a was rather insignificant (Figure 3.4a). However, under low light conditions, especially after iron enrichment (L1+Fe), an increase in the contribution of coccolithophores to 28% and a decrease in contribution of *Phaeocystis* and diatoms, to 16.5% and 31.8% respectively, was observed (Figure 3.4a). Both high light treatments (L2 and L2+Fe) showed an increase in contributions of diatoms and

coccolithophores to ca. 51% and ca. 6% respectively, and a decrease in the contribution of *Phaeocystis* to 23% (Figure 3.4a). Despite the increase in contribution of coccolithophores and decrease in contribution of *Phaeocystis*, diatoms and *Phaeocystis* still dominated the contribution to total chl-a under high light at the end of the incubation (Figures 1.4, S1.4a). This corresponds to our observation that the largest size group (>5 µm) showed the strongest increase in chl-a over the course of the high light incubations (Figure 3.3a).

The contribution of *Phaeocystis* to chl-a, in general, decreased under low light conditions compared to the initial conditions. However, the response of *Phaeocystis* (*P. antarctica*) cells acclimated to high iron availability and those acclimated to low iron availability (see 1.4.4 CHEMTAX set-up) was different. After iron enrichment, contributions (to the total chl-a) of *Phaeocystis* cells with a pigment composition indicating low iron availability ("Phaeocystis-L" in Figure 3.4) dropped drastically from 23% to non-detectable amounts. Contributions (to the total chl-a) of *Phaeocystis* cells with a pigment composition indicating high iron availability ("Phaeocystis-H" in Figure 3.4) only decreased from 22% to 17% after iron enrichment.

Photoacclimation: All treatments in the PFZ showed an increase in Fv/Fm over the course of the incubation (Figure 3.2a). However, iron addition led to stronger initial increase in Fv/Fm compared to the non-amended treatments (Figure 3.2a). The response in photochemical efficiency was rather quick: the L1 +Fe and L2 +Fe treatments showed higher Fv/Fm values than the L1 and L2 within two days of incubation (Figure 3.2a). In contrast, differences in σ_{PSII} between treatments were not statistically significant (Table S3.6).

Xanthophyll cycle pigments diadinoxanthin and diatoxanthin (DDT) are further used to assess stress and photo-acclimation strategies in this study. These are found in all of the taxa considered in this paper except chlorophytes, prasinophytes and cyanobacteria (Olaizola et al. 1994; Brunet et al. 2011), and are synthesized to protect the cell against excess light. In the PFZ, the DDT concentration as well as the ratio of DDT (photoprotective pigments) to chl-a and to light harvesting pigments fucoxanthin and 19'-hexanoyloxyfucoxanthin (Fuco+Hex; Figure S3.5a), increased in both high light treatments irrespective of iron enrichment (Table 3.2). This increase in photoprotective pigments was accompanied by an increase in the photosynthetic efficiency (Fv/Fm) especially under conditions of high light with iron enrichment (Figure S3.6).

3.5.3 Responses to increasing iron and light in the AAZ (65 °S)

Indicators of growth: In contrast to the incubations in the PFZ at 46 °S, the experiment at 65 °S in the AAZ showed a major increase in chl-a upon iron enrichment even at the lower light intensity (Figure 3.4b). The daily change in chl-a concentration under L2 +Fe conditions at 65 °S was more than three times greater than under L1 conditions (Table S3.5) resulting in statistically significant differences in chl-a concentrations at the end of the incubations between L1 and L2 +Fe (Table S3.7). The POC content remained unchanged under low light even after iron enrichment, and consequently, the chl-a:POC ratios more than doubled upon iron enrichment under low light conditions (Table S3.4). In contrast, POC content increased under high light (Figure 3.5), even without iron addition resulting in lower chl-a:POC ratios. Increased nutrient uptake rates were also observed at 65 °S upon iron enrichment under low and high light (Table S3.5). The strongest silicic acid uptake increase was observed under high light, high iron conditions and the weakest under high light without iron enrichment (L2; Table S3.4). A noticeable increase in the phaeopigment:chl-a ratios was also observed, especially at L2+Fe (0.29 µg:µg; Table 3.2), with generally higher phaeophorbide-a than phaeophytin-a concentrations (Table S3.8).

Shifts in the community composition: The chl-a derived growth rate was higher in the iron enriched incubations both under low and high light conditions (Figure 3.3b). This strong response to iron enrichment can mostly be attributed to the large cells' response (Figure 3.3b). The contribution of the smallest cells increased from 13 % to 15 % without iron enrichment, but decreased from 13 % to 11 % after iron enrichment (under both light levels). Iron enrichment thus seemed to affect both total chl-a concentration as well as community structure in the AAZ independent of the light level.

Under all treatments, the increase in total chl-a was mostly due to growth of diatoms (Figure 3.4b). Between the treatments, diatom growth was strongest upon iron enrichment: The contribution of diatoms to total chl-a increased to 80% with iron enrichment under low light and to 82% with iron enrichment under high light (Figure 3.4b). *Phaeocystis* (predominantly the high iron acclimated form) chl-a also increased upon iron enrichment compared to the non-amended treatments (up to 0.4 µg L^{-1}; Figure 3.4b), which, however resulted in only minor changes in *Phaeocystis*' contribution to total chl-a (ca. 12% in all treatments; Figure S3.4). Coccolithophores responded differently. Lower coccolithophore chl-a concentrations were observed under low light iron enriched treatments compared to the unamended treatments (0.21 µg L^{-1} and 0.23 µg L^{-1}, respectively), decreasing coccolithophores' contribution to total chl-a

to ca. 7% upon iron addition (Figure 3.4b). The contribution of all other smaller phytoplankton groups was minimal for all treatments in the AAZ. This is in agreement with the chl-a size fractionated measurements, which showed iron enrichment induced major changes in the large size fraction of the community in the AAZ incubations.

Photoacclimation: All treatments in the AAZ showed an initial increase in Fv/Fm over the course of the incubation (Figure 3.2c), matching the changes observed in chl-a and POC-derived growth (Figures 1.3 and 1.5). Iron addition resulted in strong chl-a and POC increase and similarly, iron addition led to stronger initial increases in Fv/Fm compared to the non-amended treatments (Figure 3.2c). After two days the increase in Fv/Fm reached a plateau and then began to decrease. The largest decreases occurred in the non-amended control treatments without iron addition (Figure 3.2c). The σ_{PSII} decreased for all treatments during the initial 2-3 days with the greatest decreases occurring in the iron enriched treatments (Figure 3.2d).

The DDT (diadinoxanthin + diatoxanthin) photoprotective pigment ratios to chl-a were relatively low in our AAZ incubations (Table 3.2), with lowest DDT:chl-a ratios observed under the high light treatment with iron (0.021 µg:µg; L2+Fe). This corresponds to a low DDT:(Fuco+Hex) ratio of 0.028 µg:µg (Table 3.2), indicating that the community favoured photosynthesis over photoprotection after iron addition at high light.

3.6 Discussion

The Southern Ocean is not uniform and the response of phytoplankton to the environment in which they live varies between regions (Boyd et al. 2010; Thomalla et al. 2011). This highlights the importance of understanding the factors that drive phytoplankton growth in different regions. Here we focus on the community response to iron and light variability in the Atlantic Sector of the Southern Ocean. The in-situ conditions varied largely between the stations at 46 °S and 65 °S. Hence, pre-adaptation and pre-acclimation (Flynn et al. 2015) of the phytoplankton communities incubated in our experiments were expected to differ.

3.6.1 Initial differences in environmental conditions, community distribution and acclimation

Environmental conditions: At 65 °S (AAZ), the phytoplankton were exposed to in-situ temperatures close to freezing point, long day lengths and high nitrate and silicic acid concentrations (Table 3.1). At 46°S (PFZ) phytoplankton were exposed to higher in-situ temperatures, shorter day-lengths, and lower silicic acid concentrations than in the AAZ. The mixed layer depth was deep (89 m) at 46 °S, but relatively shallow (31 m) at 65 °S. The station

at 65 °S was located within the seasonal ice zone of the AAZ. Based on satellite imagery (Cavalieri et al. 1996, updated yearly), the ice melted relatively late during the summer of 2015 at this location (Figure S3.7). This late ice melt might have caused the observed particularly shallow mixing regime and possible micronutrient release.

While surface waters of the summertime Southern Ocean in general are typically iron limited (Moore et al. 2013), Klunder et al. (2011b) observed dFe concentrations that decreased southwards along the Good Hope Line in February-March 2008. Our measured dFe concentrations in January 2015 of 0.31 nM at 46 °S and 0.19 nM at 65 °S were in agreement with the range reported by Klunder et al. (2011b) for surface waters (Figure S3.8). Iron limitation is also indicated for both stations by the dFe:NO_3 ratio of 0.016 (nM:µM) at 46 °S and 0.0075 (nM:µM) at 65 °S, much lower than the ratio of 0.5 (nM:µM) based on the extended Redfield ratio of $(C_{106}N_{16}P_1)_{x1000}Fe_8$ (Morel et al. 2003). Several factors indicate that the iron depletion at 65 °S was likely a recent occurrence following the utilisation of micronutrients released from the melting sea ice that prevailed at the station at 65 °S until a week before sampling (Figure S3.7). For instance, Fv/Fm values were low and indicated iron stress. However, only high-iron acclimated *Phaeocystis* forms and a relatively high chla:POC ratio were observed at 65 °S, which is rather indicative of iron replete conditions. The pigment acclimation reportedly requires time lags of two or more days between iron addition and biological response (Sedwick et al. 2000, 2007; Coale et al. 2003). Altogether, this would indicate that the initial community at 65 °S was sampled towards the end of a recent bloom caused by ice melt. This recent bloom arguably removed most of the released available dFe and started inducing iron limitation.

Community structure: Varying environmental conditions in the two investigated Southern Ocean water masses not only drive variability in biomass and primary productivity but also in community composition. Shifts in the community composition are important as they change the composition of exported organic matter and the trajectory of primary production through the food web (Boyd and Trull 2007; Finkel et al. 2010). In our study, picophytoplankton (0-2 µm) played a major role (38% of total chl-a) in the PFZ, while diatoms and non-calcified haptophytes (*Phaeocystis*) both contributed less than 45% each to the total chl-a, corresponding to previous findings in the Polar Frontal and Subantarctic waters (Ishikawa et al. 2002; e.g., Gervais et al. 2002). This indicates that the PFZ community was more diverse, possibly due the deep mixed layer which in turn also causes the community to be more light than iron

limited, as discussed further below. In the AAZ, in contrast, the phytoplankton community was dominated by large (>5 µm) cells. The CHEMTAX analyses revealed that diatoms largely dominated (ca. 60% w.r.t. chl-a) this phytoplankton community despite the observed low dFe concentration and very low dFe:NO_3 ratios. Either the diatom growth had only recently induced the iron depletion, and/or secondary factors such as depth of vertical mixing might have played a key role here, favouring large cells in the shallow mixed layer of the Antarctic waters (Wright et al. 2010; Swan et al. 2015). Some Antarctic diatoms can also grow with minimal iron availability by replacing ferridoxin with flavodoxin (Pankowski and Mcminn 2009). Higher silicic acid availability in the AAZ, necessary for diatom growth, is also likely to have affected the in-situ community composition. Strong grazing pressure is unlikely given the low phaeopigment:chl-a ratios.

Photophysiology and acclimation: We observed low initial photosynthetic efficiencies (Fv/Fm) at 46 °S and at 65 °S, which could indicate iron limitation in both water masses. Additionally, it could be due to region-specific causes: 1) light inhibition during daytime (due to the shallow mixed layer) in the AAZ, and 2) larger contribution of smaller phytoplankton in the PFZ. Our data set does not allow for disentangling these interacting driving forces. Light inhibition in the AAZ might have resulted from the observed lower photoprotective versus assimilatory pigments ratio. The initial average σ_{PSII} (7.9 nm^{-2} $quanta^{-1}$) at 65 °S was only slightly lower than the range observed in laboratory Southern Ocean diatom cultures, but higher than published values for coastal diatoms isolates (Strzepek et al. 2012) and much higher than at 46 °S (2.8 nm^{-2} $quanta^{-1}$). This relatively high σ_{PSII} in the AAZ may be a result of the pre-acclimation to very low iron availability and/or photoinhibition, i.e. lack of photoprotective pigments (Suggett et al. 2004 and references therein). Shifts in the phytoplankton community may also influence the σ_{PSII} (Suggett et al. 2004). However, as mentioned above, the PFZ contained a more diverse functional community, including prasinophytes and pelagophytes, for example. Prasinophytes and pelagophytes have much larger absorption cross sections compared to diatoms (Suggett et al. 2004), which means that we should expect larger σ_{PSII} in the PFZ if the σ_{PSII} was mainly driven by the community composition. Since this is not the case, photoacclimation appears to better explain the larger σ_{PSII} observed in our study in the AAZ compared to the PFZ.

3.6.2 Growth and community structure response to enrichment in iron and light

The differences in environmental conditions, community composition and acclimation, resulted in different responses to relief of iron and light limitation. The community at 46 °S

was only enhanced by iron addition if the light environment was suitable. Iron addition at low light intensities had a negligible effect on the growth. This would indicate a dependent co-limitation (Saito et al. 2008), where light is the primary limiting factor. In the ocean, such conditions would, for example, arise after a resupply of iron through deep mixing followed by a shoaling of the mixed layer. Inability of Southern Ocean phytoplankton to use the external supply of iron under unfavourable light conditions has been observed previously in areas with deep mixed layers (de Baar et al. 2005; Cassar et al. 2011). For temperate phytoplankton, Sunda and Huntsman (1997) suggested that iron enrichment might relieve light limitation as the greater requirement for photosynthetic iron-based redox proteins in low-light acclimatized algae can be met. Our findings at 46 °S, a mixed community, rather support Strzepek et al. (2012) observations that iron enrichment does not always provide relief of light limitation and that the response to iron and light availability in Southern Ocean subantarctic communities may differ from temperate phytoplankton.

However, at 65 °S, a diatom dominated community, iron enrichment indeed led to increased growth even at low light. The greater macronutrient depletion observed in our AAZ incubation media upon iron enrichment supports the assumption that the AAZ community insufficiently consumes macronutrients under iron limiting conditions explaining the prevailing excess macronutrient availability in Antarctic waters, and that only iron enrichment enables an increased utilization of macronutrients. Additional light, without iron enrichment resulted in low chl-a increase. This points towards a dependent co-limitation where iron is the predominant factor. The phytoplankton in the AAZ might only be light limited if iron limits the restructuring of the photosynthetic apparatus. The contrasting response of the phytoplankton community at 46 °S and 65 °S indicates that the potential to use iron enrichment under low light conditions mainly depends on the resident phytoplankton assemblage and pre-acclimation.

The changes observed in the community composition over the course of the incubations, provide further insight into which functional groups benefited most. At 65 °S, diatoms' contribution to total chl-a increased in all treatments, most so (up to 80%) upon iron enrichment independent of the light regime in agreement with previous studies, which showed that large diatoms benefited the most from sudden iron enrichment (Hoffmann et al. 2006 and references therein). Our observations in the PFZ were different though. The size-fractionated composition in the PFZ barely changed over the course of the six day long incubation, independent of the treatment. At this site, diatoms only increased their contribution to total chl-a under high light

conditions (from 43% up to 52%). Under low light conditions, the contribution of coccolithophores to total chl-a increased (from 0.3 to 28%) whereas the contribution of diatoms and *Phaeocystis* decreased. Nonetheless, the observed shift in the pigment composition from *Phaeocystis* acclimated to high iron availability to *Phaeocystis* acclimated to low iron availability in the PFZ supports the Deppeler and Davidson (2017) assumption of the great potential of *P. antarctica* to thrive in the future oceans.

3.6.3 Photophysiological changes in response to changes in iron and light

Changes in the cellular chl-a content are usually part of the acclimation strategies to changes in light and nutrient regimes (Behrenfeld et al. 2005). Under light limitation, one widespread acclimation strategy in phytoplankton is to increase the cellular chl-a content so that additional photosynthetic units (PSU) can be synthesized and maximum light can be captured. However, the synthesis of these units requires iron and hence the iron demand is increased under light limiting conditions. Under iron limitation on the other hand, phytoplankton are unable to produce enough PSU to capture sufficient light for photosynthesis and growth (Sunda and Huntsman 1997). Therefore, generally, iron-replete phytoplankton are known to have higher chl-a:POC ratios than iron depleted cells (Moore et al. 2007), while increased light availability generally results in a decrease in chl-a:POC ratios. In line with this, the chl-a:POC ratio increased in the AAZ upon iron enrichment, especially under low light conditions, but in the PFZ the ratio only increased upon iron enrichment and high light conditions (Table S3.4). Hence, similar to observations for growth, the change in the photosynthetic apparatus, specifically in cellular chl-a, appears to occur upon relief of iron limitation alone in the AAZ, while such changes require relief of both iron and light limitation in the PFZ.

Diatoms and haptophytes (*Phaeocystis* and coccolithophores) present an additional acclimation strategy to varying light intensities whereby they use pigments of the xanthophyll cycle, such as diadinoxanthin and diatoxanthin, for photoprotection (Brunet et al. 2011). Our PFZ experiment showed, as in Moore et al. (2007), that increases in light caused increases in the concentration of photoprotective pigments. However, this did not occur in the AAZ, despite the dominance of xanthophyll producing phytoplankton groups, diatoms and haptophytes. They were either not able to produce sufficient amounts of photoprotective pigments or used other protective strategies. The increase in chl-a degradation products (phaeopigments, especially phaeophorbide-a) under high light conditions suggests that the AAZ community might have been limited in their capacity to prevent photo-inhibition and resulting cell damage and chl-a degradation.

Typically, in the world's oceans, phytoplankton iron requirements are lower under higher irradiance than under lower irradiances. Strzepek et al. (2012), however, suggested that Southern Ocean phytoplankton – in contrast to temperate communities - respond to low light by increasing the size of PSU rather than the number of PSU. As a result, their demand for iron is not increased to the same extent under low light as they do not require extra iron to build new PSU. Hence, they might not be iron deficient when they are acclimated to low light. Strzepek et al. (2012) furthermore suggested that the increased size of PSU is reflected in high σ_{PSII} values. However, contrary to Strzepek et al. (2012) findings, the σ_{PSII} did not change noticeably over the course of our PFZ incubations (Figure 3.2b). This might be due to a lack of short-term response in the size of PSU in our six days long incubations, or to the observed shifts in the community. At 65 °S, in the AAZ, however, iron enrichment did lead to strong growth and an increase in Fv/Fm values under low light intensities compared to the non-amended treatment. The σ_{PSII} decreased in all treatments over the course of the incubation, but most dramatically so in the iron enriched incubations. Fv/Fm showed an inverse response, with most drastic increase in the iron enriched incubations. The decrease in Fv/Fm at a later stage during the incubations, especially in the non-iron amended treatments may indicate photoinhibition, potentially a result of the above mentioned low photoprotective versus assimilatory pigment ratios in the AAZ.

3.7 Conclusion

In this study, two incubation experiments were conducted showing responses of Southern Ocean phytoplankton to iron enrichment and higher irradiances. As had been suggested previously, a dependent co-limitation of iron and light in both water masses was confirmed. However, the importance of one or the other limiting factor was shown to differ regionally. The community in the PFZ showed a stronger response to light than to iron, while in the AAZ, iron was the dominant limiting factor. The latter was attributed to differences in the resident community as well as to pre-acclimation to post-bloom and a shallower surface mixed layer. At both sites, however, addition of both iron and light led to the strongest responses in chl-a, POC and photochemical efficiency, indicating that iron and light in both water masses to some extent in both locations co-limited phytoplankton photosynthesis and growth. Iron and light addition not only induced changes in growth and photochemical efficiency, but also resulted in important shifts in community structure. For example, at 46 °S, where the functional diversity was higher than at 65 °S, coccolithophore and prasinophytes contributions were higher under low light than under high light, independent of the iron addition, whereas the

diatom contribution was lower under low light and higher under high light. At 65°S in contrast, diatom contribution increased more upon iron enrichment than under high light alone. Such changes in the phytoplankton community will have major consequences on the macronutrient and carbon cycles at the ocean surface, as well as on the sinking and settling of calcium carbonate and silicate. The knowledge of region-specific responses in growth, photochemical efficiency and community composition is therefore key to improve biogeochemical models and the understanding of our future oceans.

3.8 Acknowledgements

The work leading to these results received funding from the National Research Foundation (NRF), under the SA/Norway Collaboration Programme and the South African National Antarctic Programme, grant numbers 91313 and 110731 awarded to S.F. R.P. acknowledges support from NRF through a SANCOR-NRF fellowship under grant number 94915. J.V. acknowledges funding from NRF through a Masters Innovation Scholarship. The XBT data used in this manuscript are made freely available on the Atlantic Oceanographic and Meteorological Laboratory and are funded by the NOAA Office of Climate Observations. The authors thank NASA Goddard Space Flight Center, Ocean Ecology Laboratory, Ocean Biology Processing Group, for seasonal composite chl-a concentrations. The authors furthermore thank Smit Amandla crew of the R/V SA Agulhas II, Department of Environmental Affairs (DEA), and all the scientific cruise participants of SANAE 54.

3.9 References

For the purpose of this thesis the references for this manuscript and the others, including references for supplemental information, are combined in the main reference list (on page 76) to avoid duplication.

3.10 Tables

Table 3.1. Site characteristics and initial conditions for both incubation experiments. The temperature and salinity were extracted from the CTD sensor data for both stations. The initial nutrient concentrations (NO_3^- and $Si(OH)_4$) were obtained from discrete samples taken on a separate cast at the same station. The mixed layer depth (MLD) was calculated according to the temperature criteria by de Boyer Montégut et al. (2004). Example profiles of temperature, light attenuation and chl-a concentrations at both stations are shown in Supplemental Figure S3.1 (Appendix A).

	S54-46	**S54-65**
Date	12-Jan-15	18-Jan-15
Latitude (°S)	46	65
Longitude (°E)	8	0
Region	PFZ	AAZ
Temperature (°C)	6.20	0.00
Salinity	33.8	34.0
MLD (m)	89	31
[dFe] (nM)	0.37	0.19
$[NO^-{}^3]$ (μM)	23.3	25.2
$[Si(OH)_4]$ (μM)	5.79	74.3

Table 3.2. Ratios of photoprotective versus chl-a and accessory light harvesting pigments in both incubation experiments in response to iron and/or light addition. Phaeo=Phaeopigments, DDT=diadinoxanthin+diatoxanthin (photoprotective), FH=Fuco+Hex (light-harvesting). Detailed data sets (e.g. individual pigment concentrations) can be found in Supplemental Table S3.8 (Appendix A).

	S54-46 (PFZ)			**S54-65 (AAZ)**		
	Phaeo:Chla	DDT:Chla	DDT:FH	Phaeo:Chla	DDT:Chla	DDT:FH
Initial	0.0000	0.069	0.075	0.101	0.051	0.050
L1	0.007	0.066	0.087	0.096	0.054	0.056
L1 +Fe	0.000	0.063	0.092	0.122	0.040	0.046
L2	0.022	0.083	0.122	0.163	0.055	0.065
L2 +Fe	0.022	0.087	0.120	0.286	0.021	0.028

3.11 Figures

Figure 3.1. Station positions along the Good Hope line for cruise SANAE54. The background shows a seasonal composite of chl-a concentration for the period of December 2014 to February 2015 (NASA Ocean Biology Processing Group 2014). The solid black line represents the Good Hope line. The dashed horizontal lines indicate the frontal positions (STF - subtropical front, SAF - Subantarctic Front, PF - Polar Front) along the Good Hope line. Black regions on the map represent areas where the chl-a concentration is higher than 2 µg L^{-1} whereas white regions indicate insufficient chl-a data due to ice or cloud cover.

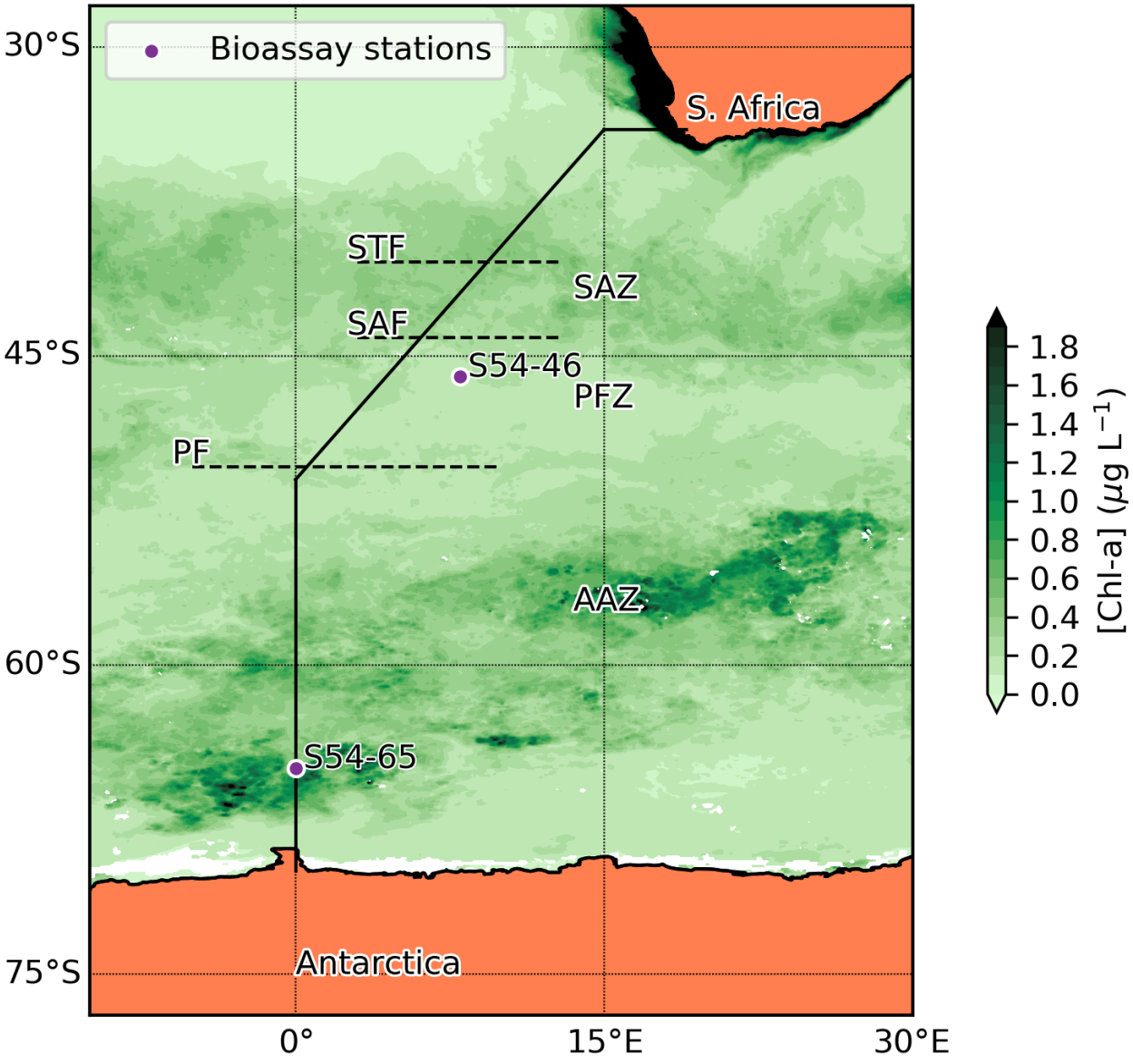

Figure 3.2. Changes in Fv/Fm (a,c) and $\sigma_{PS\ II}$ (b,d) over the course of the two summer 2015 bioassays, S54-46 (a,b), and S54-65 (c,d). The red lines indicate the low light treatments (L1) and the black lines the higher light treatments (L2). Dashed lines and triangles are for iron enriched treatments (+Fe) while solid lines and circles indicate control conditions without iron enrichment. The symbols represent individual measurements at each time point (termination). The lines represent the average values of Fv/Fm and σ_{PSII} for each treatment. The y-axes for σ_{PSII} are shown on different scales due to the large differences between the two experiments. For interpretation of the references to colour in the figure caption, the reader is referred to the online version of this article.

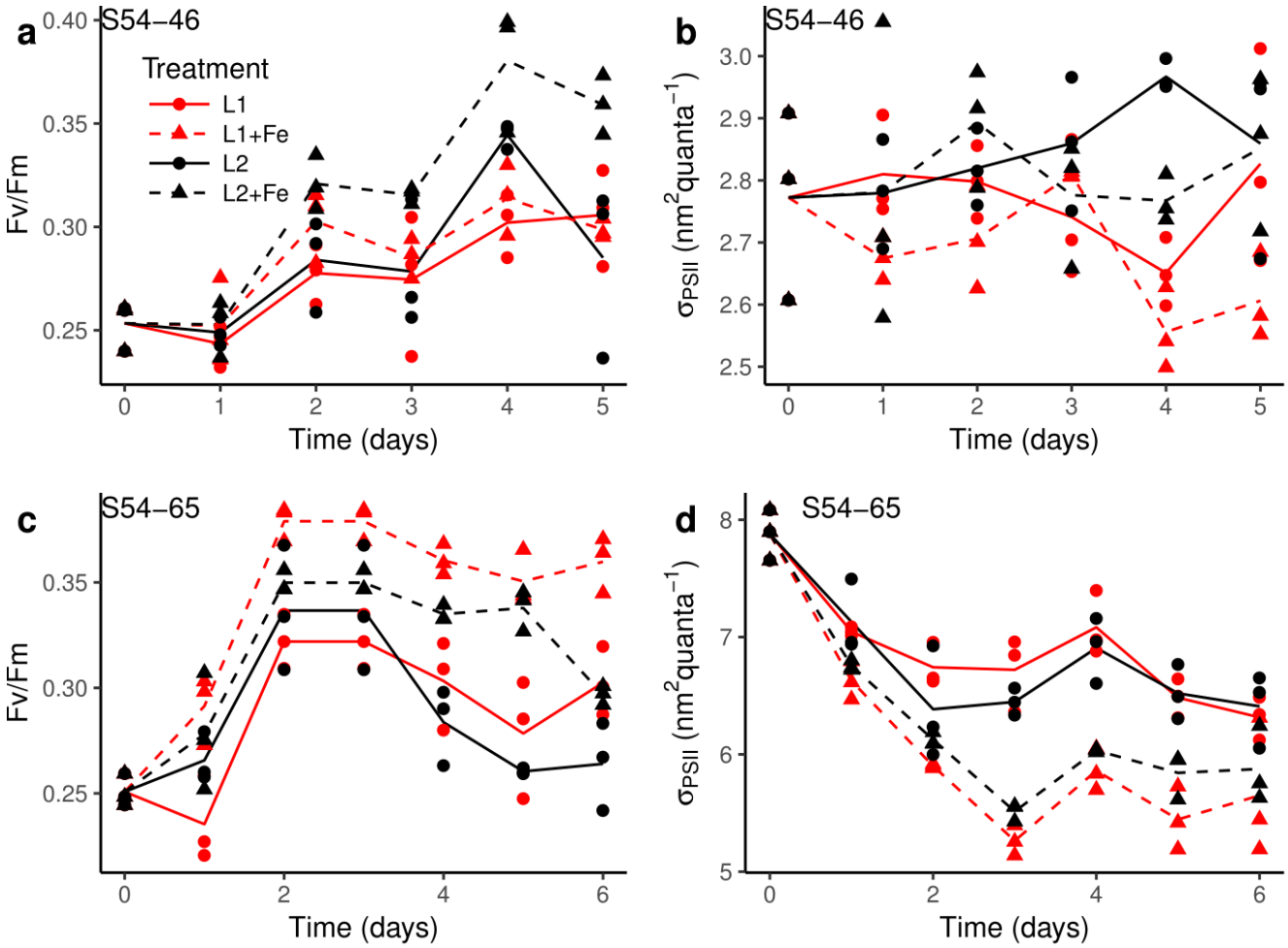

Figure 3.3. Changes in size-fractionated chl-a concentrations for S54-46 (a) and S54-65 (b). Size fractionated chl-a concentrations were measured by filtering the samples sequentially through polycarbonate filters with 5, 2 and 0.2 µm pore sizes.

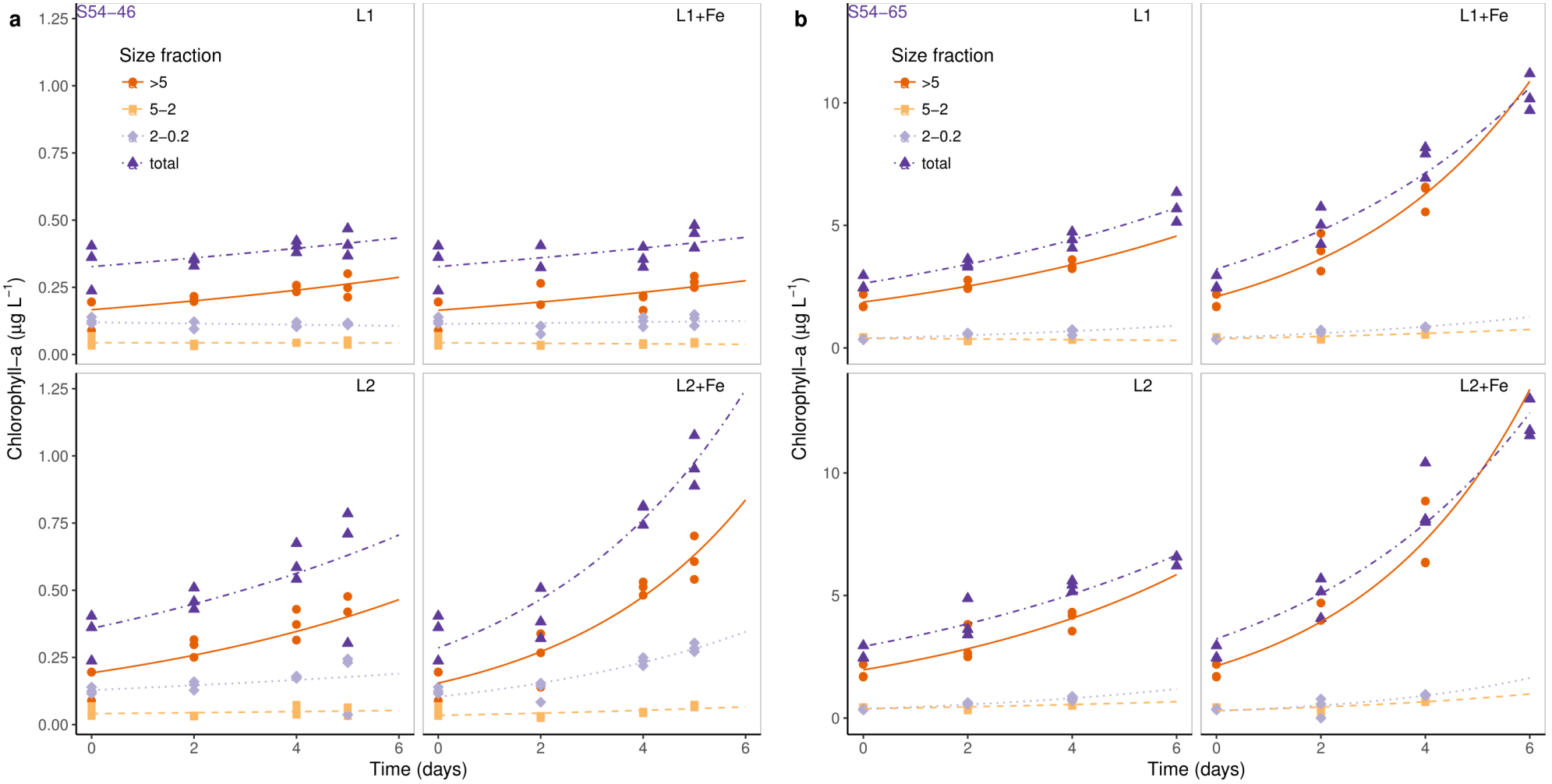

Figure 3.4. Phytoplankton composition at the end of each treatment for (a) S54-46 and (b) S54-65. Initial = Initial community with no treatment; L1 = low light; L2 = high light; +Fe = iron enrichment. Graphs were plotted using the CHEMTAX output results shown in Table S3.3. A 100% stacked bar chart is shown in Figure S3.4, Supplemental Information (Appendix A). Error bars represent standard deviations.

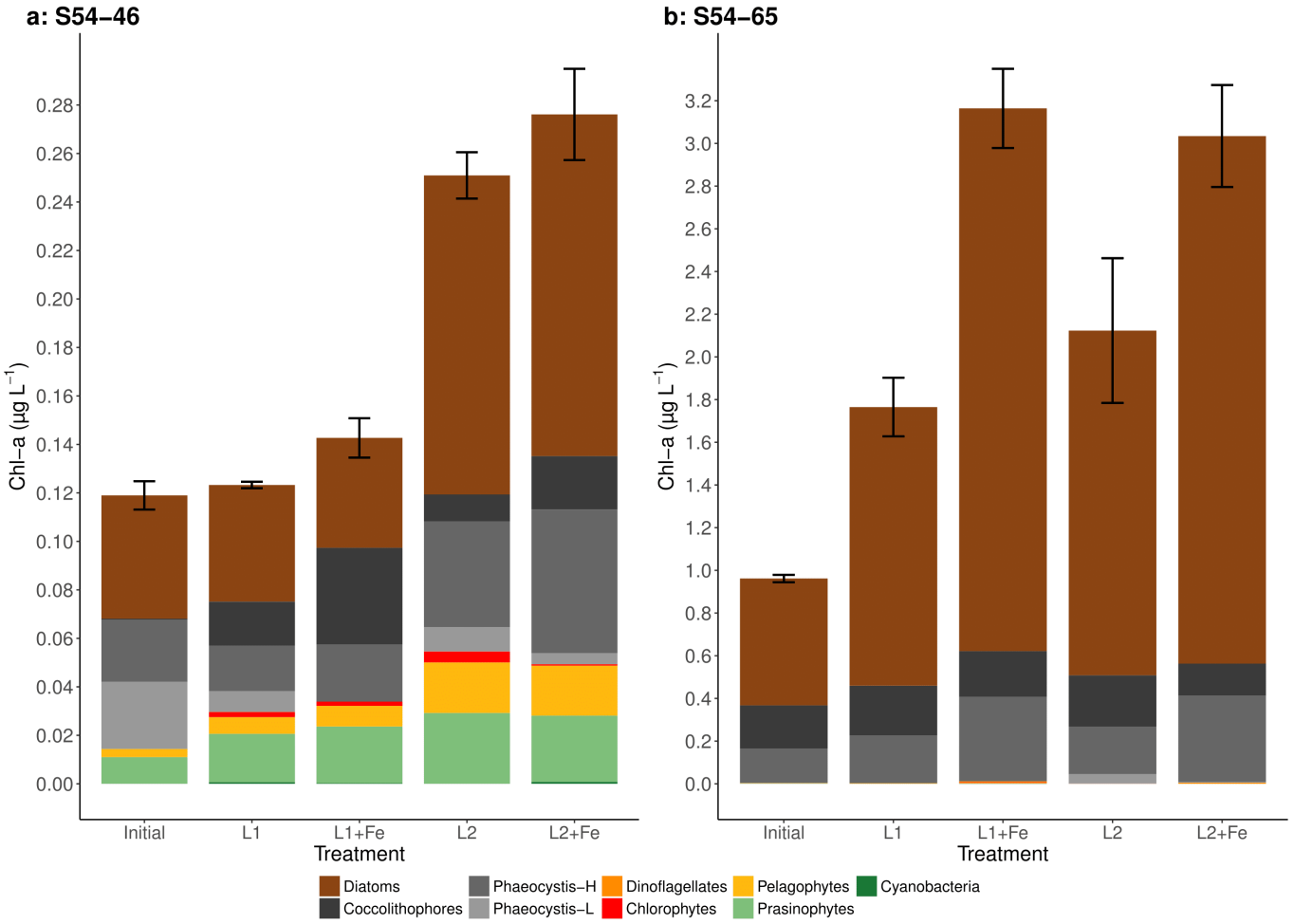

Figure 3.5. Changes in particulate organic carbon (POC) concentrations over the course of the two summer 2015 bioassays: S54-46 (a), and S54-65 (b). The red lines indicate the low light treatments (L1) and the black lines the higher light treatments (L2). Dashed lines and triangles are for iron enriched treatments (+Fe) while solid lines and circles indicate control conditions without iron enrichment. The symbols represent individual measurements at each time point (termination). The lines are exponential fits through these individual measurements points for each. The y-axes for POC (a,b) are shown on different scales due to the large differences between the two experiments.

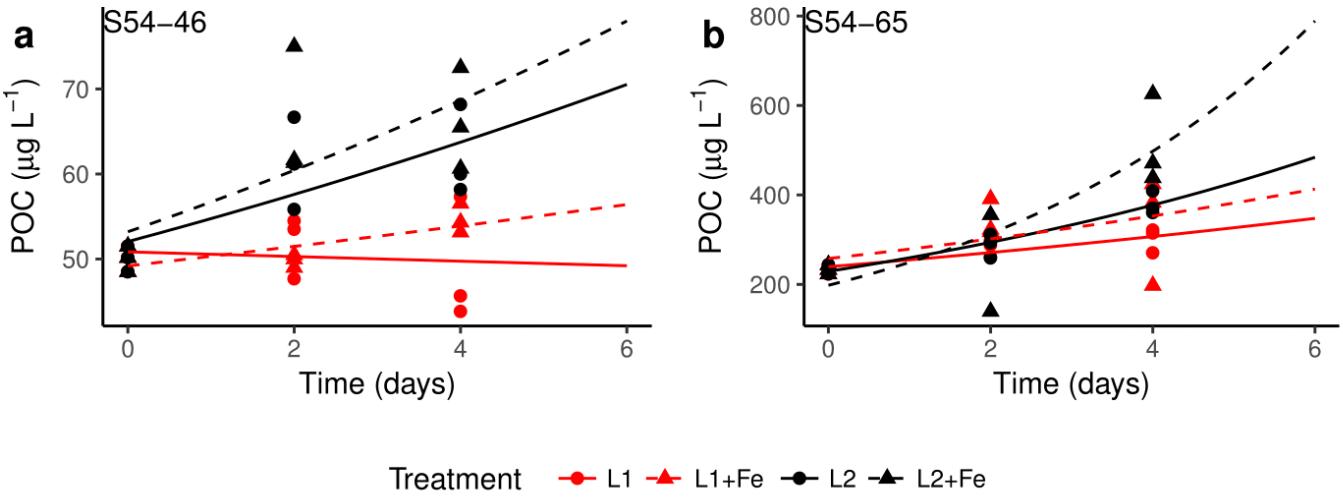

4 Chapter-4: S54 Transect Manuscript 2

4.1 Title and Authors

Manuscript in preparation intended for submission to Limnology & Oceanography.

Links between phytoplankton community composition and trace metal distribution in the surface waters of the Atlantic Southern Ocean

Johannes J. Viljoen[1]*, Ian Weir[1]*, Susanne Fietz[1,£], Ryan Cloete[1], Jean Loock[1], Raissa Philibert[1,2], Alakendra N. Roychoudhury[1]

[1]Centre for Trace Metal and Experimental Biogeochemistry, Department of Earth Sciences, University of Stellenbosch, 7600 Stellenbosch, South Africa

[2]Coastal Ocean Research Institute, Vancouver, British Columbia

[*]these authors contributed equally

[£]corresponding author: Department of Earth Sciences, Stellenbosch University, 7600 Stellenbosch, South Africa, sfietz@sun.ac.za, +27218083117

4.2 Abstract

Phytoplankton and trace metal distribution are intrinsically linked in the ocean by metabolic requirements and uptake. Traditionally, the relationship between phytoplankton and trace metals have been addressed through incubation studies, in which species are commonly studied in isolation and/or in terms of selected trace metals. This study assesses in-situ phytoplankton community variability in terms of trace metal distribution in summer surface waters of the Atlantic Southern Ocean along the GEOTRACES GIPY_05 transect. A multi-parameter approach is implemented to address phytoplankton community variability both spatially and temporally, combining an array of biogeochemical variables encountered in the five major oceanic zones across the transect. Diatoms were the dominant phytoplankton group south of the Polar Front, where silicic acid concentrations greatly increased, with notable *Phaeocystis* and coccolithophore contribution. Furthermore, zinc (Zn) and manganese (Mn) were most strongly correlated with silicic acid in this region, indicative of a community simultaneously utilizing these metals and silicic acid, a community such as diatoms. North of the Polar Front communities were *Phaeocystis*-dominated with notable diatom contribution and important cyanobacteria contribution in the Subtropical zone which may be linked with unusual cobalt (Co) depletion. *Phaeocystis* dominance north of the Polar Front is most likely attributed to limiting silicic acid concentrations and deep mixed layers, while the abundance of smaller phytoplankton groups may be related to warmer, higher salinity waters. Seasonally, highest chlorophyll-a concentrations in the study area were encountered in January and on the reoccupation of selected stations there was an obvious shift in community structure and macronutrient ratios. Our findings indicate that an influx and/or abundance of trace metals linked to hydrothermal plume activity and ice melt, is closely related to increasing biomass and community diversification. Such a diversification in community structure could not be explained by macronutrients and physical variables. The timing of such trace metal fluxes also proved to be a pivotal factor, particularly for iron in some instances, which seemed to be preferentially depleted to near-limiting concentrations and may have driven under-utilization of certain metals such as nickel to prevent further iron stress. The study highlights the importance of considering trace metals as an additional variable when accounting for phytoplankton variability in the open ocean, although it is unclear whether trace metal distributions drive the community composition or vice versa.

Keywords: GEOTRACES; hydrothermal plume; multi-parameter; austral summer; pigments

4.3 Introduction

The fundamental role macronutrients play in marine algal photosynthesis has been well-documented (Redfield 1958; Arrigo 1999) However, our understanding of the relationship between trace metals and phytoplankton communities is traditionally hindered by a lack of parallel trace metal and community composition data. Due to group-specific nutrient requirements, the phytoplankton composition greatly influences the biogeochemical cycles, including those of trace elements. In turn, availability of nutrients, including essential trace nutrients drive the phytoplankton community composition because of group and taxa-specific requirements of essential nutrients. Accordingly, current initiatives aim at providing multi-parameter data sets focussed on trace metal, macronutrient and community assemblages. Trace metals are essential micronutrients responsible for an array of photosynthetic and metabolic functions in marine phytoplankton, for instance, iron (Fe) is required in the enzyme that catalyses carbon and nitrogen (N) fixation, zinc (Zn) is part of the carbonic anhydrase, responsible for the hydration and dehydration of CO_2 , while manganese (Mn) is essential for O_2-evolving enzymes, responsible for the oxidation of water during photosynthesis (Twining and Baines 2013). Metal requirements differ between functional groups and taxa where their requirements can fluctuate in response to environmental conditions, such as light. The extended Redfield ratio describes the proportions with which phytoplankton utilise major nutrients and is defined as 180C: 23N: 1P: 5x10-3Fe: 2x10-3Zn: 1x10-3Mn: 5x10-4Ni: 4x10-4Cd: 2x10-4Cu: 4x10-5Co. It follows that trace metal distribution exerts a strong control on primary production and which groups of phytoplankton constitute that production.

Phytoplankton form the base of the marine food web and are of particular significance in the Southern Ocean, especially in the summer and spring period when large blooms develop supporting a profusion of Antarctic life. Furthermore, phytoplankton play a critical role in biogeochemical cycles which mediate the global climate (Deppeler and Davidson 2017). The Southern Ocean, in particular, accounts for ~4% of global carbon fluxes (Takahashi et al. 2009) and 40% of anthropogenic CO_2 taken up by oceans (Deppeler and Davidson 2017). Those global carbon fluxes into the ocean are largely driven by phytoplankton growth and the subsequent sinking to the deep ocean and sequestration of the phytoplankton organic matter. Different phytoplankton groups have different roles in the food-web as well as in the CO_2 uptake (van Leeuwe et al. 2015). For example, studies have shown that although certain species of

dinoflagellates uptake greater volumes of CO_2 than diatoms, their nutrient requirements differ (Chitari and Anil 2017). Therefore, we need to understand which phytoplankton groups are dominant to improve biogeochemical climate models that are used for studying climate change (Deppeler and Davidson 2017).

Few studies have been done to assess the driving factors of phytoplankton productivity and community structure across different zones in the Southern Ocean that include macronutrients and essential trace metals (Wright et al. 2010; Gibberd et al. 2013). Seasonal studies from the Ross Sea, for example, show that phytoplankton community assemblages heavily influence biogeochemical characteristics and cycles in this region, demonstrating that changes in the dominant groups and taxa impart distinctive nutrient removal ratios in the residing water mass (Arrigo 1999; Smith and Asper 2001). This paper presents an analysis on the surface distribution and structure of phytoplankton communities on the GIPY-05 transect in the Atlantic Southern Ocean. This transect includes the crossing of a mid-ocean ridge and the marginal ice zone. The aim of this study is the assessment of the relationship between micro- to macronutrient concentrations and phytoplankton communities.

4.4 Methods

4.4.1 Cruise Track

This study focuses on sampling conducted on the R/V SA Agulhas II during the South African National Antarctic Expedition (SANAE) 54 from December 2014 to February 2015 along the GEOTRACES GIPY_05 transect in the Atlantic Southern Ocean (Figure 4.1). This cruise was conducted over a period of ten weeks. The first leg went from Cape Town, South Africa, to the Antarctic shelf following the Bonus Good Hope monitoring line (05/12/2014 – 16/12/2014; herein referred to as “December”). A section not further discussed here followed north-westward to South Georgia and from South Georgia north-east to reach the Good Hope Line again at 46 °S (29/12/2014 – 6/1/2015). The third leg started at 46 °S and followed the Good Hope Line southward (6/1/2015 – 23/1/2015; herein referred to as “January”) and the fourth leg returned north along the same line (7/2/2015 – 15/2/2015; herein referred to as “February”). Three major fronts of the Antarctic Circumpolar Current (ACC) were crossed, Sub-Tropical Front (STF; 40.4 °S), Sub-Antarctic Front (SAF; 44.1 °S) and Polar Front (PF; 50.4 °S; Figure 4.1). The Southern Boundary (SBdy) of the ACC was located at ~55.44°S. The frontal positions at the time of this

study were identified based on temperature data from the eXpendable BathyThermographs (XBT) transects AX25 (NOAA 2015) using criteria in Orsi et al. (1995). Using the fronts and the SBdy, we classified the Southern Ocean surface waters in our study into five distinctive zones: Sub-Tropical Zone (STZ), Sub-Antarctic Zone (SAZ), Polar Frontal Zone (PFZ), Antarctic Zone (AAZ) and Weddell Gyre (WG; Figure 4.1).

4.4.2 Sampling and Analysis

Three sampling strategies were adopted in this study: 1) temperature and salinity data were recorded continuously at 10min intervals by the ship's on-board system from the underway supply located at around 5-6 m water depth at the ship's bow; 2) samples for all other parameters except for trace metals were taken from the underway supply at lower resolution (details follow below); 3) water samples for trace metals were collected using a GoFlo bottle array according to GEOTRACES trace metal clean standards at six stations (details follow below).

4.4.2.1 Pigments and determination of phytoplankton community composition

Seawater was collected for chl-a and accessory pigment analysis from the continuous underway supply at around 5-6 m water depth from the ship's bow. Water was collected approximately at every degree south and additionally when approaching a CTD (trace metal) station. The resulting sample set contained 33 samples representing surface phytoplankton communities across all major water masses (STZ, SAZ, PFZ, AAZ and WG). These surface pigment samples were taken as single samples due to logistical constraints of an extremely tight time schedule aboard. The water was filtered under dim light through Whatmann® GF/F glass fibre filters (0.7 µm nominal pore size) and filters were immediately stored at -80 °C until analysis after the cruise. The frozen filters were extracted and analysed for phytoplankton pigments by High-Performance Liquid Chromatography (HPLC) at Laboratoire d'Océanographie de Villefranche/Mer (LOV – CNRS) as described by Ras et al. (2008). The calculation of phytoplankton community composition using the pigment data was done using CHEMTAX software (Mackey et al. 1996; Wright et al. 2010; details provided in Supplemental Information). The degradation (phaeo-) pigments, phaeophorbide-a and phaeophytin-a and the photoprotective pigments diadinoxanthin (DD) and diatoxanthin (DT) were used to assess degradation and photophysiology.

4.4.2.2 Macronutrient, biogenic silica and SEM imagery

Surface water was collected from the continuous underway supply for the analysis of dissolved nutrients (NO_3^-, NO_2^-, $Si(OH)_4$ and PO_4^{3-}). Samples were frozen at -20 °C immediately after sampling and analysed within one to two months after sampling. A Lachat Quick-Chem Flow injection autoanalyser was used for the analysis of NO_3^-, NO_2^- and $Si(OH)_4$ (Wolters 2002; Egan 2008). Phosphate was analysed manually according to methods described by Grasshoff et al. (1983). The analytical error of the NO_3^- + NO_2^-, PO_4^{3-} , and $Si(OH)_4$ quantification is ± 0.04 μM, ± 0.06 μM and ± 0.02μM, respectively (Grasshoff et al. 1983). Samples collected for particulate silica analysis were collected underway when approaching a CTD cast station or departing the station. Approximately 1L of seawater was filtered onto a 0.45µm Omnipore Membrane filter through the bow intake of the ship while underway. The filter was then oven-dried for 12 hours at 60 °C. The biogenic silica (BSi) was determined using the NaOH digestion method described by Ragueneau and Tréguer (1994). Biogenic silica is hydrolysed by a hot NaOH solution and analysed for silicic acid using the colorimetric detection method of Grasshoff et al. (1983). The reduced silicomolybdic acid species was measured on a Genesys 10-S UV Spectrophotometer at 810nm. A blank filter interference of 0.0399 ±0.002µM is reported for the NaOH digestion, with other errors negligible (<1.6%). After NaOH extraction, filters were assayed for lithogenic silica (LSi) by HF addition. The LSi fraction is not reported herein, as concentrations attained from blank filters, subject to HF addition, were high and variable (0.5-1.5µM). These samples were also used for Scanning Electron Microscope (SEM) imaging, to aid in the identification of phytoplankton with mineralized skeletons. This work supported our phytoplankton community composition determination described above.

4.4.2.3 Dissolved trace metals

Trace metal samples were collected from six CTD stations (Figure 4.1) using GoFlo bottles on a titanium frame, and sub-sampling in a certified class 100 clean container on board. All sampling and material cleaning procedures strictly followed GEOTRACES standards (Cutter and Bruland 2012; Cutter et al. 2014). Only dissolved trace metals are reported here, sampled in low density polyethylene (LDPE) bottles after online filtration through 0.2µm Sartobran filters. Prior to analysis, samples were pre-concentrated using a seaFAST-pico SC-4 DX module (Elemental Scientific Inc.) in the certified class 100 laboratory at Stellenbosch University. Pre-concentrated samples were then analysed using an Inductively Coupled Plasma Mass Spectrometry (Agilent

7900 ICP-MS) at Stellenbosch University. Details on materials used, washing procedures, instrument calibration and method validation can be found in Cloete et al. (under revision) and Loock et al. (submitted). Full depth profiles for a suite of bioactive trace metals (copper, zinc, nickel, cobalt, manganese and cadmium) are also provided by those authors. Here we focus on the surface phytoplankton community and nutrient concentrations. The shallowest depth of the vertical trace metal profiles (15-16m water depths) was used as surface concentrations. All concentrations referred to in this study are of dissolved metal species, except for cobalt, where lack of UV radiation during sample processing means that the analysed cobalt only encompasses the labile fraction Loock et al. (submitted).

4.5 Results

Temperature and salinity: As expected, sea surface temperatures (SSTs) generally decreased from north to south with sub-zero temperatures in proximity of the Antarctic shelf (Figure 4.2a). Salinity also decreased from north to south, especially through the STZ and SAZ (Figure 4.2b). Higher variability was observed in close proximity to the fronts and to the ice shelf. Seasonal progression of temperature towards warmer waters from December to February was observed, while salinities varied little with the seasonal (Figure 4.2).

Macronutrients: Nitrate surface concentrations were low throughout the STZ in December (avg. 1.3µM), while displaying a southward increase to 25µM in the SAZ and ~30µM in the PFZ and AAZ (Figure 4.3a, Table S4.1). South of 55 °S (i.e. the SBdy), nitrate concentrations were decreased again to <25µM. Average nitrate concentrations in the PFZ and northern AAZ showed large depletion in January and February (~18µM). Phosphate gradually increased southward from <0.5µM in the STZ reaching values >3µM in certain sections of the WG in December (Figure 4.3b). As a consequence, nitrate to phosphate (N/P) ratios were low in the STZ and WG, but elevated in the SAZ, PFZ and AAZ, i.e. between the STF and the SBdy (Figure S4.1, Table S4.1). January and February phosphate concentrations indicated depletion with seasonal progression, but followed a similar north-south trend as observed in December. For example, January surface phosphate concentrations averaged 1.1µM in the PFZ, but increased south across the AAZ to >2.5µM at ~67 °S (Figure 4.3b, Table S4.1). As a consequence, the N/P ratios varied only slightly across the water masses (Figure S4.1, Table S4.1). Relatively low concentrations of silicic acid (avg. <3µM) persisted throughout the STZ, SAZ and PFZ in December, followed by a sharp rise

at the PF to about 15µM (Figure 4.3c, Table S4.1). Silicic acid concentrations rapidly increased south of the PF reaching concentrations as high as 87µM upon approaching the Antarctic Shelf. Ratios of silicic acid versus nitrate and phosphate (Si/N and Si/P), showed similar trends with high Si/N and Si/P ratios in the STZ, very low ratios in the SAZ and PFZ, increasing ratios in the AAZ, and highest ratios in the WG (Figure S4.1, Table S4.1). In January and February, low concentrations of silicic acid (avg. 2.7µM) also prevailed in the STZ, SAZ and PFZ, that increased south of the PF in the AAZ (avg. 11.5µM), and WG (53µM). However, as in December, silicic acid concentrations declined in the proximity of the Antarctic shelf (~70 °S; Figure 4.3c).

Dissolved trace nutrients: Sampling for determination of dissolved trace metal concentration only occurred at six stations during the fourth leg of SANAE54, in January 2015 (Figure 4.1). The main dissolved trace metals investigated here, showed very different surface water profiles along the transect. Three principal components accounted for almost all (98%) the variance in the trace metal distribution (Table 4.2a). Copper and Ni mainly followed a similar trend as nitrate and both correlated well with the first (negatively) and second (positively) factor of the Principal Component Analysis (Table 4.2a, Figure S4.2a). Low concentrations in the STZ and increasing concentrations southwards (Figure 4.4a) from 0.5 to 1.8 nM and from 2.4 to 6.0 nM were recorded for Cu and Ni, respectively (Table 4.1a). Copper and Ni both showed nutrient-type depth profiles (i.e. depth profiles significantly, positively correlated to nitrate and phosphate) at all stations (Table 4.1b) pointing to biological uptake at surface. Zinc and Mn showed maximum concentrations at 36 °S (9.4 and 0.96 nM, respectively; Table 4.1a), which strongly decreased across the PFZ, AAZ and most of the WG, while increasing again close to the ice shelf at 68 °S (Figure 4.4c). Both, Zn and Mn, correlated well with the first component, but only weakly with the second (Table 4.2a, Figure S4.2a). The Zn and Mn maximum observed at surface at 36 °S coincides with the observation that neither Zn nor Mn show nutrient-type depth profiles at this station (Table 4.1b). Indeed, Mn only showed nutrient-type depth profiles, i.e. biological uptake at surface, at two stations, ~50 °S and ~60 °S (Table 4.1b). Iron, Co and Cd showed different surface profiles, with increasing concentrations from the STZ to the PFZ, decreasing concentrations across the PFZ, AAZ and most of the WG (Figure 4.4b). However, while Co and Cd correlated strongly with the second component, Fe was not correlated to either the first or the second component, but strongly correlated to a third component (Table 4.2a). Most prominent distinction between the transect profiles was the drastic increase in Co and Cd closest to the ice

shelf, while Fe decreased (Figure 4.4b). Out of these three metals, only Cd showed nutrient type depth profiles at all measured stations (Table 4.1b). Iron depth profiles differed from typical nutrient-type profiles at ~54 °S and at ~60 °S and cobalt only showed nutrient-type depth profiles at 36 °S and 50 °S, indicating that cobalt was only utilised in the surface at those two stations.

Phytoplankton community: The total chlorophyll a (chl-a) concentrations generally increased from north to south, ranging from 0.03 to 0.57 µg L^{-1}. Higher chl-a concentrations were seen close to the ice edge (Figure 4.3d). Strongest correlation with regard to macronutrients was found between chl-a and silicic acid concentration, even though total chl-a was also correlated (at 90% confidence interval) with nitrate and phosphate (Table 4.3a). Total chl-a was furthermore weakly (at 90% confidence interval) correlated to Cu and Zn (Table 4.3b). No significant correlation was found between the surface chl-a concentrations and the mixed-layer depth (MLD; not shown). Phaeopigments were not detected in the STZ, SAZ and PFZ, indicating low grazing pressure and cell degradation (Jeffrey et al. 1997; Wright et al. 2010; Carreto et al. 2016). However, phaeophorbide-a and phaeophytin-a both occurred south of the PF with maximum concentrations of 0.03 and 0.008 µg L^{-1}, respectively (Figure S4.3a). Maximum phaeopigment:chla ratio (0.2 µg:µg) was observed at 65 °S (Figure S4.3a).

Two principal components explain 46% of the variance in phytoplankton distribution (Table 4.2, Figure S4.2b). The first component correlated with high diatom chl-a concentrations (Table 4.2). Contribution of diatoms to total chl-a generally increased from north to south ranging from ca. 30 to 90%, with diatom chl-a concentrations ranging from ca. 0.01 to 0.3 µgL^{-1} (Figures 2.3d, S2.4), but decreased south of 69 °S within proximity of the ice. Diatom chl-a concentrations were significantly correlated with silicic acid, phosphate and Cu concentrations (Table 4.3). No significant correlation was found between the surface diatom (or any other phytoplankton group investigated here) chl-a concentrations and the MLD (not shown). SEM imaging at 36 °S indicated a low cell abundance, comprised predominantly of small centric diatoms (<5µm), which reaffirm low chl-a concentrations (0.03 µgL^{-1}) dominated by diatom contribution. The surface BSi concentrations also increased from 0.35µM at 36 °S to 4.6µM at 50 °S, remained similarly high until 60 °S (Table 4.4). SEM imaging at station 53.6 °S, in the AAZ, indicated diatoms were small to medium sized (~7-55µm) and comprised of *Chaetoceros* spp, *Thalassioisira* spp and *Fragilairiopsis* spp. Noticeably lower BSi values (<0.76µM) were encountered within proximity

of the ice (Table 4.4). However, a very prominent peak in BSi of 13.8 µM was observed at 65 °S that did not correspond to a peak in diatom chl-a (Table 4.4). The BSi:diatom-chla ratio (µmol:µg) ranged between 2 and 6 throughout most of the transect, with the exception of a prominent peak in the ratio at 50 °S and very low ratios close to the ice edge (Table 4.4).

The contribution of the haptophyte *Phaeocystis* (*P. antarctica*, refer to supplemental information, Appendix B) to total chl-a increased from 36 °S to reach its maximum of 63% at 42 °S, but decreased southwards thereafter (Figures 2.3d, S2.2). The *Phaeocystis* chl-a was not correlated to any macronutrient and only showed weak correlation with Mn and Cd (Table 4.3). Two forms of *P. antarctica* can be differentiated based on their composition of light-harvesting pigments ratios, regulated according to the availability of dissolved iron (DiTullio et al. 2007; Wright et al. 2010). Along our transect, the two forms showed generally opposite trends (Figures 2.3d, S2.2). The chl-a concentration from *P. antarctica* with the characteristic pigmentation pattern of iron replete conditions (*Phaeocystis*-H) increased southwards, while chl-a concentration from *P. antarctica* with the characteristic pigmentation pattern of iron depleted conditions (*Phaeocystis*-L) decreased southwards (Figures 2.3d, S2.2). As a consequence, the chl-a concentration from *Phaeocystis*-H correlated with principal component one, similarly to diatom chl-a, while chl-a concentration from *Phaeocystis*-L correlated with a separate component, distinct to all other groups investigated in this study (Table 4.2). Neither form was correlated to Fe concentration nor any other trace metal investigated (not shown).

Coccolithophores chl-a concentrations were correlated to the first principal component along with diatoms and *Phaeocystis*-H (Table 4.2). Coccolith platelets have been observed using SEM imaging at station 53.6 °S, most likely belonging to the species *Emiliania huxleyi*. Coccolithophore chl-a ranged between 0.0004 and 0.04 μgL^{-1} showing a general increase from north to south. However, coccolithophores showed a sudden increase to ca. 34% of total chl-a (i.e. ~0.20 μgL^{-1}) at ca. 67 °S within the WG (Figures 2.3d, S2.2). This coccolithophore increase encountered at ca. 67 °S coincided with the maximum chl-a concentration of the total community (Figure 4.3d).

Some pigments, such as diadinoxanthin and diatoxanthin (DDT), generally found in diatoms and haptophytes including *Phaeocystis* and coccolithophores, can furthermore be used as indicators of photoacclimation (Alderkamp et al. 2011; Brunet et al. 2011). Photoprotective pigments (diadino-

and diatoxanthin) were not detected in the STZ, but concentrations increased southwards, except close to the ice edge (Figure S4.3b). Consequently, the ratio of the photoprotective (DDT) versus light-harvesting (fucoxanthin and 19′-hex-fucoxanthin) pigments (DDT:FH) was lowest close to the ice edge (0.07 µg:µg), but ranged between 0.09 and 0.2 across all other water masses (except in the STZ; Figure S4.3b).

Other phytoplankton groups showed only minor contributions to total chl-a (<20%) and few general north-south trends. Cyanobacteria and chlorophytes correlated with a second principal component (Figure S4.2b), but neither was correlated to macro- or micronutrient concentrations (not shown). Cyanobacteria, for example, dominated the phytoplankton community with a contribution of ca 36% in the STZ at 36 °S, but contributed <2% southwards (Figure 4.3d). All other groups correlated best with the third principal component (Table 4.2) and their occurrence did not show trends across the water masses. For instance, sudden peaks in contribution to total chl-a by dinoflagellates (19%) and cryptophytes (17%) were observed at 55.3 °S and 52.8 °S, respectively, while prasinophytes showed a prominent peak close to the Antarctic ice at 70 °S (Figure 4.3d). Interestingly, a correlation between pelagophyte chl-a concentration and Fe was found as well as a weak correlation with Co (Table 4.3).

Several sample sites were revisited on different legs of the SANAE54 expedition, allowing for an evaluation of seasonal progression. The community structure at 44 °S for example, was very similar between December and January (Figure 4.3d). At 49 °S, the December community contained important contributions of picophytoplankton, such as flagellate eukaryotes and cyanobacteria, not seen in February at this station. Three samples were furthermore taken in close proximity of 70°S in December and January. One sample was collected at 70 °S on 16 December, one at 69.7 °S on 20 January, and a third at 70.1 °S on 23 January. The December community showed a chl-a concentration of 0.26 μgL^{-1} in the range of the two January communities (0.38 and 0.11 μgL^{-1}). Diatoms dominated all three communities with around 63-64% contribution to total chl-a, while contributions of coccolithophores (16%) and *Phaeocystis*-L (20%) were higher in December compared to the January communities.

4.6 Discussion

This multi-parameter approach promotes understanding the dynamics of phytoplankton community composition in the Atlantic Southern Ocean. In the absence of single, predominant nutrients driving the community composition across all water masses in our study, variable and potentially interacting nutrient drivers will first be addressed here for each of the major oceanic zones individually. Potential impact of other driving factors, such as changes in temperature and light regimes will also be discussed.

4.6.1 STZ

The STZ was characterized by low chl-a concentrations, especially at the northern most station ca. 36 °S. Here the community was dominated by diatoms and cyanobacteria with both contributing equal proportions. At 39 °S the contribution of cyanobacteria to total chl-a dropped to less than 2% at 39 °S. However, diatoms did not dominate, but a rather diverse community was found, with important contributions by prasinophytes and dinoflagellates. Low diatom contribution to the community was accompanied by low BSi concentration, but relatively high BSi:diatom chl-a ratios, indicative of smaller cells. Higher contribution of smaller phytoplankton groups in the STZ might be a result of the warmer waters (Schlüter et al. 2011; Mendes et al. 2015; van Leeuwe et al. 2015) and/or due to the particularly low nitrate and phosphate concentrations (Hudson and Morel 1990; van Leeuwe et al. 2015). Additionally, low silicic acid concentrations may have been driving lower diatom contribution allowing higher contribution of other phytoplankton groups. Our community structure data only encompassed early December conditions at 36 °S, but based on the observed increased SST and low nutrient concentrations and ratios, similar community shifts could also be assumed for February. Important contribution of cyanobacteria in February, for example, is supported by trace metal data. For example, at 36 °S, Co concentrations are heavily depleted in the surface displaying a strong positive correlation between Co and phosphate in the upper 1000m, indicative of typical nutrient-like behaviour of Co (Loock et al. submitted). The strong Co uptake is accompanied by a depletion in Cu, Ni, Cd and Fe, but weak surface depletion of other bioactive trace elements (Zn, Mn). Cyanobacteria, abundant at this particular STZ station, demonstrate an absolute requirement for Co (Saito and Moffett 2002). Their dominance may therefore explain the observed unusual strong depletion in cobalt at station 36 °S.

4.6.2 SAZ

The SAZ community, determined in February, was characterized by a low chl-a concentration, similar to the STZ, and dominated by *Phaeocystis* (63.4 %) with a noticeable diatom contribution. *Phaeocystis*-dominated waters in February have been reported in the SAZ by Gibberd et al. (2013); albeit at much higher total chl-a concentrations (ca. 0.45 μgL^{-1}) and ca. 2.5 fold higher nitrate and phosphate concentrations. This suggests that lower chl-a concentrations reported herein may be linked to a more depleted February nitrate and phosphate pool. Substantial nitrate removal (-81%) accompanied by an increase in Si/N ratio was evident from December to February. Despite this increase, the Si/N ratios <1 are likely to inhibit diatom growth (Brzezinski 1985) lessening diatom competition for other nutrients and allowing other groups such as *Phaeocystis* to dominate the community structure.

4.6.3 PFZ

The majority of communities encountered in the PFZ are comprised predominantly of diatoms and *Phaeocystis*. High nitrate concentrations (30 µM), noticeably higher than global averages (19 µM) reported for this region (Garcia et al. 2013), and high N/P molar ratios (35:1) were observed in December in the PFZ. It is unlikely that the high nitrate concentrations were driven by spring ice melt and northward transport of nutrient-rich meltwaters, as one would expect to see equally elevated phosphate and silicate concentrations. Klausmeier et al. (2004) have shown that under exponential growth (i.e. growth during the bloom season) N/P molar ratios exceeding 35:1 are a result of either limiting irradiance, nitrate, phosphate or a combination. On the same cruise, Viljoen et al. (2018; Chapter-3) established that within the deep MLD's, which characterize the PFZ, the residing community was predominantly affected by light limitation with iron as co-limiting factor. The under-utilization of nitrate in the PFZ was therefore possibly caused by light and iron co-limitation, along with limiting silicic acid concentrations. The nitrate was, however, largely removed between December and February (-68%), possibly as a result of shifts in the community structure. For example, at 44 °S, the December community was diatom dominated, but shifted to a *Phaeocystis* dominance in February.

Trace nutrient data are available in the PFZ at 46°S. The community at 46 °S was diatom-dominated with large contributions from *Phaeocystis* and coccolithophores. While *Phaeocystis* already was a major contributor to total chl-a across the STZ and SAZ, coccolithophores contribution was negligible. Coccolithophores can occur within a range of 2–15.7 °C (Findlay and

Giraudeau 2000) and the decrease of water temperatures south of the STF to below 15 °C might therefore have been favourable for coccolithophore growth in the PFZ. BSi concentrations were higher than at 36 °S and the N/P ratios (~14:1) at this station correspond with diatom-dominated waters (Smith and Asper 2001). The Si/N (0.3:1) and Si/P (3:1) ratios, in contrast, suggest diatom productivity was still limited by silicic acid. Copper and Zn showed typical nutrient-like behaviour and bio-utilization (Cloete et al. under revision). Surface zinc concentrations decreased drastically from the STZ to the PFZ, showing strongest depth profile correlation with silicic acid (compared to correlations with nitrate and phosphate). This points to simultaneous uptake of Zn and silicic acid, thus a community dependant on silicic acid and Zn, such as diatoms. Copper also showed strongest depth profile correlation with silicic acid (Cloete et al. under revision). Cadmium, in contrast, showed typical nutrient behaviour, but strongest correlation with nitrate and phosphate, possibly indicating preferential uptake by groups other than diatoms, e.g. *Phaeocystis* and coccolithophores. Manganese and Co, in contrast, did not indicate surface depletion. This is surprising as coccolithophores have a requirement for Co, although it can be replaced by Zn (Xu et al. 2007). Surface Fe at 46 °S was the highest encountered at all stations, but was not accompanied by high chl-a concentration. This dissolved Fe pool might not be fully accessible for biological uptake and might be limiting. For example, pigment composition indicated dominance of the *Phaeocystis* form acclimated to low-iron availability (*Phaeocystis*-L) across the STZ and SAZ and PFZ. As mentioned above, alternatively, Viljoen et al. (2018) have shown that at this particular station macro- and micronutrient under-utilization is possibly related to light limitation.

At 49 °S (December) and 50 °S (January), the communities were *Phaeocystis*-dominated, with large contributions of diatoms, and smaller contributions from other picoplankton. Macronutrient concentrations and ratios differed greatly between the two sites. At both stations nitrate appeared to be largely under-utilized while low, possibly limiting, silicic acid concentrations prevailed. The deepest MLD on the transect (102m) was observed at 50 °S, which might explain *Phaeocystis* dominance at this station (Arrigo 1999). *Phaeocystis* have been shown to be more abundant in deeply mixed waters due to their photosynthetic properties that allow for efficient light usage under varying light conditions (Alderkamp et al. 2012a) and their ability to form colonies that are more resistant to turbulent water (Schoemann et al. 2005; Rousseau et al. 2007). The station at 49 °S was revisited in February, revealing a shift to a diatom-dominated community. February N/P molar ratios (~14:1) agree with a shift to more diatom-dominated waters (Smith and Asper 2001). An

increase in SST from December and February (5.8 to 6.5 °C) may potentially alleviate water column stability, resulting in a more stratified water column and shallower MLD favouring diatom growth (Arrigo 1999). Silicic acid concentrations increased slightly and phosphate concentrations have remained similar from December to February, while nitrate has seen large removal to near-limiting concentrations, suggestive of a late summer community removing nitrate at a much more rapid rate than other macronutrients. Low chl-a concentrations, coupled with rapid, preferential, nitrate removal suggest that there might be another factor, such as heterotrophic bacterial uptake (Kirchman and Wheeler 1998) responsible for the large nitrate removal with seasonal progression. Alternatively, near-limiting concentrations of essential trace metals such as Fe could also result in the low chl-a encountered at 50 °S. This stations is one of the two stations where surface depletion and nutrient-type depth profiles were found for Mn and Co (Loock et al. submitted). Cobalt was more strongly correlated with phosphate and nitrate than silicic acid which may suggest that the majority of Co is not taken up by diatoms but other groups such as *Phaeocystis* (Sunda and Huntsman 1995a).

4.6.4 AAZ

Waters in the AAZ, between the Polar Front and the Southern Boundary of the ACC, are characterized by a relatively diverse community structure which was dominated by diatoms with notable coccolithophore, haptophyte, pelagophyte and prasinophyte contributions. Nitrate concentrations were still high in December and silicic acid concentrations increased drastically southward across the AAZ. In late summer (February), nitrate concentrations were considerably lower than in December while phosphate and silicic acid concentrations remained rather unchanged. A relatively deep MLD (100m) was encountered at station 53.6 °S, accompanied by relatively high surface concentration of all trace metals (compared to other stations along the transect). Elevated trace metal concentrations have been previously reported in the region around 54 °S and may be attributed to the Bouvet Triple Junction (52-56 °S) hydrothermal plume activity (Klunder et al. 2011b). The abundance of trace metals may have induced the higher biomass and diversification as well as led to enhanced and preferential uptake of nitrate. Degradation pigments were detected at 53.6 °S that were absent north of the PF, which point to a possibly mature community. Therefore, it is thought that a trace metal influx prior to our trace metal sampling may have caused an early stage local bloom and that our occupation of this station reflects waning bloom conditions. The lower phytoplankton productivity observed in December and February in

the same area also support the concept of a short lived phytoplankton bloom within January caused by a periodic trace metal influx.

Loock et al. (submitted) and Cloete et al. (under revision) showed that Co, Cd and Zn were more strongly utilized in the surface than Cu and Ni, most likely because phytoplankton have a smaller requirement for Cu and Ni compared to Fe and Zn, for example (Twining and Baines 2013). Copper might have been utilized by *Thalassiosira*, which have been shown to have a greater Cu requirement under Fe limitation (Peers and Price 2006), but the absence or low contribution of typical Cu utilising groups, such as cyanobacteria, chlorophytes and prasinophytes may be driving under-utilization of Cu. Nickel may also be more important for cyanobacteria and picoeukaryotes than other algal groups in the community (Dupont et al. 2010). Iron limitation may further decrease the Ni requirement of diatoms by halting urease activity in order to prevent further iron stress (Dupont et al. 2010).

4.6.5 WG

The WG is the largest subpolar cyclone and best defined in the Southern Ocean as being a pertinent source of Antarctic Bottom Water (Deacon 1963). The community structure in the WG was characterized by the highest chl-a concentration in the study area, albeit lower community diversity. High silicic acid concentrations as well as a shoaling of the MLD, are environmental factors which favour diatom productivity at the expense of the community (Sedwick et al. 2007). Pigment data further suggests diatom-dominance throughout the season, which is strongly supported by average Si/N and N/P ratios in this region (Arrigo 1999; Smith and Asper 2001). High BSi concentration and high BSi to diatom chl-a ratio at 65 °S further suggest that we encountered diatom bloom conditions at least at some stations. Nevertheless, coccolithophores and *Phaeocystis* also largely contribute to total chl-a. Temperatures in the WG fall on the low end of the temperature range reported for coccolithophores (Findlay and Giraudeau 2000). Gibberd et al. (2013), showed negligible coccolithophore contribution in the WG region in 2008/2009, under similar macronutrient but lower SST conditions. We speculate here that the higher SST observed in 2014/2015 may have led to coccolithophore growth in the WG. Throughout most of the WG, *Phaeocystis* was dominant in its state acclimated to high iron conditions (*Phaeocystis*-H), even though the Fe concentrations were low, possibly limiting. This may be a result of acclimation to earlier high Fe surface concentrations released from ice melt approximately a week prior to our

sampling (Viljoen et al. 2018). Highest phaeopigment:chl-a ratios were recorded in the WG indicative of post-bloom communities at the time of sampling at some stations.

At 60 °S and 65 °S, for example, a low salinity feature and a temperature inversion is observed at these stations, accompanied by a shoaling of the MLD (50m), most likely a result of low density waters from ice melt producing stratified waters in this region (Wright et al. 2010). The shoaling of the MLD may possibly create a stratified water column which may drive diatom dominance in this region. Water column stratification caused by melt waters could have acted as a hydrographic barrier and may have limited vertical resupply of nutrients. Depth profiles at station 60 °S and 65 °S both showed large surface depletion of bio-utilized trace metals (excluding Ni and Cu) and of macronutrients in the water column. Iron, for example, showed near-limiting concentrations (Moore et al. 2013) and was possibly a key factor controlling the low chl-a concentration. Viljoen et al. (2018) have shown through incubation experiments that iron is limiting at 65 °S. In addition, co-limitation with other trace metals may have played a role. For example, the strong Mn depletion may be related to the importance of Mn in iron deficient waters as Fe-deficient conditions increase the Mn demand (Peers and Price 2004). Loock et al., (submitted) furthermore highlighted large Co surface depletion and have attributed this to bloom conditions depleting a range of micronutrients, thereby creating a selection pressure which may promote Co substitution through removal of primary enzymatic nutrients.

Conditions south of 68 °S, close to the ice edge, changed drastically and with it the community. For example, at station 68 °S the highest biomass, and some of the highest surface trace metal concentrations were encountered, with the highest coccolithophore contribution (34%) to any community structure in the study area. The large coccolithophore biomass and greater contribution to the community structure may be linked with trace metal concentrations and ratios, particularly Fe, Co and Cd. *Emiliania huxleyi*, for example, have been shown to have a lower cellular requirement for Fe than diatoms (Brand 1991; Sunda and Huntsman 1995b; Muggli and Harrison 1996). Furthermore, various studies have hypothesized that its low Fe requirement allows it to grow in regions where diatoms are limited by Fe (Brand 1991; Muggli and Harrison 1997). Ho et al. (2003) have further shown coccolithophores to have a higher quota for Co and Cd than diatoms. Therefore, large coccolithophore contribution in the waters may be related to iron approaching

limiting concentrations, inhibiting further diatom growth as well as an abundance of essential metals, particularly Co and Cd, essential in coccolithophore metabolic functions.

The presence of the high iron acclimated-form of *Phaeocystis* indicates that there was possibly high availability of Fe prior to the sampling as it has been documented that they take at least two days to fully acclimate to high iron conditions by adjusting their photosynthetic pigments (Sedwick et al. 2007; Viljoen et al. 2018). Therefore, we assume a recent ice melt accompanied by augmented trace metal supply in which Fe is preferentially utilized to near limiting concentrations. Elevated trace metal surface concentrations in this region are partly attributed to ice melt and subsequent input of associated trace metals into the surface waters (Grotti et al. 2001). Extensive iron utilization was coupled with limited bio-utilization of other metals probably due to highest phytoplankton requirements for Fe (Twining and Baines 2013).

4.7 Conclusion

In this study, as in previous studies within the Atlantic Southern Ocean, we have seen a variety of physical (temperature, salinity, mixed-layer depth and the resulting water column structure) and chemical (macronutrients) properties shape and influence phytoplankton abundance and community structure. It is well established that certain factors like macronutrients and temperature, that differs regionally, affect which phytoplankton is present and in what quantities. However, often phytoplankton occurrence and the community structure differences are not always fully explained by these properties or by just a single parameter. Here in lies the advantage of a multiple parameter in-situ observational approach such as this study to address phytoplankton community variability both spatially and temporally, combining an array of biogeochemical variables encountered in various oceanic regions.

Micronutrients (essential trace metals) is one of the driving factors that can be used to account for those differences that are not always fully explained by physical properties and/or macronutrients alone. Zn and Mn were most strongly correlated with silicic acid south of the PF, indicative of a diatom-dominated community that are dependent on both silicic acid and these metals. The importance of considering the influence of a suite of trace metals has also been shown in this study when localised blooms could not be explained by the other parameters or iron alone. Our findings indicate that an influx and/or abundance of a suite of trace metals linked to hydrothermal plume activity and ice melt, is closely related to increasing biomass and community diversification.

Although, in some instances, it is unclear whether trace metal distributions drive the community composition or vice versa. Iron did affect whole community productivity and structure the most and because of that when iron is preferentially depleted to near-limiting concentrations it may have driven under-utilization of certain metals. Iron limitation showed to further decrease the Ni requirement of diatoms by halting urease activity in order to prevent further iron stress (Dupont et al. 2010).

The importance of time was also evident in this study such as the timing of the hydrothermal and ice-melt trace metal fluxes that proved to be a pivotal factor in the assessment of blooms and their age. Therefore, we recommend caution for future studies that involves these essential micronutrients and to incorporate the consideration of the timing of phytoplankton sampling relative to the time of an event like the release of trace metals from hydrothermal vents or melting ice.

4.8 Acknowledgements

The work leading to these results received funding from the National Research Foundation (NRF), under the SA/Norway Collaboration Programme and the South African National Antarctic Programme, grant numbers 91313 and 110731 awarded to S. Fietz. J.J. Viljoen acknowledges funding from NRF through a Masters Innovation Scholarship. I. Weir acknowledges the financial assistance of the NRF through the South African National Antarctic Programme grant number 110731. The authors furthermore thank the crew of the R/V SA Agulhas II, Department of Environmental Affairs (DEA), and all the scientific cruise participants of SANAE 54.

4.9 References

For the purpose of this thesis the references for this manuscript and the others, including references for supplemental information, are combined in the main reference list (on page 76) to avoid duplication.

4.10 Tables

Table 4.1. A) Trace metal concentrations (in nM) determined at six stations across the Atlantic sector of the Southern Ocean measured during the third (January) and fourth (February) legs of voyage SANAE54 (see Figure 4.1 for cruise map). B) Assessment of nutrient-type behaviour considering depth profile. Nutrient-type behaviour is assumed herein if correlation between depths profiles for metal and nitrate and phosphate were significantly and positively correlated.

A)

			concentrations at surface (µM)						
Date	**Latitude (N)**	**Longitude (E)**	**Cd**	**Cu**	**Fe**	**Zn**	**Ni**	**Mn**	**Co**
5/2/2015	-36.00	13.35	0.01	0.50	0.17	9.37	2.37	0.96	0.008
12/1/2015	-46.03	8.00	0.25	1.00	0.38	1.46	5.07	0.24	0.033
14/1/2015	-50.71	2.03	0.25	0.94	0.23	1.27	4.98	0.13	0.020
15/1/2015	-54.22	0.00	0.34	1.45	0.25	1.55	5.42	0.21	0.024
16/1/2015	-60.25	0.01	0.22	1.49	0.14	1.33	5.98	0.03	0.014
18/1/2015	-65.04	0.12	0.12	1.29	0.22	1.02	4.65	0.04	0.009
19/1/2015	-67.98	0.05	0.69	1.83	0.11	4.56	6.02	0.26	0.030

B)

			depth profile significantly, positively correlated to N and P (i.e. nutrient-type)						
Date	**Latitude (N)**	**Longitude (E)**	**Cd**	**Cu**	**Fe**	**Zn**	**Ni**	**Mn**	**Co**
5/2/2015	-36.00	13.35	y	y	y	no	y	no	y
12/1/2015	-46.03	8.00	y	y	y	y	y	no	no
14/1/2015	-50.71	2.03	y	y	y	y	y	y	y
15/1/2015	-54.22	0.00	y	y	no	y	y	no	no
16/1/2015	-60.25	0.01	y	y	no	y	y	y	no
18/1/2015	-65.04	0.12	y	y	y	y	y	no	no
19/1/2015	-67.98	0.05	y	y	y	y	y	no	no

Table 4.2. Rotated component matrices derived from Principal Component Analysis for (A) trace metal concentrations. B) phytoplankton group chl-a concentrations. Highlighted correlation coefficients indicate significant correlation at 95% confidence interval.

A)	Components		
	1	2	3
% of variance	40.8	34.9	22.2
Cd	-0.17	**0.94**	-0.27
Cu	-0.58	0.62	-0.48
Fe	-0.13	-0.03	**0.98**
Zn	**0.95**	-0.08	-0.28
Ni	-0.77	0.60	-0.14
Mn	**0.98**	-0.17	-0.01
Co	-0.14	**0.89**	0.44

B)	Component			
	1	2	3	4
% of variance	26.1	19.5	18.8	13.0
Cyano.	-0.12	**0.96**	-0.01	0.04
Prasino.	-0.27	-0.10	**0.74**	-0.02
Dinoflag.	0.32	-0.06	**0.66**	-0.21
Crypto.	-0.33	-0.15	-0.03	-0.77
Phaeocy-H	**0.84**	-0.09	0.44	-0.01
Phaeocy-L	-0.50	-0.17	0.04	**0.71**
Cocco.	**0.74**	-0.09	-0.18	0.17
Pelago.	-0.04	-0.04	**0.80**	0.36
Chloro.	-0.14	**0.95**	-0.16	-0.01
Diatoms	**0.89**	-0.21	-0.11	-0.10

Table 4.3. Kendall-Tau correlation between selected phytoplankton group chl-a concentrations and A) macronutrients, where sample size was n=24 and B) dissolved trace nutrients, where sample size was n=6. Only phytoplankton groups with at least one significant correlation are included in this table. Highlighted correlation coefficients indicate significant correlation at least at 90% confidence interval. * indicates significant correlation at 95% confidence interval and ** at 99%.

A)		total chla	Diatoms	Phaeoc.	Cocco.	Pelago.
N	Correlation Coefficient	**0.28**	0.22	0.16	0.12	0.23
	Sig. (2-tailed)	**0.05**	0.14	0.28	0.41	0.12
P	Correlation Coefficient	**0.28**	**0.29***	0.07	0.20	0.02
	Sig. (2-tailed)	**0.06**	**0.04**	0.64	0.17	0.92
Si	Correlation Coefficient	**0.44****	**0.54****	-0.12	**0.46****	-0.22
	Sig. (2-tailed)	**0.00**	**0.00**	0.43	**0.00**	0.14

B)		total chla	Diatoms	Phaeoc.	Cocco.	Pelago.
Cu	Correlation Coefficient	**0.60**	**0.60**	0.47	0.33	-0.33
	Sig. (2-tailed)	**0.09**	**0.09**	0.19	0.35	0.35
Ni	Correlation Coefficient	0.33	0.33	0.20	0.33	-0.07
	Sig. (2-tailed)	0.35	0.35	0.57	0.35	0.85
Zn	Correlation Coefficient	**0.60**	0.33	0.47	0.33	0.20
	Sig. (2-tailed)	**0.09**	0.35	0.19	0.35	0.57
Mn	Correlation Coefficient	0.47	0.20	**0.60**	0.47	0.33
	Sig. (2-tailed)	0.19	0.57	**0.09**	0.19	0.35
Cd	Correlation Coefficient	0.47	0.20	**0.60**	0.20	0.33
	Sig. (2-tailed)	0.19	0.57	**0.09**	0.57	0.35
Co	Correlation Coefficient	0.20	-0.07	0.33	0.20	**0.60**
	Sig. (2-tailed)	0.57	0.85	0.35	0.57	**0.09**
Fe	Correlation Coefficient	-0.20	-0.47	-0.07	-0.20	**0.73***
	Sig. (2-tailed)	0.57	0.19	0.85	0.57	**0.04**

Table 4.4. Biogenic silica (BSi) and ratio of BSi versus diatom-chl-a concentration determined at eight stations across the Atlantic sector of the Southern Ocean (see Figure 4.1 for cruise map).

Date	Latitude (N)	Longitude (E)	BSi (µM)	BSi/ (diatom chla) (µmol:µg)
5/2/2015	-36.00	13.35	0.35	32
12/1/2015	-46.03	8.00	1.20	13
14/1/2015	-50.71	2.03	4.61	171
15/1/2015	-54.22	0.00	3.72	22
16/1/2015	-60.25	0.01	3.59	33
18/1/2015	-65.04	0.12	13.8	69
19/1/2015	-67.98	0.05	0.38	1.2
20/1/2015	-69.79	-1.94	0.69	2.2
23/1/2015	-70.09	-1.59	0.17	2.4

4.11 Figures

Figure 4.1. Map Station positions along the Good Hope line for the SANAE54 cruise. The background shows the ocean floor bathymetry from Ocean Data View (Schlitzer 2015). The solid black line represents the Good Hope line. The dashed horizontal lines indicate the frontal positions (STF - subtropical front, SAF - Subantarctic Front, PF - Polar Front and Sbdy - Southern ACC boundary) along the Good Hope line. The red diamond symbols indicate the trace metal station locations (Table 4.1).

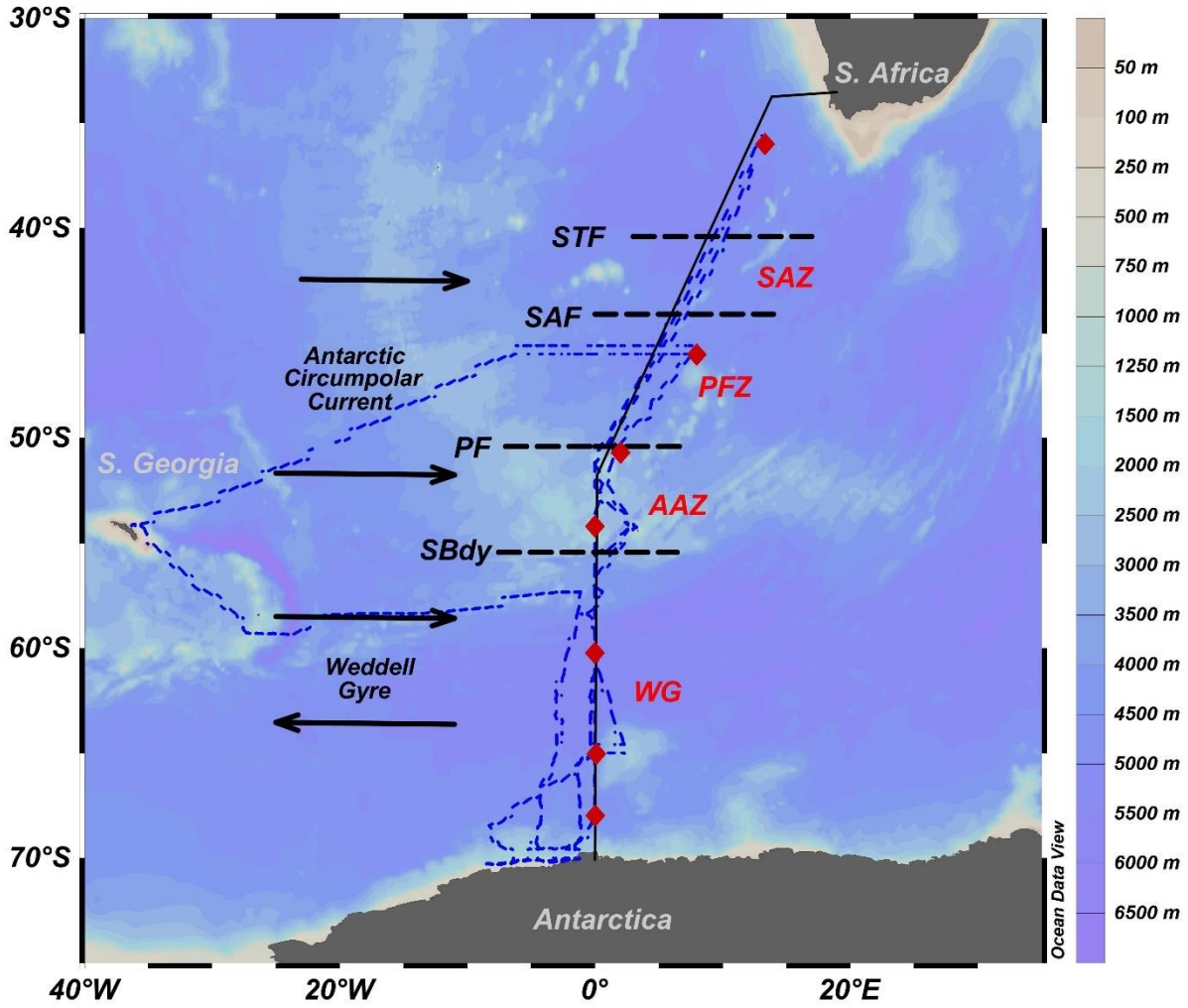

Figure 4.2. Surface (ca. 5-6m) temperature (a) and salinity (b) along the Good Hope Line during the first (05/12/2014 – 16/12/2014; "December"), third (29/12/2014 – 6/1/2015; "January") and fourth (7/2/2015 – 15/2/2015; "February") legs of voyage SANAE54 on board R/V SA Agulhas II.

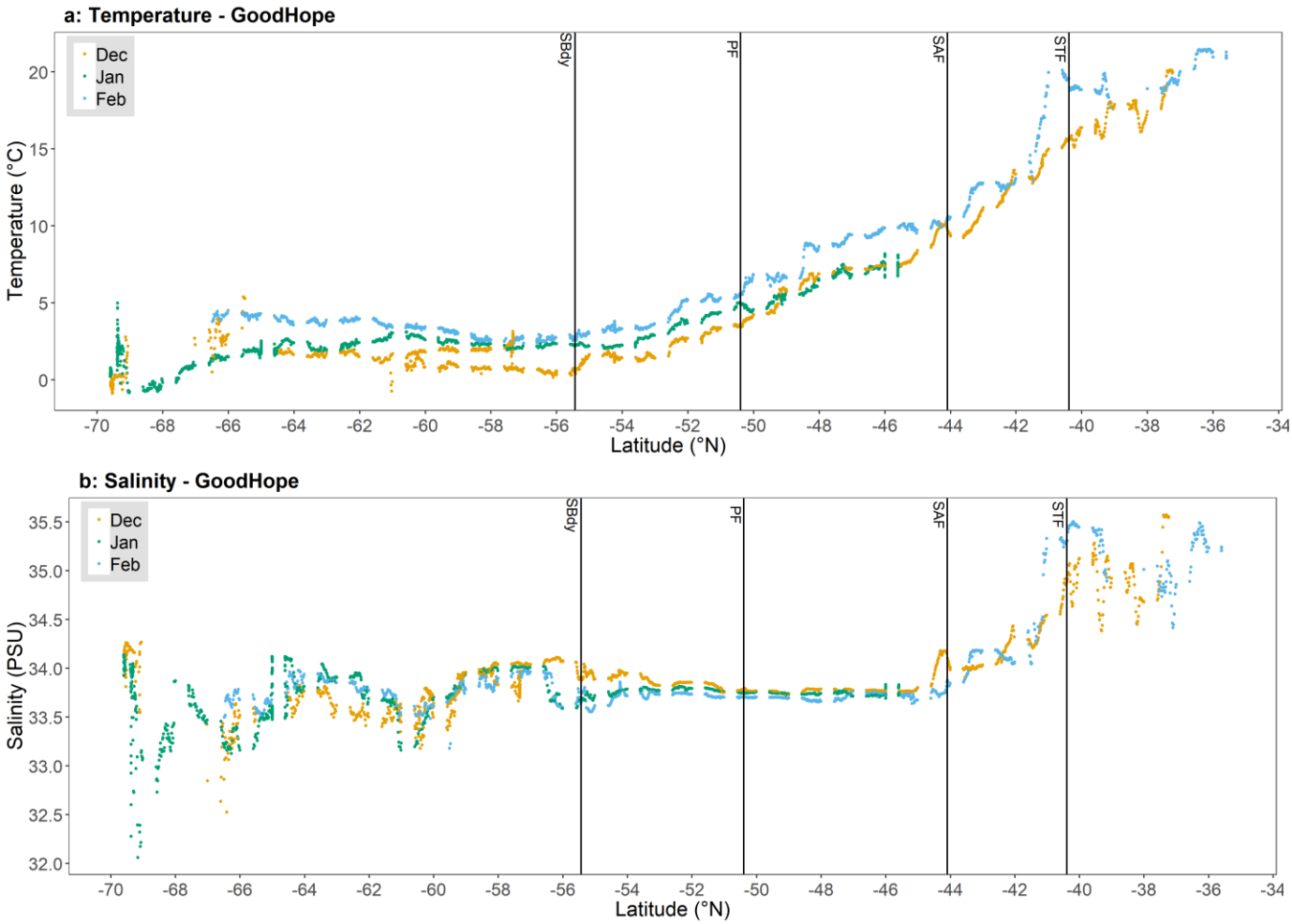

Figure 4.3. Macronutrient concentrations and phytoplankton community structure along Good Hope Line of the SANAE54 cruise (see Figure 4.1 for cruise map).

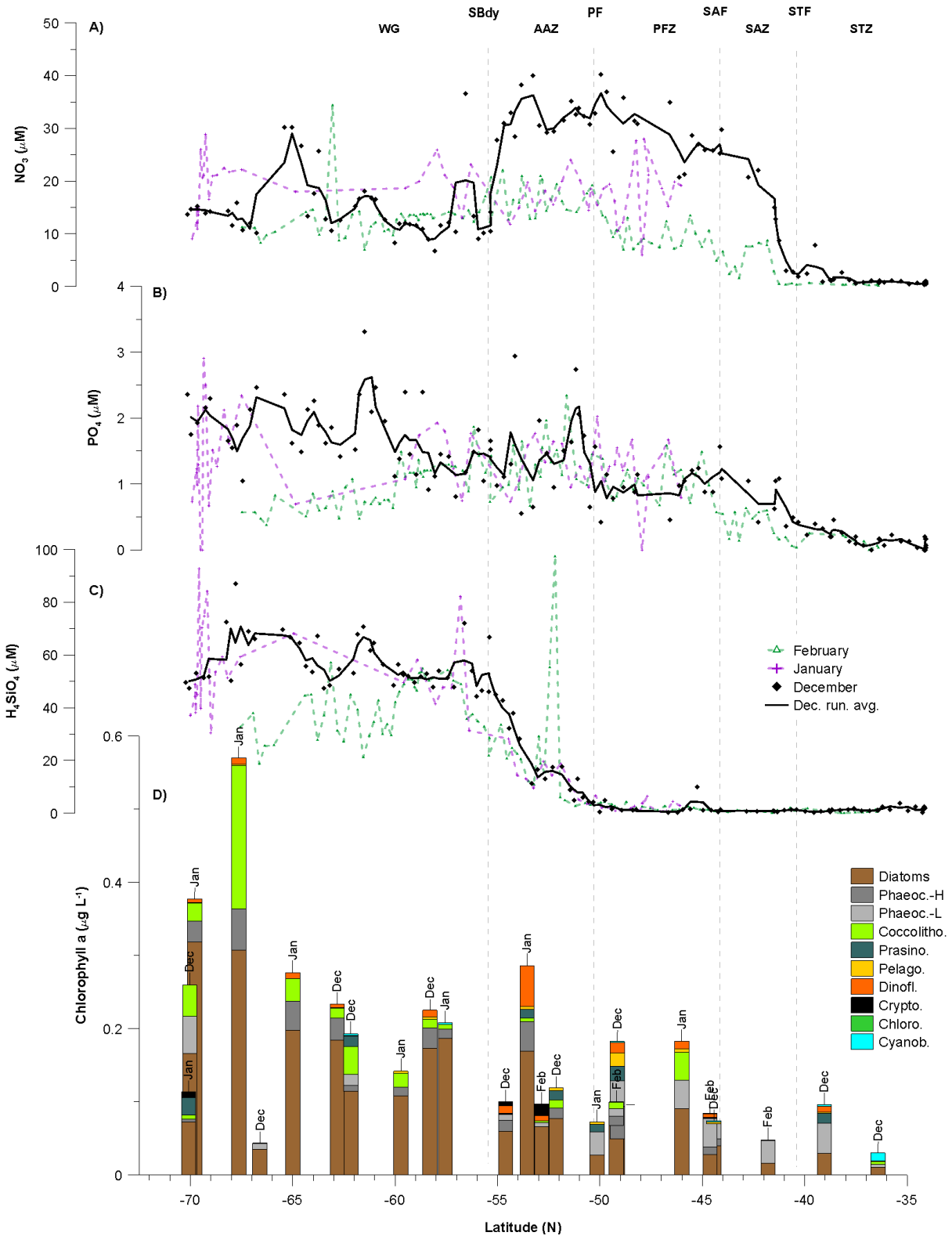

Figure 4.4. Surface dissolved trace metal distribution for seven stations along the cruise transect (Figure 4.1). A) Cu (*10) and Ni; note that nitrate concentrations are shown in panel A to illustrate the similar trends of some trace metals. B) Fe, Co (*10) and Cd. C) Zn and Mn (*10)

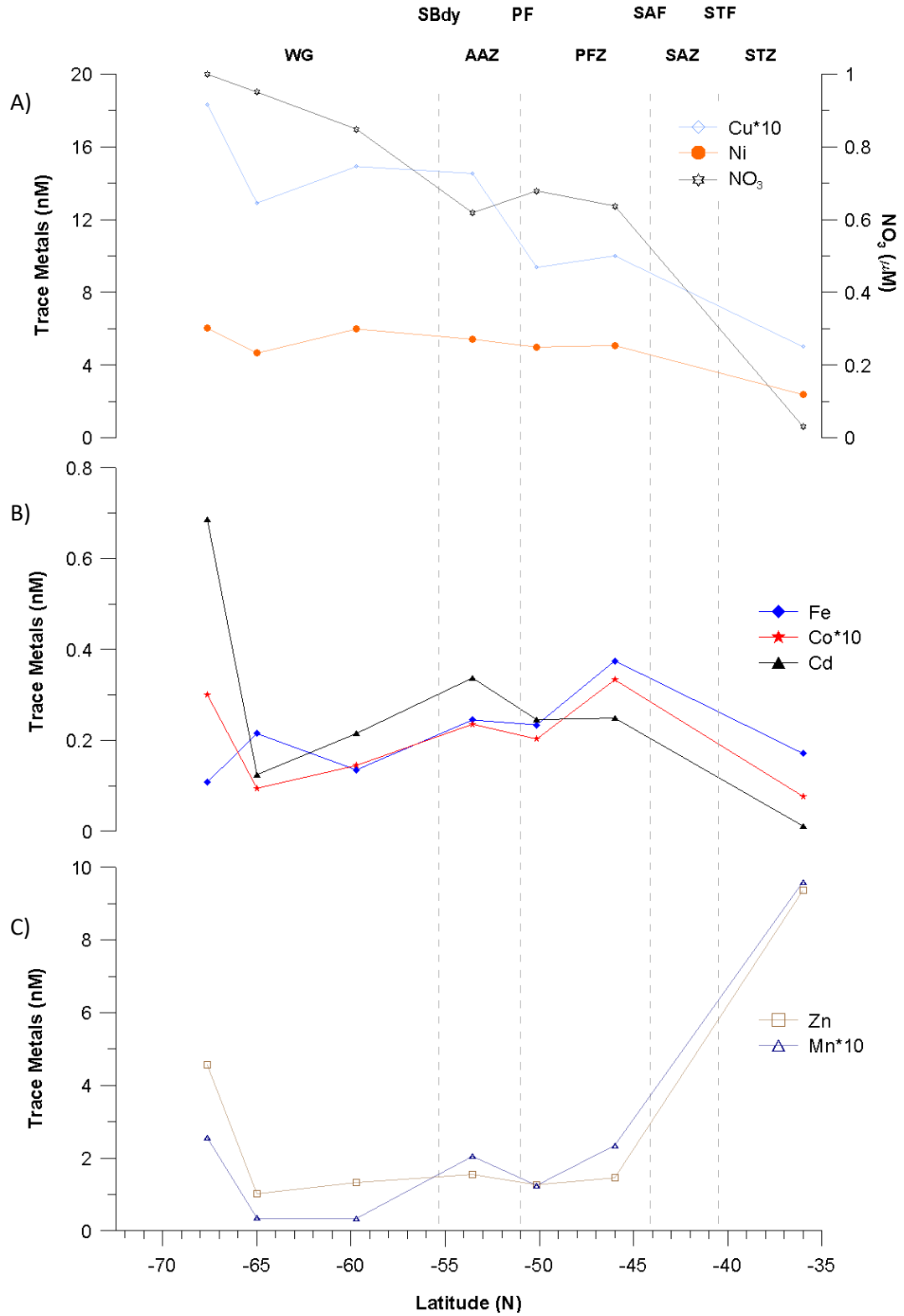

5 Chapter-5: S54 Surface versus Depth Manuscript 3

5.1 Title and Authors:

Manuscript in preparation intended for publication in Polar Biology

How representative are surface and chla-max communities: can we use only one or do we need both to understand phytoplankton dynamics in the Southern Ocean?

Johannes J. Viljoen and Susanne Fietz

Centre for Trace Metal and Experimental Biogeochemistry, Department of Earth Sciences, University of Stellenbosch, 7600 Stellenbosch, South Africa

5.2 Introduction

The distinct properties of the various oceanic regions largely determine the phytoplankton community structure, which in turn affects the food webs and general ocean ecosystem functioning (Schlüter et al. 2011; Gibberd et al. 2013; Mendes et al. 2015). The properties of different water masses has been projected to change in the future (Deppeler and Davidson 2017) and changes in the phytoplankton structure can therefore be expected to occur in the future. These possible changes to specific controlling factors of phytoplankton dynamics, which can have large consequences (Sedwick et al. 2007; Alderkamp et al. 2010), needs to be investigated on large scale studies as well as small scale, like region- and/or group-specific incubation experiments (DiTullio et al. 2007; Viljoen et al. 2018).

Very often studies on the response to selected potentially limiting factors are conducted on bulk communities collected from one water depth due to logistical sampling constraints (Moore et al. 2007; Feng et al. 2010; Viljoen et al. 2018). It is then assumed that the communities from the selected depth are representative of the upper water column, e.g. the mixed-layer (ML). It has to be noted though, that in addition to the latitudinal changes between water masses, variations in the vertical structure of the water column results in depth gradients of irradiance, nutrients as well as temperature which has been shown to play a role in the acclimation of phytoplankton cells (Cheah et al. 2013). This may lead to variability in phytoplankton community and photo-acclimation with depth (Alderkamp et al. 2011). In the Indian Ocean the phytoplankton community structure changes at surface between water masses and also with depth. This was mainly attributed to changes in temperature, nutrients and the depth of the ML, e.g. in the Subtropical regions where stratification increases the contribution of picophytoplankton at the surface due to the physical

barrier preventing the introduction of nutrients into the surface euphotic layers, limiting the growth of nano- and microphytoplankton (Schlüter et al. 2011; Mendes et al. 2015).

We postulate here that over and above the community structure, the photophysiology also changes with depth even within the ML. Therefore, it might not be suitable to only sample one depth within a region as resident phytoplankton may have different acclimations at different depths. In this study we will therefore focus on vertical changes in the phytoplankton community structure and their acclimation status in the Polar Frontal (PFZ) and Antarctic (AAZ and WG) waters of the Atlantic Southern Ocean.

The study done on the surface phytoplankton community of the SANAE 54 (S54) cruise transect (Viljoen et al. in preparation; Chapter-4), gave us great insight into the controls of phytoplankton community structure and dynamics of the surface and their links to macronutrient and trace metal distribution. The study done on the incubation experiments conducted on S54 (Viljoen et al. 2018; Chapter-3), gave us a better idea of the direct effect of increased availability of iron under low in situ and high light can have on algal productivity and specifically the variation in community composition. For each incubation station (S54-46 and S54-65; Figure 5.1), a corresponding surface phytoplankton community was sampled at ca. 5-6m depth. Water for the S54 incubation experiments at 46 °S (S54-46) and 65 °S (S54-65) was collected from the respective apparent depth of fluorescence maximum (fl-max), at ca. 78m and 40m respectively (Table 5.1; Viljoen et al. 2018). Therefore, the surface community composition can be compared to that of the initial community of the incubation experiments, which will allow for observations of phytoplankton community structure and acclimation change with depth. This will further be discussed in how these changes with depth differs within two stations which have considerable different water column characteristics and ML depth. Hence for this study, we discuss the change in phytoplankton community structure with depth within the two regions and how they change their pigment photoprotective acclimation strategies.

5.3 Methodology

5.3.1 Cruise Track and Sampling

The data that are used for this study was collected during the 54th South African National Antarctic Expedition (SANAE) from December 2014 to February 2015 (from here on referred to as S54). The cruise track mainly followed the Good Hope monitoring line from Cape Town, South Africa,

into the Atlantic Southern Ocean (Figure 3.1) crossing the Subtropical Front (40.4 °S), Subantarctic Front (44.1 °S), Polar Front (50.4 °S) and the Southern Boundary (SBdy) of the Antarctic Circumpolar Current (ACC) to the Antarctic ice shelf (Viljoen et al. 2018).

Two sampling stations, one at 46 °S (S54-46) located in the Polar Frontal Zone and the other at 65 °S (S54-65) located in the Antarctic Zone are discussed here. The following depths have been sampled for the surface and apparent fluorescence maximum (fl-max): 5m and 78m at 46 °S and 5m and 40m at 65 °S (Table 5.1). Detailed sampling methods for pigments, ancillary data and macronutrients are described in Viljoen et al. (2018) and Viljoen et al. (in preparation). Sampling was done from the ship's underway water supply for the surface and from Niskin CTD casts for depth profiles on board the RV SA Agulhas II.

5.3.2 Analysis of phytoplankton community structure, ancillary data and macronutrients

Pigment analyses are described in detail in Viljoen et al. (2018). Briefly, pigments were analysed at Laboratoire d'Océanographie de Villefranche-sur-Mer using HPLC (Ras et al. 2008), and phytoplankton group composition estimated using CHEMTAX software (Mackey et al. 1996). Phytoplankton groups: cyanobacteria, chlorophytes and cryptophytes are not included in this study as their pigment signatures were not detected in the samples discussed here. Further details on the optimisation and choice of pigments for the surface samples can be found in Viljoen et al. (in preparation) and for fl-max samples in Viljoen et al. (2018) and their respective supplementary sections (Appendix A,B). A summary of the specific pigment ratios used in this study, indicative for photoacclimation and degradation, is provided in Table 5.2 and detailed pigment concentration data can be found for the surface and fl-max in Table S5.1. A peculiarity of the Southern Ocean community is the pigment based distinction between *Phaeocystis* cells acclimated to high and low iron availability (Wright et al. 2010). Details of this distinction are provided in Viljoen et al. (2018) based on observations by DiTullio et al. (2007) and Wright et al. (2010). In the following (as in previous chapters of this thesis) *Phaeocystis antarctica* with a pigment composition indicating acclimation to high iron availability is indicated as *Phaeocystis*-H and *Phaeocystis antarctica* with a pigment composition indicating acclimation to low iron availability is indicated as *Phaeocystis*-L. Temperature, salinity, PAR and fluorescence profiles were obtained from sensors mounted on the CTD rosette and can be found in Viljoen et al. (2018) supplementary Figure S3.1 (Appendix A p100) and summarised for the surface and fl-max of each station in Table 5.1. The fluorescence

signal (Figure S3.1) was corrected for quenching and calibrated against bottle measurements of chl-a. The mixed layer depth (Table 5.1) was identified by Viljoen et al. (2018) from the temperature profiles according to de Boyer Montégut et al. (2004). Nutrient concentrations, for the two stations at 46 °S and 65 °S, were determined using a flow injection autoanalyser for NO_3^- + NO_2^- and $Si(OH)_4$ (Wolters 2002; Egan 2008), while PO_4^{3-} concentrations were determined manually according to the methods described by Grasshoff et al. (1983). Further details on nutrient analysis and data can be found in Viljoen et al. (2018) and Viljoen et al. (in preparation).

5.4 Results

5.4.1 Site Characteristics

Table 5.1 summarises the in-situ conditions for both station at the surface and the fl-max. Station S54-46 was located in the PFZ at 46 °S with a deep ML of 89m and sampled in the early afternoon with a PAR of ca. 4400 and 15 µE m^{-2} s^{-1} at the surface and fl-max depth (ca. 78m) respectively (Table 5.1). Temperatures were relatively low at the surface at 7.5 °C that decreased to 6.2 °Cat the fl-max community. The nitrate concentration at the surface were high (22.6 µM) and silicic acid concentration low (3.16 µM) which was similar but slightly increased at the fl-max depth (23 µM and 5.8 µM respectively). The dFe concentrations at 46 °S were 0.38 nM at the surface (Viljoen et al. in preparation) and 0.37 nM at 75m depth (Viljoen et al. 2018; Table 5.1).

Station S54-65 was sampled early morning at 65 °S within the WG (Figure 5.1), with a relatively shallow ML of 31m. At surface a PAR of ca. 200 µE m^{-2} s^{-1} was recorded with values close to zero at the fl-max depth of ca. 40m that time of the day. At 65 °S conditions was characterized by much lower temperatures at surface (1.9 °C) and at 40m depth (0 °C), which results in a water column structure with a pronounced temperature minimum (Viljoen et al. 2018; Figure S3.1). Station S54-65 also had high nitrate and silicic acid concentrations at surface (20.6 and 44.93 µM respectively) and increased towards the chl-max (25.2 and 74.3 µM respectively). The dFe concentrations at 65 °S were 0.22 nM at surface (Viljoen et al. in preparation) and 0.19 nM at the fl-max (Viljoen et al. 2018; Table 5.1).

5.4.2 Chla and degradation (phaeopigments)

At 46 °S chl-a concentrations were relatively low at the surface at 0.18 µg L^{-1} that decreased to 0.12 µg L^{-1} at the fl-max community. Phaeopigments (sum of degradation pigments phaeophytin-a and phaeophorbide-a) were below detection limit at surface and at the fl-max (Table 5.2). In

contrast, conditions at 65 °S showed much higher chl-a concentrations at surface (0.28 µg L^{-1}) that increased 3 fold to the fl-max depth (0.96 µg L^{-1}) and result in a pronounced chl-a maximum (chl-max) within the profile at 40m (Viljoen et al. 2018; Figure S3.1). Phaeopigments (Phaeo) were detected at 65 °S, indicating some degradion, probably grazing, with 2 fold higher Phaeo:Chla ratios in the surface (0.2 µg:µg) than at the pronounced chl-max (0.1 µg:µg). At the surface more than 90% of the phaeopigments consisted of phaeophorbide-a which decreased to 76% at the fl-max (Table 5.2). The phaeophytin-a versus chl-a ratio (Phyt:Chla) increased from surface (0.015 µg:µg) to the fl-max depth (0.024 µg:µg) at ca. 40m.

5.4.3 Phytoplankton community structure

The phytoplankton community at 46°S with a chl-a concentration of 0.18 µg L^{-1} (Figure 5.2a), is dominated by diatoms (50%) in the surface waters along with relatively high contributions, almost equal, of coccolithophores and *Phaeocystis*-L (21%; see methodology for details on *Phaeocystis*-L) and minor contributions from dinoflagellates (5.6%) and pelagophytes (2.6%). The community composition at the fl-max, with a chl-a concentration of 0.12 µg L^{-1}, no longer contains dinoflagellates but does show a contribution of ca. 9 % prasinophytes, a decrease in diatoms and coccolithophores (to 43% and 0.3% respectively), increase of *Phaeocystis*-L (23%) and the addition of *Phaeocystis*-H (22%; see methodology for details on *Phaeocystis*-H) to the community.

In contrast to 46 °S, the surface waters at 65 °S with a chl-a concentration of 0.28 µg L^{-1} (Figure 3.2b), contained a community with increased diatom dominating contribution (72%) decreased coccolithophores (11%) and *Phaeocystis*-L is replaced by *Phaeocystis*-H (14%). However, with the large amount of macronutrients available south of the PF, that now includes silicic acid, we would expect the algal productivity to be much higher, but we only see a change in community composition and not a major increase in total biomass. As previously stated, this can be attributed to the limitations by low micronutrient concentrations, especially iron, as shown with dFe concentrations (Table 5.1). The fl-max community at 65 °S with the pronounced 3-fold chl-a increase (0.96 µg L^{-1}), just below the ML, showed composition changes from surface to fl-max that included a major decrease in diatoms (62%), increase in coccolithophores (21%) and *Phaeocystis*-H (17%) and a decrease in dinoflagellates to where they are no longer part of the community. Pelagophytes and prasinophytes also now contribute minor amounts to the

community. However, diatoms, coccolithophores and *Phaeocystis* all showed major group specific chl-a concentration increases which resulted in the total community chl-a increase.

5.4.4 Acclimation (photoprotective pigments)

At 46 °S the DDT (sum of photoprotective pigments diadinoxanthin and diatoxanthin) concentrations were higher at the surface than at fl-max (Figure 5.3a). This resulted in higher ratios of DDT:Chla (0.079 µg:µg) and DDT versus light-harvesting pigments fucoxanthin and 19'-hexanoyloxyfucoxanthin (DDT:Fuco+Hex; 0.089 µg:µg) compared to the fl-max (0.069 and 0.074 µg:µg respectively). At 65 °S, with the chl-max sampled just below the shallow mixed layer (Table 5.1), the DDT:Chla ratio between the surface (0.08 µg:µg) and the chl-max (0.05 µg:µg) differed much more compared to the more deeply mixed water column at 46 °S (Figure 3.3b). The DDT:FH ratios show an even larger difference between the surface (0.11 µg:µg) and the fl-max (0.05 µg:µg).

5.5 Discussion

The comparison of surface phytoplankton communities with those deeper down the water column at the fl-max gave great insight into the change in phytoplankton composition with depth within two different zones of the Atlantic Southern Ocean. In the sections below we will discuss how the community structure, their acclimation to the light, their drivers and consequences changes vertical between the surface and the fl-max within a deeply mixed PFZ station (S54-46) and shallow mixed WG zone station (S54-65).

5.5.1 Deeply mixed PFZ station S54-46

Productivity, degradation and community structure: At 46°S, within the deeply mixed PFZ waters, diatoms dominate the surface waters along with relatively high contributions of coccolithophores and *Phaeocystis*-L within a community of fairly low chl-a concentrations relative to the rest of the S54 cruise (Viljoen et al. in preparation). The community sampled at 78m depth, still within the well mixed layer of 89m, showed slightly lower productivity which resulted from a decrease in coccolithophores and disappearance of dinoflagellates from the community. Both the fluorescence (Figure S3.1) and nutrient profiles (Figure S3.1) of the S54-46 stations show well mixed conditions within the ML with nutrient concentrations being fairly similar for the upper 85m. Therefore, the high contribution of coccolithophore pigment signatures was most likely due to the light difference between the two, although the communities should be fairly similar within a well-mixed layer.

However, the decrease in coccolithophores was accompanied by an increase in *Phaeocystis* that now also contains a significant proportion of the high-iron state *P. antarctica* (*Phaeocystis*-H). Therefore, the *P. antarctica* pigment group at the surface acclimated to low iron concentrations was still present at the fl-max (higher mixing) but had produced just as much *P. antarctica* with pigment signatures characteristic of a higher iron environment to double the total *Phaeocystis* contribution. Possibly, due to the deeper mixed layer allowing contact with water of higher available iron concentrations.

Acclimation: For this PFZ station, it appears that light, in conjunction with depth in the water column, exerts a strong role on the productivity and the community structure within this region. This is supported by Alderkamp et al. (2010) and Moore et al. (2007) who did extensive studies on in situ bloom observation and experiments assessing phytoplankton light acclimation and photochemical efficiencies (Fv/Fm) and specifically also used the xanthophyll cycle photoprotective pigments diadinoxanthin and diatoxanthin (DDT) to assess the relative photoprotective pigment quantities of different communities and if they would rather favour photosynthetic pigment production or photoprotective to resist photoinhibition. There is a higher productivity and contribution of coccolithophores at the surface, where coccolithophores is showed by Viljoen et al. (2018) to be highly depended on light intensity. As mentioned above, although the fluorescence signal was shown to be relatively uniform between surface and the 89m deep ML by Viljoen et al. (2018; Figure S3.1), chl-a concentrations were ca. 0.06 µg L^{-1} higher at the surface (46S-Surface; Figure 5.2). Therefore, it could be speculated that cells collected further up the water column to be less light limited than those at the 78m fl-max sampling depth (46S-FlMax; Figure 3.2), which could indicate that the results from the 46 °S experiment reflect a very depth-specific phytoplankton community. The possibility of this being a niche community that lives just above the thermocline, even within a deep ML (89m), are supported by the DDT ratios being lower here at the fl-max indicating that these cells are slightly less acclimated to high light environments than the surface sampled cells. Additionally, it would seem that the surface community at 46 °S is similar to that of the community at low light incubation treatment of Viljoen et al. (2018; Figure 3.4) in that it shows a larger coccolithophore contribution (dependent on light). The only difference in community structure being that the low light community contains noticeable amounts of prasinophytes, chlorophytes and *Phaeocystis*-H, which can be accounted for by the initial community, before they were incubated, contained minor amounts of them which was then

stimulated under the favourable light conditions for 5 days. Therefore, due to the surface community being pre-acclimated to higher light conditions they would have displayed even higher resistance to photoinhibition within higher light intensity treatments than the incubated fl-max community from 78m depth.

After what was observed after the surface community was also considered when studying the well mixed PFZ, it indicates, in addition to what Viljoen et al. (2018) stated about a deeply mixed PFZ community structure and its photoacclimation abilities being affected by light, that even within a well-mixed layer it is important to consider the surface and/or multiple depth sampled communities when assessing the factors affecting community structure. As well as their photo acclimation which have been shown now to have varying pre-acclimated cells at different depths.

5.5.2 Stratified shallow mixed AAZ/WG station S54-65

Productivity, degradation and community structure: At 65°S a major increase in diatom abundance to ca. 72% was observed that lead to a high total chl-a concentration. This relatively high chl-a concentration, along with the low dissolved iron concentrations compared to other trace metals (Viljoen et al. in preparation), the fact that *Phaeocystis* at the surface at 65°S only consisted of the high-iron state end member *Phaeocystis*-H, and ice presence at 65°S a week before ship arrival indicated the likelihood of waning bloom conditions supported by the release of melt water (Cavalieri et al. 1996; Viljoen et al. 2018). However, the composition at 65 °S showed changes from surface to chl-a maximum that included a major decrease in diatom contribution to total chl-a along with an increase in coccolithophores that resulted in the major chl-a increase to three times more than at surface. Phaeopigments was detected at this station with surface Phaeo:Chla ratios double (0.2) than that of the chl-max (0.1), which indicates higher grazing pressures at the surface. Grazers were possibly trapped in the shallow mixed layer at 65 °S caused by the ice melt. Most of the phaeopigments were phaeophorbid-a (Table 5.2), indicating the presence of both dying cells and/or detritus and faecal pellets (Szymczak-Zyła et al. 2008; Wright et al. 2010), which indicates that most of the grazing had already taken place at the time of sampling.

Acclimation: The DDT:Chla ratio was noticeably higher (0.084) at surface, even though the total chl-a concentration was lower than at the fl-max (0.051). This would preliminary indicate that the light environment, and therefore the acclimation of the phytoplankton cells, was different at the surface than at the fl-max. This is most likely due to the surface community being located within

a shallow ML (Moore et al. 2007; Alderkamp et al. 2011), caused by the recent ice melts, and the fl-max community just below the ML. Shallow mixed layers have been shown to be generally more productive due to the favourable, less variable, light conditions. Therefore, communities grown in these more stable conditions would have a lower DDT production, as they would need less photoprotection, but higher production of photosynthetic pigments (Moore et al. 2007), like Fuco and Hex. The measurement of lower DDT:Chla ratios at depth within a, most likely matured, high chl-max community with structure similar to the surface further indicates a change in the intra-cellular mechanics of photosynthesis with depth. The lower DDT:FH ratio at depth is also responsible for the high productivity here, where the low variability of irradiance at this depth causes the cell to decrease their ratio of photoprotective versus photosynthetic pigments and thereby increasing metabolic rates (Cheah et al. 2013), at this station and depth where iron limitation started to occur only recently (Viljoen et al. 2018).

5.6 Conclusion

There seems to be a whole issue with surface versus depth and the possibility of sampling a niche community which could lead to the results from an experiment to reflect a very depth-specific acclimated phytoplankton community and not that of a regional representative one. This study showed how different the acclimation of phytoplankton can be between two different depths and this is exemplified by regional differences in water column structure and dynamics. At 46 °S, although community structure seems similar due to the well ML, there is a difference between surface and depth communities in the iron and especially light acclimation of the phytoplankton cells. At 65 °S we clearly saw how a more stratified water column could enforce the phytoplankton cells sampled at different depths, within and below the ML, to adopt different acclimation strategies to the different sets of light and iron availabilities they are experiencing. The studying of irradiance for example by Cheah et al. (2013) showed that communities sampled at different depths will result in different responses. We therefore recommend that as far as possible, within in-situ observation studies and especially incubation studies of iron-light interactions, more than one depth of sampling should be done in order to account for the change in the acclimation of cells to the complex iron and light interactions observed in the ocean with depth. Should there be logistical constraints, low stratification and no major inversions of abiotic properties, such as temperature and macronutrients, be present as within a deeply mixed layer, one depth could be

sampled. However, caution should be taken in the interpretation of phytoplankton results from only one depth.

5.7 Acknowledgements

The authors thank the SANAE 54 team for the sampling, and Raissa Philibert for the analysis of the macronutrient data used in this manuscript. The work leading to these results received funding from the National Research Foundation (NRF), under the SA/Norway Collaboration Programme and the South African National Antarctic Programme, grant numbers 91313 and 110731 awarded to S. Fietz. J.J. Viljoen acknowledges funding from NRF through a Masters Innovation Scholarship.

5.8 References

For the purpose of this thesis the references for this manuscript and the others, including references for supplemental information, are combined in the main reference list (on page 76) to avoid duplication.

5.9 Tables

Table 5.1. Site characteristics at surface and fl-max for both stations. Profiles of nutrient concentrations (NO_3^- and $Si(OH)_4$) at both stations are shown in Supplemental Figure S5.1. #Light level at 10m. Example profiles of temperature, light attenuation and fluorescence (chl-a) are shown in Supplemental Figure S3.1 (Viljoen et al. 2018).

	S54-46		**S54-65**	
	Surface	**Fl-Max**	**Surface**	**Fl-Max**
Date	12-Jan-15		18-Jan-15	
Latitude (°S)	46		65	
Longitude (°E)	8		0	
Region	PFZ		AAZ	
MLD (m)	89		31	
Time of day	Early Afternoon		Early Morning	
Sampling Depth (m)	5-6	75-80	5-6	40
PAR (µE m-2 s-1)	4400	15	200	25#
Temperature (°C)	7,5	6,2	1,9	0
Salinity	33,72	33,79	33,57	34
[NO- 3] (µM)	22,6	23,3	20,6	25,2
[Si(OH)4] (µM)	3,16	5,79	44,93	74,30
[dFe] (nM)	0,38	0,37	0,22	0,19
Chl-a (µg/L)	0,18	0,12	0,28	0,96

Table 5.2. Ratios of photoprotective (DDT) versus chl-a and accessory light harvesting (FH) pigments for both stations at surface and fl-max. Phaeo=Phaeopigments, Phorb=Phaeophorbide-a, Phyt=Phaeophytin-a, DDT=diadinoxanthin+diatoxanthin, FH=Fuco+Hex. Detailed pigment data set (e.g. individual pigment concentrations) can be found in Supplemental Table S5.1. Data shown within Figure 5.3.

	S54-46			**S54-65**				
	Phaeo :Chla	DDT :Chla	DDT :FH	Phaeo :Chla	Phorb :Chla	Phyt :Chla	DDT :Chla	DDT: FH
Surface	0	0,0788	0,0889	0,1960	0,1808	0,0152	0,0843	0,1131
Fl-Max	0	0.0686	0.0745	0.1011	0.0772	0.0239	0.0507	0.0495

5.10 Figures

Figure 5.1. Station positions (Two red diamond symbols; S54-46 and S54-65) along the Good Hope line for SANAE54 cruise. The background shows the ocean floor bathymetry from Ocean Data View (Schlitzer 2015). The solid black line represents the Good Hope line. The dashed horizontal lines indicate the frontal positions (STF - subtropical front, SAF - Subantarctic Front, PF - Polar Front and Sbdy - Southern ACC boundary) along the Good Hope line.

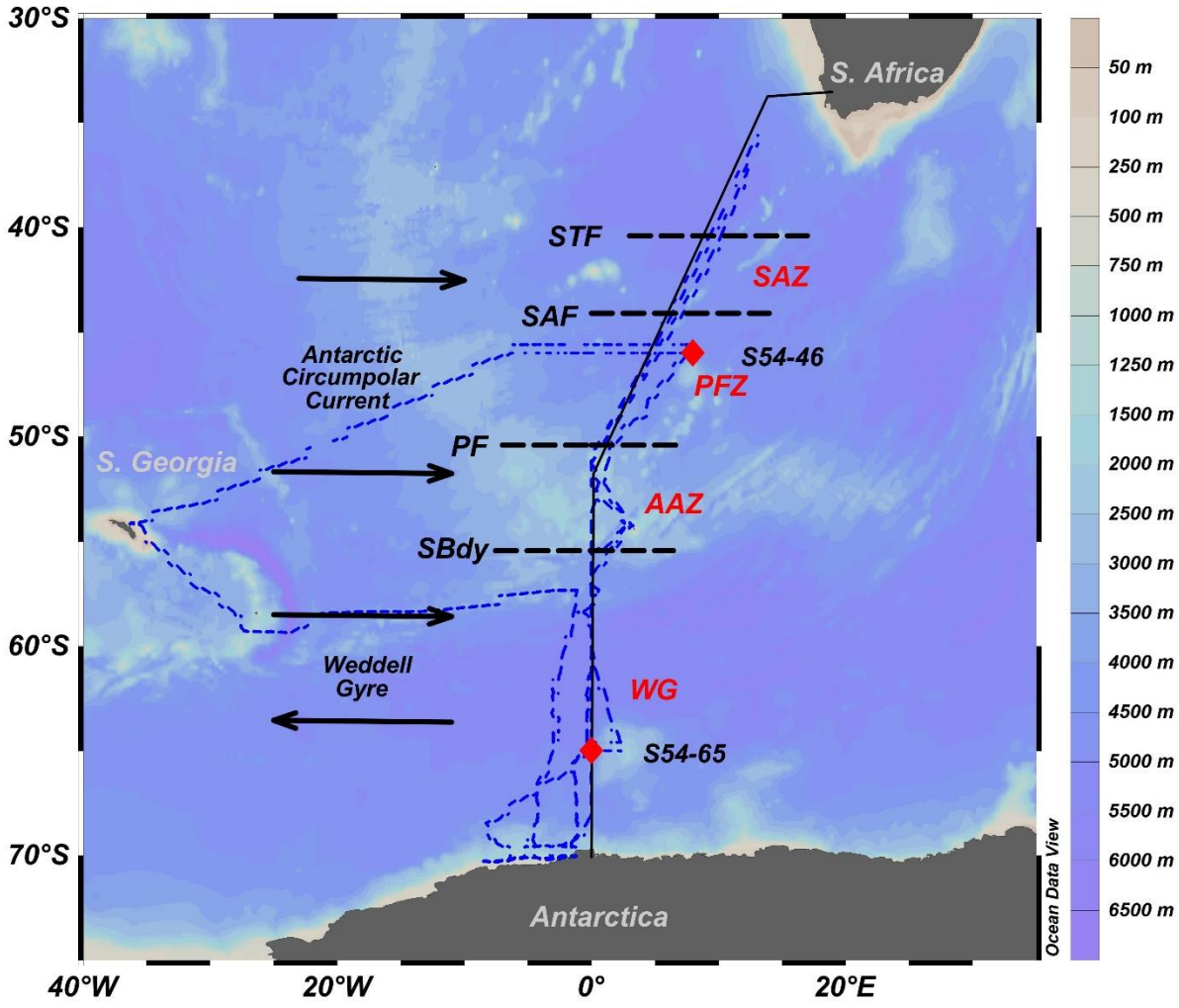

Figure 5.2. Phytoplankton composition in chl-a concentration (µg L^{-1}) at each depth (Surface and FlMax) for both stations at 46 °S: (a) S54-46 and 65 °S: (b) S54-65. The total stacked chl-a concentration indicates the total chl-a measured at that community. Graphs were plotted using the CHEMTAX output results shown in Supplemental Table S5.2.

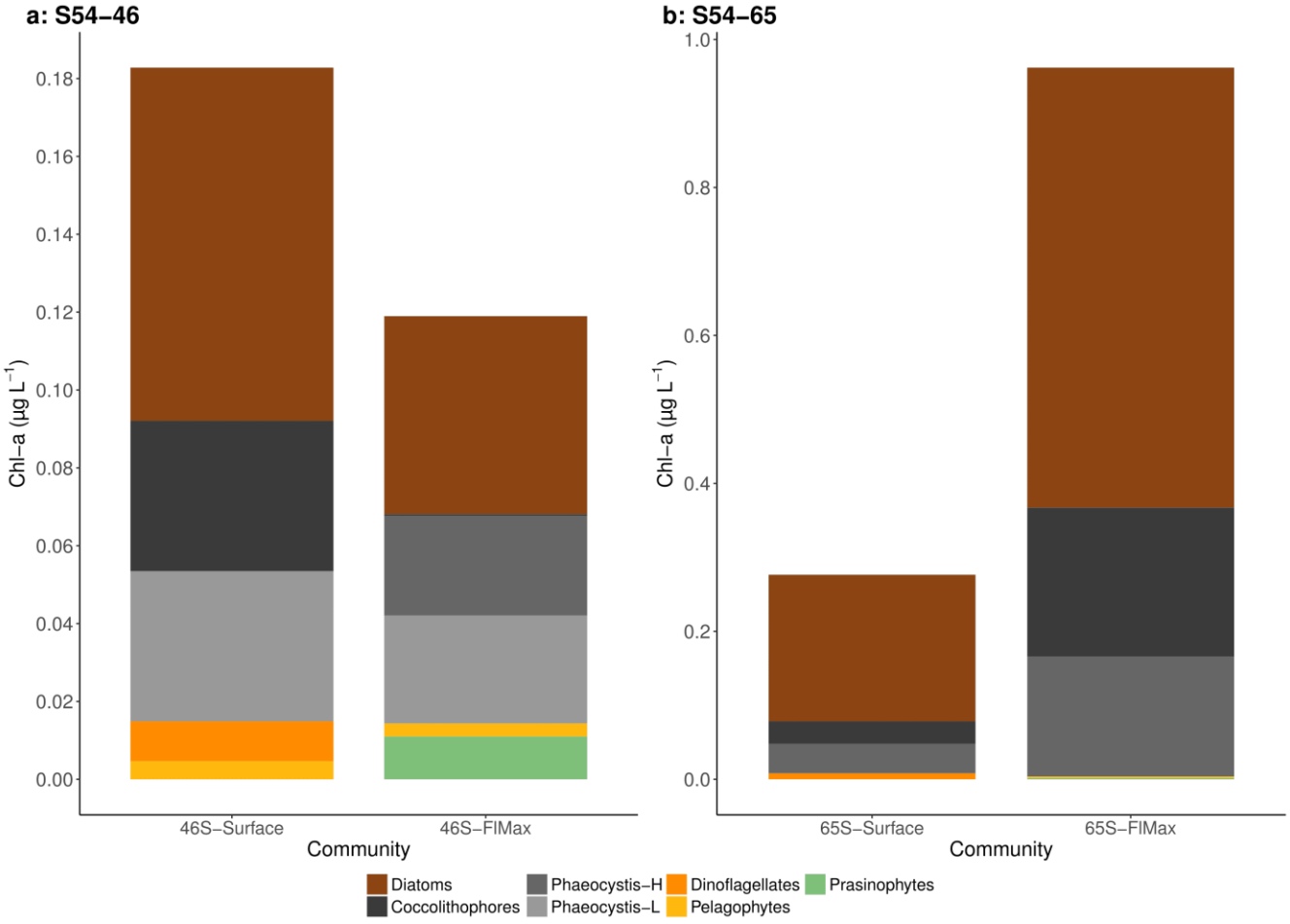

Figure 5.3. Pigment ratios (Phaeo:Chla, DDT:Chla and DDT:FH) measured within each community (Surface and FlMax) for both stations (a) S54-46 and (b) S54-65. Phaeopigments not detected at 46 °S therefore, Phaeo:Chla ratio not shown for (a) S54-46. Graphs were plotted using the phytoplankton pigment ratio results shown in Table 5.2.

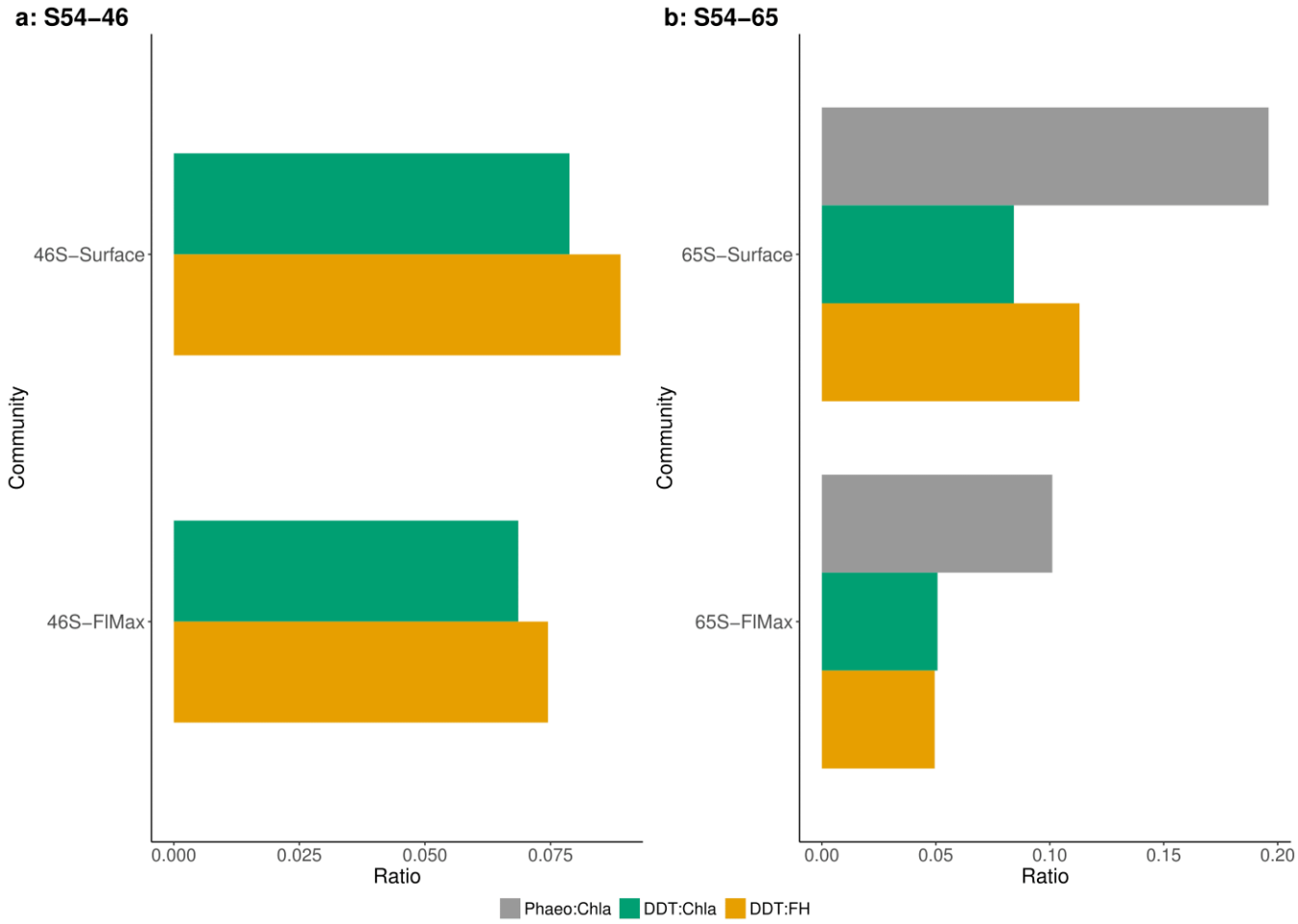

6 General Conclusion

This multi-manuscript study reports an elucidated understanding of the consequences key environmental changes has on phytoplankton community structure, productivity and their acclimation abilities for the Atlantic Sector of the Southern Ocean.

Manuscripts I showed that in the Atlantic sector of the Southern Ocean irradiance is limiting significant phytoplankton growth (in chlorophyll-a and particulate organic carbon) north of the Polar Front while iron addition resulted in growth stimulation even at low light levels in the Antarctic zone. Although photochemical efficiency (Fv/Fm) increased upon iron fertilization in both water masses, indicating stress relief, the acclimation strategies fundamentally differed between the two communities.

However, herein also lies the issue, which manuscripts III covered, of sampling a niche community when only one depth is sampled which could lead to results of a very depth-specific acclimated phytoplankton community and not that of a regional representative one. Due to changes in irradiance with vertical depth, acclimation of phytoplankton can vary between two different depths, including deep mixed layers, which is exemplified by regional differences in water column structure and dynamics. It is therefore essential to take both biogeographical differences between Southern Ocean water masses and vertical depth acclimation into account when interpreting ecosystem dynamics. Furthermore, it is recommended that for phytoplankton incubation experiment studies, especially of iron-light interactions, more than one depth should be sampled in order to account for acclimation changes of cells to the complex iron and light interactions observed in the ocean with depth and yes, caution should be taken in the interpretation of phytoplankton incubation results from only one depth.

Moreover, the findings of manuscript II indicate that on a regional scale an influx and/or abundance of trace metals linked to hydrothermal plume activity and ice melt, is closely related to increasing biomass and community diversification. Such a diversification in community structure could not be explained by macronutrients and physical variables. Herein lied the advantage a multi-parameter approach that highlights the importance of considering trace metals as an additional variable when accounting for phytoplankton variability in the open ocean. Therefore, caution should be taken by studies that involves these essential micronutrients and to incorporate the

consideration of the timing of phytoplankton sampling relative to the time of an event like the release of trace metals from hydrothermal vents or melting ice.

The work presented here demonstrates the noteworthy significance of how even the smallest changes from irradiance to the availability of trace metals and when they are released, can influence phytoplankton functioning and dynamics to a point where the number of vertical samples taken for incubation experiments is of utmost importance. Therefore, this study can conclude that, at least for the Atlantic Southern Ocean, the present state and future of phytoplankton dynamics greatly depends on key environmental changes such as irradiance, varying degrees of iron-light co-limitation and the proven strong influence of trace metal availability.

7 References

Reference list for the whole thesis including the Appendices.

Alderkamp, A.-C., H. J. W. de Baar, R. J. W. Visser, and K. R. Arrigo. 2010. Can photoinhibition control phytoplankton abundance in deeply mixed water columns of the Southern Ocean? Limnol. Oceanogr. **55**: 1248–1264. doi:10.4319/lo.2010.55.3.1248

Alderkamp, A. C., V. Garcon, H. J. W. de Baar, and K. R. Arrigo. 2011. Short-term photoacclimation effects on photoinhibition of phytoplankton in the Drake Passage (Southern Ocean). Deep Sea Res. I **58**: 943–955. doi:10.1016/j.dsr.2011.07.001

Alderkamp, A. C., G. Kulk, A. G. J. Buma, R. J. W. Visser, G. L. Van Dijken, M. M. Mills, and K. R. Arrigo. 2012a. The effect of iron limitation on the photophysiology of phaeocystis antarctica (prymnesiophyceae) and fragilariopsis cylindrus (bacillariophyceae) under dynamic irradiance. J. Phycol. **48**: 45–59. doi:10.1111/j.1529-8817.2011.01098.x

Alderkamp, A. C., M. M. Mills, G. L. van Dijken, and others. 2012b. Iron from melting glaciers fuels phytoplankton blooms in the Amundsen Sea (Southern Ocean): Phytoplankton characteristics and productivity. Deep Sea Res. II **71**–**76**: 32–48. doi:10.1016/j.dsr2.2012.03.005

Arrigo, K. R. 1999. Phytoplankton Community Structure and the Drawdown of Nutrients and CO2 in the Southern Ocean. Science. **283**: 365–367. doi:10.1126/science.283.5400.365

de Baar, H. J. W., P. W. Boyd, K. H. Coale, and others. 2005. Synthesis of iron fertilization experiments: From the Iron Age in the Age of Enlightenment. J. Geophys. Res. **110**: C09S16. doi:10.1029/2004JC002601

de Baar, H. J. W., A. G. J. Buma, R. F. Nolting, G. C. Cadee, G. Jacques, and P. J. Treguer. 1990. On iron limitation of the Southern Ocean : experimental observations in the Weddell and Scotia Seas. Mar. Ecol. Prog. Ser. **65**: 105–122. doi:10.3354/meps065105

Behrenfeld, M. J., E. Boss, D. A. Siegel, and D. M. Shea. 2005. Carbon-based ocean productivity and phytoplankton physiology from space. Global Biogeochem. Cycles **19**: 1–14. doi:10.1029/2004GB002299

Behrenfeld, M. J., and A. J. Milligan. 2013. Photophysiological Expressions of Iron Stress in Phytoplankton. Ann. Rev. Mar. Sci. **5**: 217–246. doi:10.1146/annurev-marine-121211-172356

Billany, W., S. Swart, J. Hermes, and C. J. C. Reason. 2010. Variability of the Southern Ocean fronts at the Greenwich Meridian. J. Mar. Syst. **82**: 304–310. doi:10.1016/j.jmarsys.2010.06.005

Boyd, P. W., and E. R. Abraham. 2001. Iron-mediated changes in phytoplankton photosynthetic competence during SOIREE. Deep Sea Res. II **48**: 2529–2550. doi:10.1016/S0967-0645(01)00007-8

Boyd, P. W., and M. J. Ellwood. 2010. The biogeochemical cycle of iron in the ocean. Nat. Geosci. **3**: 675–682. doi:10.1038/ngeo964

Boyd, P. W., R. Strzepek, F. Fu, and D. A. Hutchins. 2010. Environmental control of open-ocean phytoplankton groups: Now and in the future. Limnol. Oceanogr. **55**: 1353–1376. doi:10.4319/lo.2010.55.3.1353

Boyd, P. W., and T. W. Trull. 2007. Understanding the export of biogenic particles in oceanic waters: Is there consensus? Prog. Oceanogr. **72**: 276–312. doi:10.1016/j.pocean.2006.10.007

Boyd, P. W., A. J. Watson, C. S. Law, and others. 2000. A mesoscale phytoplankton bloom in the polar Southern Ocean stimulated by iron fertilization. Nature **407**: 695–702. doi:10.1038/35037500

de Boyer Montégut, C., G. Madec, A. S. Fischer, A. Lazar, and D. Iudicone. 2004. Mixed layer depth over the global ocean: An examination of profile data and a profile-based climatology. J. Geophys. Res. C Ocean. **109**: 1–20. doi:10.1029/2004JC002378

Boyer, T. P., J. I. Antonov, O. K. Baranova, and others. 2013. World Ocean Database 2013, S. Levitus and M. Alexey [eds.]. NOAA Atlas NESDIS 72.

Brand, L. E. 1991. Minimum iron requirements of marine phytoplankton and the implications for the biogeochemical control of new production. Limnol. Oceanogr. **36**: 1756–1771. doi:10.4319/lo.1991.36.8.1756

Brunet, C., G. Johnsen, J. Lavaud, and S. Roy. 2011. Pigments and photoacclimation processes, p. 445–471. *In* S. Roy, C. Llewellyn, E.S. Egeland, and G. Johnsen [eds.], Phytoplankton Pigments: Characterization, Chemotaxonomy and Applications in Oceanography. Cambridge University Press.

Brzezinski, M. A. 1985. The Si:C:N ratio of marine diatoms: interspecific variability and the effect of some environmental variables. J. Phycol. **21**: 347–357. doi:10.1111/j.0022-3646.1985.00347.x

Carreto, J. I., N. G. Montoya, M. O. Carignan, R. Akselman, E. M. Acha, and C. Derisio. 2016. Environmental and biological factors controlling the spring phytoplankton bloom at the Patagonian shelf-break front – Degraded fucoxanthin pigments and the importance of microzooplankton grazing. Prog. Oceanogr. **146**: 1–21. doi:10.1016/j.pocean.2016.05.002

Carter, L., I. N. McCave, and M. J. M. Williams. 2008. Chapter 4 Circulation and Water Masses of the Southern Ocean: A Review. Dev. Earth Environ. Sci. **8**: 85–114. doi:10.1016/S1571-9197(08)00004-9

Cassar, N., P. J. DiFiore, B. A. Barnett, and others. 2011. The influence of iron and light on net community production in the Subantarctic and Polar Frontal Zones. Biogeosciences **8**: 227–237. doi:10.5194/bg-8-227-2011

Cavalieri, D. J., C. L. Parkinson, P. Gloersen, and H. J. Zwally. 1996. Sea ice concentrations from Nimbus-7 SMMR and DMSP SSM/I-SSMIS Passive Microwave Data, Version 1. [December 2013 - January 2015 daily data].doi:10.5067/8GQ8LZQVL0VL

Cheah, W., A. McMinn, F. B. Griffiths, K. J. Westwood, S. W. Wright, and L. A. Clementson. 2013. Response of Phytoplankton Photophysiology to Varying Environmental Conditions in the Sub-Antarctic and Polar Frontal Zone S. Lin [ed.]. PLoS One **8**: e72165.

doi:10.1371/journal.pone.0072165

Chitari, R. R., and A. C. Anil. 2017. Estimation of diatom and dinoflagellate cell volumes from surface waters of the Northern Indian Ocean. Oceanologia **59**: 389–395. doi:10.1016/j.oceano.2017.03.001

Cloete, R., J. C. Loock, T. N. Mtshali, S. Fietz, and A. N. Roychoudhury. Winter and summer distributions of Copper, Zinc and Nickel along the International GEOTRACES section GIPY05: Insights into deep winter mixing. Chem. Geol. (revisions submitted) (manuscript nr. CHEMGE-S-18-00174).

Coale, K. H., K. S. Johnson, F. P. Chavez, and others. 2004. Southern Ocean Iron Enrichment Experiment: Carbon Cycling in High- and Low-Si Waters. Science. **304**: 408–414. doi:10.1126/science.1089778

Coale, K. H., X. Wang, S. J. Tanner, and K. S. Johnson. 2003. Phytoplankton growth and biological response to iron and zinc addition in the Ross Sea and Antarctic Circumpolar Current along 170°W. Deep Sea Res. II **50**: 635–653. doi:10.1016/S0967-0645(02)00588-X

Cutter, G. A., and K. W. Bruland. 2012. Rapid and noncontaminating sampling system for trace elements in global ocean surveys. Limnol. Oceanogr. Methods **10**: 425–436. doi:10.4319/lom.2012.10.425

Cutter, G., L. Codispoti, P. Croot, R. Francois, M. Lohan, and M. Rutgers Van Der Loeff. 2014. Sampling and Sample-handling Protocols for GEOTRACES Cruises. **2**.

Deacon, G. E. R. 1963. The Southern Ocean, p. 281–296. *In* M.N. Hill [ed.], The sea. Interscience.

Deppeler, S. L., and A. T. Davidson. 2017. Southern Ocean Phytoplankton in a Changing Climate. Front. Mar. Sci. **4**: 40. doi:10.3389/fmars.2017.00040

DiTullio, G. R., N. Garcia, S. F. Riseman, and P. N. Sedwick. 2007. Effects of iron concentration on pigment composition in Phaeocystis antarctica grown at low irradiance. Biogeochemistry **83**: 71–81. doi:10.1007/978-1-4020-6214-8_7

Dunn, O. J. 1964. Multiple Comparisons Using Rank Sums. Technometrics **6**: 241–252. doi:10.1080/00401706.1964.10490181

Dupont, C. L., K. N. Buck, B. Palenik, and K. Barbeau. 2010. Nickel utilization in phytoplankton assemblages from contrasting oceanic regimes. Deep Sea Res. I **57**: 553–566. doi:10.1016/j.dsr.2009.12.014

Egan, L. 2008. Determination of Nitrate and/or Nitrite in Brackish or Seawater by Flow Injection Analysis. QuikChem® Method 31-107-04-1-C.

Feng, Y., C. E. Hare, J. M. Rose, and others. 2010. Interactive effects of iron, irradiance and CO2 on Ross Sea phytoplankton. Deep Sea Res. I **57**: 368–383. doi:10.1016/j.dsr.2009.10.013

Findlay, C. S., and J. Giraudeau. 2000. Extant calcareous nannoplankton in the Australian Sector of the Southern Ocean (austral summers 1994 and 1995). Mar. Micropaleontol. **40**: 417–

439. doi:10.1016/S0377-8398(00)00046-3

Finkel, Z. V., J. Beardall, K. J. Flynn, A. Quigg, T. A. V Rees, and J. A. Raven. 2010. Phytoplankton in a changing world: Cell size and elemental stoichiometry. J. Plankton Res. **32**: 119–137. doi:10.1093/plankt/fbp098

Flynn, K. J., M. St John, J. A. Raven, D. O. F. Skibinski, J. I. Allen, A. Mitra, and E. E. Hofmann. 2015. Acclimation, adaptation, traits and trade-offs in plankton functional type models: reconciling terminology for biology and modelling. J. Plankton Res. **37**: 683–691. doi:10.1093/plankt/fbv036

Garcia, H. E., R. A. Locarnini, T. P. Boyer, J. I. Antonov, O. K. Baranova, M. M. Zweng, J. R. Reagan, and D. R. Johnson. 2013. World Ocean Atlas 2013. Vol. 4: Dissolved Inorganic Nutrients (phosphate, nitrate, silicate). S. Levitus, Ed.; A. Mishonov, Tech. Ed. NOAA Atlas NESDIS **76**: 25. doi:10.1182/blood-2011-06-357442

Gervais, F., U. Riebesell, and M. Y. Gorbunov. 2002. Changes in primary productivity and chlorophyll a in response to iron fertilization in the Southern Polar Frontal Zone. Limnol. Oceanogr. **47**: 1324–1335. doi:10.4319/lo.2002.47.5.1324

Gibberd, M. J., E. Kean, R. Barlow, S. Thomalla, and M. Lucas. 2013. Phytoplankton chemotaxonomy in the Atlantic sector of the Southern Ocean during late summer 2009. Deep Sea Res. I **78**: 70–78. doi:10.1016/j.dsr.2013.04.007

Grasshoff, K., M. Ehrhardt, K. Kremling, and T. Almgren. 1983. Methods of seawater analysis, Verlag Chemie.

Grotti, M., F. Soggia, M. L. Abelmoschi, P. Rivaro, E. Magi, and R. Frache. 2001. Temporal distribution of trace metals in Antarctic coastal waters. Mar. Chem. **76**: 189–209. doi:10.1016/S0304-4203(01)00063-9

Ho, T.-Y., A. Quigg, Z. V. Finkel, A. J. Milligan, K. Wyman, P. G. Falkowski, and F. M. M. Morel. 2003. The Elemental Composition of Some Marine Phytoplankton. J. Phycol. **39**: 1145–1159. doi:10.1111/j.0022-3646.2003.03-090.x

Hoffmann, L. J., I. Peeken, K. Lochte, P. Assmy, and M. Veldhuis. 2006. Different reactions of Southern Ocean phytoplankton size classes to iron fertilization. Limnol. Oceanogr. **51**: 1217–1229. doi:10.4319/lo.2006.51.3.1217

Howes, E. L., F. Joos, C. M. Eakin, and J.-P. Gattuso. 2015. An updated synthesis of the observed and projected impacts of climate change on the chemical, physical and biological processes in the oceans. Front. Mar. Sci. **2**: 36. doi:10.3389/fmars.2015.00036

Hudson, R. J. M., and F. M. M. Morel. 1990. lron transport in marine phytoplankton: Kinetics of cellular and medium coordination reactions. Limnol. Oceanogr. **35**: 1002–1020. doi:10.4319/lo.1990.35.5.1002

Ishikawa, A., S. W. Wright, R. Van Den Enden, A. T. Davidson, and H. J. Marchant. 2002. Abundance,size structure and community composition of phytoplankton in the Southern Ocean in the austral summer 1999/2000. Polar Biosci **15**: 11–26.

Jeffrey, S. W., R. F. C. Mantoura, and S. W. Wright. 1997. Phytoplankton pigments in

oceanography: guidelines to modern oceanography, United Nations Educational, Scientific and Cultural Organization.

Kirchman, D. L., and P. A. Wheeler. 1998. Uptake of ammonium and nitrate by heterotrophic bacteria and phytoplankton in the sub-Arctic Pacific. Deep Sea Res. I **45**: 347–365. doi:10.1016/S0967-0637(97)00075-7

Klausmeier, C. A., E. Litchman, T. Daufresne, and S. A. Levin. 2004. Optimal nitrogen-to phosphorus stoichiometry of phytoplankton. Nature **429**: 171–174. doi:1.1029/2001GL014649

Klunder, M. B., P. Laan, R. Middag, H. J. W. de Baar, and J. C. van Ooijen. 2011a. Dissolved iron measured on water bottle samples during POLARSTERN cruise ANT-XXIV/3.doi:10.1594/PANGAEA.780271

Klunder, M. B., P. Laan, R. Middag, H. J. W. De Baar, and J. C. van Ooijen. 2011b. Dissolved iron in the Southern Ocean (Atlantic sector). Deep Sea Res. II **58**: 2678–2694. doi:10.1016/j.dsr2.2010.10.042

Lance, V. P., M. R. Hiscock, A. K. Hilting, D. A. Stuebe, R. R. Bidigare, W. O. Smith, and R. T. Barber. 2007. Primary productivity, differential size fraction and pigment composition responses in two Southern Ocean in situ iron enrichments. Deep Sea Res. I **54**: 747–773. doi:10.1016/J.DSR.2007.02.008

van Leeuwe, M. A., G. Kattner, T. van Oijen, J. T. M. de Jong, and H. J. W. de Baar. 2015. Phytoplankton and pigment patterns across frontal zones in the Atlantic sector of the Southern Ocean. Mar. Chem. **177**: 510–517. doi:10.1016/j.marchem.2015.08.003

Loock, J., R. Cloete, T. Mtshali, S. Fietz, and A. Roychoudhury. The biogeochemistry of Co, Mn and Cd on a seasonal re-occupation of the Southern Ocean. Chem. Geol. (revisions submitted) (manuscript nr. CHEMGE-S-18-00176).

Mackey, M. D., D. J. Mackey, H. W. Higgins, and S. W. Wright. 1996. CHEMTAX- a program for estimating class abundances from chemical markers : application to HPLC measurements of phytoplankton. Mar. Ecol. Prog. Ser. **144**: 265–283. doi:doi:10.3354/meps144265

Martin, J. H., R. M. Gordon, and S. E. Fitzwater. 1990. Iron in Antarctic waters. Nature **345**: 156–158. doi:10.1038/345156a0

Mendes, C. R. B., R. Kerr, V. M. Tavano, F. A. Cavalheiro, C. A. E. Garcia, D. R. Gauns Dessai, and N. Anilkumar. 2015. Cross-front phytoplankton pigments and chemotaxonomic groups in the Indian sector of the Southern Ocean. Deep Sea Res. II **118**: 221–232. doi:10.1016/j.dsr2.2015.01.003

Mills, M. M., A.-C. Alderkamp, C.-E. Thuróczy, G. L. van Dijken, P. Laan, and H. J. W. de Baar. 2012. Phytoplankton biomass and pigment responses to Fe amendments in the Pine Island and Amundsen polynyas. Deep Sea Res. II **71**–**76**: 61–76. doi:10.1016/J.DSR2.2012.03.008

Moore, C. M., M. M. Mills, K. R. Arrigo, and others. 2013. Processes and patterns of oceanic nutrient limitation. Nat. Geosci. **6**: 701–710. doi:10.1038/ngeo1765

Moore, C. M., S. Seeyave, A. E. Hickman, J. T. Allen, M. I. Lucas, H. Planquette, R. T. Pollard, and A. J. Poulton. 2007. Iron-light interactions during the CROZet natural iron bloom and EXport experiment (CROZEX) I: Phytoplankton growth and photophysiology. Deep Sea Res. II **54**: 2045–2065. doi:10.1016/j.dsr2.2007.06.011

Morel, F. M. M., A. J. Milligan, and M. A. Saito. 2003. Marine Bioinorganic Chemistry: The Role of Trace Metals in the Oceanic Cycles of Major Nutrients, p. 113–143. *In* Treatise on Geochemistry. Elsevier.

Muggli, D. L., and P. J. Harrison. 1996. Effects of nitrogen source on the physiology and metal nutrition of Emiliania huxleyi grown under different iron and light conditions. Mar. Ecol. Prog. Ser. **130**: 255–267. doi:10.3354/meps130255

Muggli, D. L., and P. J. Harrison. 1997. Effects of iron on two oceanic phytoplankters grown in natural NE subarctic pacific seawater with no artificial chelators present. J. Exp. Mar. Bio. Ecol. **212**: 225–237.

NASA Ocean Biology Processing Group. 2014. VIIRSN Level-3 Standard Mapped Image. Maint. by NASA Ocean Biol. Distrib. Act. Arch. Cent. (OB.DAAC), Goddard Sp. Flight Center, Greenbelt MD.

NOAA. 2015. High density XBT transects: AX25.

van Oijen, T., M. A. van Leeuwe, E. Granum, F. J. Weissing, R. G. J. Bellerby, W. W. C. Gieskes, and H. J. W. de Baar. 2004. Light rather than iron controls photosynthate production and allocation in Southern Ocean phytoplankton populations during austral autumn. J. Plankton Res. **26**: 885–900. doi:10.1093/plankt/fbh088

Olaizola, M., J. La Roche, Z. Kolber, and P. G. Falkowski. 1994. Non-photochemical fluorescence quenching and the diadinoxanthin cycle in a marine diatom. Photosynth. Res. **41**: 357–370. doi:10.1007/BF00019413

Orsi, A. H., T. Whitworth, and W. D. Nowlin. 1995. On the meridional extent and fronts of the Antarctic Circumpolar Current. Deep Sea Res. I **42**: 641–673. doi:10.1016/0967-0637(95)00021-W

Pankowski, A., and A. Mcminn. 2009. Iron availability regulates growth, photosynthesis, and production of ferredoxin and flavodoxin in Antarctic sea ice diatoms. Aquat. Biol. **4**: 273–288. doi:10.3354/ab00116

Peers, G., and N. M. Price. 2004. A role for manganese in superoxide dismutases and growth of iron-deficient diatoms. Limnol. Oceanogr. **49**: 1774–1783. doi:10.4319/lo.2004.49.5.1774

Peers, G., and N. M. Price. 2006. Copper-containing plastocyanin used for electron transport by an oceanic diatom. Nature **441**: 341–344. doi:10.1038/nature04630

Peloquin, J., J. Hall, K. Safi, and others. 2011. Control of the phytoplankton response during the SAGE experiment: A synthesis. Deep Sea Res. II **58**: 824–838. doi:10.1016/J.DSR2.2010.10.019

Petrou, K., C. S. Hassler, M. A. Doblin, K. Shelly, V. Schoemann, R. van den Enden, S. Wright, and P. J. Ralph. 2011. Iron-limitation and high light stress on phytoplankton populations

from the Australian Sub-Antarctic Zone (SAZ). Deep Sea Res. II **58**: 2200–2211. doi:10.1016/J.DSR2.2011.05.020

Petrou, K., S. Trimborn, B. Rost, P. J. Ralph, and C. S. Hassler. 2014. The impact of iron limitation on the physiology of the Antarctic diatom Chaetoceros simplex. Mar. Biol. **161**: 925–937. doi:10.1007/s00227-014-2392-z

Pollard, R. T., M. I. Lucas, and J. F. Read. 2002. Physical controls on biogeochemical zonation in the Southern Ocean. Deep Sea Res. II **49**: 3289–3305. doi:10.1016/S0967-0645(02)00084-X

R Core Team. 2015. R: A Language and Environment for Statistical Computing.

Ragueneau, O., and P. Tréguer. 1994. Determination of biogenic silica in coastal waters: applicability and limits of the alkaline digestion method. Mar. Chem. **45**: 43–51. doi:10.1016/0304-4203(94)90090-6

Ras, J., H. Claustre, and J. Uitz. 2008. Spatial variability of phytoplankton pigment distributions in the Subtropical South Pacific Ocean: comparison between in situ and predicted data. Biogeosciences **5**: 353–369. doi:10.5194/bgd-4-3409-2007

Raven, J. A. 1990. Predictions of Mn and Fe use efficiencies of phototrophic growth as a function of light availability for growth and of C assimilation pathway. New Phytol. **116**: 1–18. doi:10.1111/j.1469-8137.1990.tb00505.x

Redfield, A. C. 1958. The biological control of chemical factors in the environent. Am. Sci. **46**: 230. doi:10.2307/27827150

Rousseau, V., M.-J. Chrétiennot-Dinet, A. Jacobsen, P. Verity, and S. Whipple. 2007. The life cycle of Phaeocystis: state of knowledge and presumptive role in ecology. Biogeochemistry **83**: 29–47. doi:10.1007/s10533-007-9085-3

Saito, M. A., T. J. Goepfert, and J. T. Ritt. 2008. Some thoughts Three definitions on the concept of colimitation : and the importance of bioavailability. Limnol. Oceanogr. **53**: 276–290. doi:10.4319/lo.2008.53.1.0276

Saito, M. A., and J. W. Moffett. 2002. Temporal and spatial variability of cobalt in the Atlantic Ocean. Geochim. Cosmochim. Acta **66**: 1943–1953. doi:10.1016/S0016-7037(02)00829-3

Schlitzer, R. 2002. Carbon export fluxes in the Southern Ocean: Results from inverse modeling and comparison with satellite-based estimates. Deep Sea Res. II **49**: 1623–1644. doi:10.1016/S0967-0645(02)00004-8

Schlitzer, R. 2015. Ocean Data View.

Schlüter, L., P. Henriksen, T. G. Nielsen, and H. H. Jakobsen. 2011. Phytoplankton composition and biomass across the southern Indian Ocean. Deep Sea Res. I **58**: 546–556. doi:10.1016/j.dsr.2011.02.007

Schoemann, V., S. Becquevort, J. Stefels, V. Rousseau, and C. Lancelot. 2005. Phaeocystis blooms in the global ocean and their controlling mechanisms: a review. J. Sea Res. **53**: 43–66. doi:10.1016/j.seares.2004.01.008

Sedwick, P. N., G. R. DiTullio, and D. J. Mackey. 2000. Iron and manganese in the Ross Sea, Antarctica: Seasonal iron limitation in Antarctic shelf waters. J. Geophys. Res. Ocean. **105**: 11321–11336. doi:10.1029/2000JC000256

Sedwick, P. N., N. S. Garcia, S. F. Riseman, C. M. Marsay, and G. R. DiTullio. 2007. Evidence for high iron requirements of colonial Phaeocystis antarctica at low irradiance. Biogeochemistry **83**: 83–97. doi:10.1007/s10533-007-9081-7

Sidak, Z. 1967. Rectangular Confidence Regions for the Means of Multivariate Normal Distributions. J. Am. Stat. Assoc. **62**: 626. doi:10.2307/2283989

Smith, W. O., and V. L. Asper. 2001. The influence of phytoplankton assemblage composition on biogeochemical characteristics and cycles in the southern Ross Sea, Antarctica. Deep Sea Res. I **48**: 137–161. doi:10.1016/S0967-0637(00)00045-5

Strzepek, R. F., and P. J. Harrison. 2004. Photosynthetic architecture differs in coastal and oceanic diatoms. Nature **431**: 689–692. doi:10.1038/nature02954

Strzepek, R. F., K. A. Hunter, R. D. Frew, P. J. Harrison, and P. W. Boyd. 2012. Iron-light interactions differ in Southern Ocean phytoplankton. Limnol. Oceanogr. **57**: 1182–1200. doi:10.4319/lo.2012.57.4.1182

Suggett, D. J., H. L. MacIntyre, and R. J. Geider. 2004. Evaluation of biophysical and optical determinations of light absorption by photosystem II in phytoplankton. Limnol. Oceanogr. Methods **2**: 316–332. doi:10.4319/lom.2004.2.316

Sunda, W. G. 1997. Control of dissolved iron concentrations in the world ocean, A comment. Mar. Chem. **57**: 169–172. doi:10.1016/S0304-4203(97)00045-5

Sunda, W. G., and S. A. Huntsman. 1995a. Cobalt and zinc interreplacement in marine phytoplankton: Biological and geochemical implications. Limnol. Oceanogr. **40**: 1404–1417. doi:10.4319/lo.1995.40.8.1404

Sunda, W. G., and S. A. Huntsman. 1995b. Iron Uptake and Growth Limitation in Oceanic and Coastal Phytoplankton. Mar. Chem. **50**: 189–206. doi:10.1016/0304-4203(95)00035-p

Sunda, W. G., and S. A. Huntsman. 1997. Interrelated influence of iron , light and cell size on marine phytoplankton growth light and cell size on marine. Nature **2051**: 389–392. doi:10.1038/37093

Swan, C. M., M. Vogt, N. Gruber, and C. Laufkoetter. 2015. A global seasonal surface ocean climatology of phytoplankton types based on CHEMTAX analysis of HPLC pigments. Deep Sea Res. I. doi:10.1016/j.dsr.2015.12.002

Szymczak-Zyła, M., G. Kowalewska, and J. W. Louda. 2008. The influence of microorganisms on chlorophyll a degradation in the marine environment. Limnol. Oceanogr. **53**: 851–862. doi:10.4319/lo.2008.53.2.0851

Takahashi, T., S. C. Sutherland, R. Wanninkhof, and others. 2009. Climatological mean and decadal change in surface ocean pCO2, and net sea–air CO2 flux over the global oceans. Deep Sea Res. II **56**: 554–577. doi:10.1016/J.DSR2.2008.12.009

Thomalla, S. J., N. Fauchereau, S. Swart, and P. M. S. Monteiro. 2011. Regional scale characteristics of the seasonal cycle of chlorophyll in the Southern Ocean. Biogeosciences **8**: 2849–2866. doi:10.5194/bg-8-2849-2011

Timmermans, K. R., M. S. Davey, B. Van der Wagt, J. Snoek, R. J. Geider, M. J. W. Veldhuis, L. J. A. Gerringa, and H. J. W. De Baar. 2001. Co-limitation by iron and light of Chaetoceros brevis, C. dichaeta and C. calcitrans (Bacillariophyceae). Mar. Ecol. Prog. Ser. **217**: 287–297. doi:10.3354/meps217287

Timmermans, K. R., B. Van Der Wagt, M. J. W. Veldhuis, A. Maatman, and H. J. W. De Baar. 2005. Physiological responses of three species of marine pico-phytoplankton to ammonium, phosphate, iron and light limitation. J. Sea Res. **53**: 109–120. doi:10.1016/j.seares.2004.05.003

Twining, B. S., and S. B. Baines. 2013. The Trace Metal Composition of Marine Phytoplankton. Ann. Rev. Mar. Sci. **5**: 191–215. doi:10.1146/annurev-marine-121211-172322

Viljoen, J. J., R. Philibert, N. Van Horsten, T. Mtshali, A. N. Roychoudhury, S. Thomalla, and S. Fietz. 2018. Phytoplankton response in growth, photophysiology and community structure to iron and light in the Polar Frontal Zone and Antarctic waters. Deep Sea Res. I. doi:10.1016/J.DSR.2018.09.006

Viljoen, J. J., I. Weir, S. Fietz, R. Cloete, J. Loock, R. Philibert, and A. N. Roychoudhury. Links between phytoplankton community composition and trace metal distribution in the surface waters of the Atlantic Southern Ocean. (in preparation).

Wickham, H. 2009. Ggplot2 : Elegant graphics for data analysis, Springer-Verlag New York.

Wolters, M. 2002. Determination of Silicate in Brackish or Seawater by Flow Injection Analysis. QuikChem® Method 31-114-27-1-D.

Wright, S. W., R. L. van den Enden, I. Pearce, A. T. Davidson, F. J. Scott, and K. J. Westwood. 2010. Phytoplankton community structure and stocks in the Southern Ocean (30-80E) determined by CHEMTAX analysis of HPLC pigment signatures. Deep Sea Res. II **57**: 758–778. doi:10.1016/j.dsr2.2009.06.015

Xu, Y., D. Tang, Y. Shaked, and F. M. M. Morel. 2007. Zinc, cadmium, and cobalt interreplacement and relative use efficiencies in the coccolithophore Emiliania huxleyi. Limnol. Oceanogr. **52**: 2294–2305. doi:10.4319/lo.2007.52.5.2294

8 Appendix A: Chapter-3 Supplemental Information

Supplemental Information to manuscript

Manuscript accepted to Deep Sea Research Part I. Published online September 2018.

Phytoplankton response in growth, photophysiology and community structure to iron and light in the Polar Frontal Zone and Antarctic waters

Johannes J. Viljoen[1*]

Raïssa Philibert[1*,¥]

Natasha Van Horsten[1,2]

Thato Mtshali[2]

Alakendra N. Roychoudhury[1]

Sandy Thomalla[2]

Susanne Fietz[1,£]

[1]Department of Earth Sciences, Stellenbosch University, 7600 Stellenbosch, South Africa

[2]Southern Ocean Carbon and Climate Observatory, CSIR, 7599 Stellenbosch, South Africa

[*]these authors contributed equally

[¥]Current address: Coastal Ocean Research Institute, Vancouver, British Columbia

[£]corresponding author: Department of Earth Sciences, Stellenbosch University, 7600 Stellenbosch, South Africa, sfietz@sun.ac.za, +27218083117

8.1 Supplementary methods

8.1.1 Protocol for acid washing of incubation material and bottles

The 50L LDPE carboys used for homogenisation and 2.4L polycarbonate bottles used for incubations, as well as all other material required for the incubation process (e.g., plastic measuring cylinders) were soaked for one month in Decon 90® detergent (Decon Laboratories Limited, UK) and one week to one month in 1 M HCl (32% trace metal grade, Merck Millipore, USA). The bottles and other sampling material were soaked in a bath so that both inside and outside were in contact with the detergent or acid. The bottles and other sampling material were rinsed with Milli-Q® water (three to five times) after each washing step (detergent, 1M HCl and 0.5 M HCl). The bottles were then filled with 0.1 M HCl (30% Suprapur®, Merck Millipore, USA) and stored double bagged for at least another month prior to their use. Shortly before use, the bottles were removed from the double bags shortly and rinsed with Milli-Q® water.

8.1.2 Detailed incubation scheme during SANAE 54 (S54) summer cruise

Nine acid washed 2.4-L polycarbonate incubation bottles were prepared for each of the four treatments (Figure S3.1) and filled up to 1.6 L to allow headspace for gas exchange. Three bottles were prepared to be used for control samples at time zero (T0), which represented the initial conditions. The sample bottles were shaken gently every 2 to 4 hours over the course of the incubation in order to prevent particles from settling. The incubator doors were covered with black plastic sheets to prevent outside light interference when opening incubators to mix bottles. Three major terminations were conducted for each experiment. Three bottles (triplicates) per treatment were terminated after two days, four days and six days. Photophysiology measurements were conducted every 24 hours from the time of sampling using the samples to be terminated the following day. For instance, photophysiology measurements done after the first 24 hours were performed on samples meant to be filtered after two days. The samples were incubated under 8:16 and 4:20 dark/light cycles for S54-46 and S54-65 respectively, in accordance with in-situ day:night cycles at the time of sampling. The high light (L2) was set at 65 µE m^{-2} s^{-1} for both incubations. The low light level (L1) was set at the in-situ PAR (15 µE m^{-2} s^{-1}) for S54-46. For S54-65, the measured in-situ PAR at the sampling depth (40 m) was 0 µE m^{-2} s^{-1} and the euphotic depth was very shallow (20 m) as there was a rapid attenuation of light within the upper water column due to the large biomass. Therefore, the L1 was set at a level that would be appropriate for growth. This was taken as 25 µE m^{-2} s^{-1} (PAR at 10 m depth).

8.1.3 Details on analytical methods

Concentrations of total chl-a, particulate organic carbon (POC) and dissolved nutrients (NO_3^-, NO_2^-, $Si(OH)_4$, and PO_4^{3-}) were measured to determine differences in growth and nutrient uptake rates between treatments. Chlorophyll-a (chl-a) and POC concentrations were measured at T0 and each termination, while nutrients were only analysed at T0 and the final terminations.

Size-fractionated chl-a was measured in order to obtain information on the phytoplankton community size structure. 400ml of the samples were filtered successively onto 5, 2 and 0.2 µm polycarbonate filters. The sum of chl-a in all three fractions was taken as total chl-a concentration. For both experiments (S54-46 and S54-65), the chl-a was extracted in 90%

acetone at -20 °C for 24 hours. The fluorescence was measured on a Turner Design Trilogy® fluorometer using the chl-a non-acidified module. The fluorometer was calibrated prior to analysis using a chl-a standard (Sigma-Aldrich, USA). This same method was also used to measure chlorophyll concentrations from discrete samples from each CTD cast in order to calibrate the CTD fluorescence sensor.

For POC, 600 to 700 ml sample was vacuum filtered through a pre-combusted (at 400 °C for 12 to 24 hours) Whatmann glass fibre filter (GFF, nominal pore size 0.7 µm). Samples were acid-fumed to remove inorganic carbon and oven-dried. They were subsequently analysed using a Flash EA 1112 series elemental analyser (Thermo Finnigan, Italy) coupled to a Delta Plus XP isotope ratio mass spectrometer (IRMS) detector (Thermo Electron, Germany). The carbon content of each sample was determined using standards of known carbon content by weight, such as a proteinaceous gel (Merck Millipore, USA), *Acacia saligna* leaves and Valine (Sigma-Aldrich, USA). Cross-laboratory comparisons have shown the accuracy of this measurement to be within 1% of the true value (unpublished).

The samples collected for macronutrient analysis were frozen at -20 °C immediately after sampling and analysed upon return in the laboratory. The nutrient concentrations were determined for NO_3^-, NO_2^-, and $Si(OH)_4$ by using a Lachat Quick-Chem Flow injection autonalyser (Wolters 2002; Egan 2008) and PO_4^{3-} manually according to methods described by Grasshoff et al. (1983). The analytical error of the NO_3^-+ NO_2^-, PO_4^{3-} , and $Si(OH)_4$ quantification is ± 0.04 µM, ± 0.06 µM and ± 0.02 µM, respectively (Grasshoff et al. 1983).

High resolution photophysiology analysis was conducted by measuring Fv/Fm and σ_{PSII} every 24 hours from the start of the incubation during SANAE 54 using a Fast Repetition Rate fluorometry (FRRf) system (FastAct base unit and FastOcean sensor, 2220-173-PL, Chelsea SMD Telecommunications (Pty) LTD, UK). The FRRf was set up to conduct single turnover mode analyses for high resolution and time course terminations to measure Fv/Fm and σ_{PSII}. Samples were dark adapted for 30 minutes before analysis. LEDs were adjusted to ensure an $R_{\sigma PS\ II}$ value (probability of PSII reaction centre being closed during first flashlet) between 0.04 and 0.05. For both experiments, blanks were obtained by running 0.7 µm filtered seawater at the same LED settings used for bioassay samples.

8.1.4 Details regarding the choice of specific pigments and phytoplankton groups in the CHEMTAX processing for S54 incubation experiments

CHEMTAX v1.95 (Mackey et al. 1996) was used to define the contribution of major functional phytoplankton groups to the total chlorophyll-a (chl-a). CHEMTAX is a matrix factorisation programme that relies on "marker" pigment composition in the different phytoplankton groups. The programme requires given initial ratios of accessory pigments against chl-a and then provides an estimate of group contribution to total chl-a through a suite of iterations. The optimisation of the community structure estimate requires some prior assumptions on the expected phytoplankton group composition and typical pigment ratios for those groups in the respective region. The main choices of phytoplankton groups and initial pigment ratios are described in detail in the main section of this paper. Here we provide additional explanations on less typical selections of groups and "marker" pigments.

Choice of groups: Nine phytoplankton groups were chosen: cyanobacteria, prasinophytes, dinoflagellates, *Phaeocystis*-H (High iron-acclimated state of *Phaeocystis antarctica*, a species within the haptophyte phytoplankton group), *Phaeocystis*-L (Low iron-acclimated state of *P. antarctica*), coccolithophores (haptophytes-6), pelagophytes (pelago-1), chlorophytes and diatoms (Table S3.2). The interpretation of HPLC pigment data for the assessment of community composition can be difficult due to "marker" pigments that are present in several groups. Therefore, the selection of group also depends the pigments detected through the HPLC analysis and groups expected based on existing literature. Cyanobacteria were included in the CHEMTAX calculations for our Southern Ocean incubations due to the presence of zeaxanthin within some of the samples, even though cyanobacteria occurrence in the Antarctic waters are unlikely (Wright et al. 2010). Zeaxanthin occurs in chlorophytes and cyanobacteria but is a dominant pigment only in cyanobacteria (Table S3.2; Mendes et al. 2015). Therefore, if only chlorophytes were included and a high zeaxanthin concentration was detected, chlorophytes would be inaccurately attributed a high contribution to total chl-a, when in fact this high concentration would be due to a high cyanobacteria signature. Lutein, which is one of the characteristic pigments of chlorophytes, was below the detection limit suggesting that this group played a minor role in our incubations.

Choice of pigments: The following pigments were included in our analysis: Chl-c3; Chl-c1c2; peridinin (Peri); 19'-butanoyloxyfucoxanthin (19-But); fucoxanthin (Fuco); neoxanthin (Neo); prasinoxanthin (Pras); violaxanthin (Violax); 19'-hexanoyloxyfucoxanthin (19-Hex); zeaxanthin (Zea); Chl-b (Table S3.1). These pigments were selected out of all the detected pigments as they are known to be indicative of the identified phytoplankton groups. Since the published optimised ratios from Wright et al. (2010) for the Southern Ocean do not contain zeaxanthin values and no other literature was found that reports zeaxanthin ratios for phytoplankton studies that include pelagophytes and coccolithophores in the same initial pigment ratio set, ratios for the Indian SAZ from Mendes et al. (2015) were used in our study. Some pigments known to be prominent and suitable marker pigments in other oceanic regions, such as lutein, for example, were below detection limit in our Atlantic Southern Ocean study. However, to ensure that the number of pigments used for the CHEMTAX analyses is higher than the number of phytoplankton groups (i.e. nine; Mackey et al. 1996), we added the pigment pair chl-c1c2 to the suite of marker pigments used in our CHEMTAX processing. This chl-c1c2 ratio is a combined signal of the chl-c1 and chl-c2 pigments, which could not be separated by the HPLC system used.

The chl-c1c2 was included as it was the only pigment left within our HPLC-pigment data set that is not drastically influenced by degradation or photo-acclimation (further discussed in section below). A recent CHEMTAX study on Atlantic Southern Ocean phytoplankton (Gibberd et al. 2013), within the same region as our study, reported discrepancies between their final optimised ratios for chl-c1c2 and chl-c3 for *P. antarctica*, and other previous studies in the Southern Ocean. Gibberd et al. (2013) suggested that their observations of unexpected variations in final ratios could be explained by the presence of a phytoplankton group not included in their CHEMTAX analysis. We therefore, included one of their suggested groups to our analyses, pelagophytes. The presence of pelagophytes (pelago-1) in our samples was supported by the presence of their dominant marker pigment 19'-butanoyloxyfucoxanthin (19-

But; Schlüter et al. 2011). The addition of pelagophytes to our CHEMTAX calculations proved valuable for the incubation experiments, since the CHEMTAX results showed that they were present in many of our samples. For all 19-But ratios, we used the latest and geographically, closest available ratios optimised for the Indian SAZ (Mendes et al. 2015).

8.1.5 Details on the removal of diadinoxanthin and diatoxanthin from the CHEMTAX pigments

Some pigments although detected were omitted from the CHEMTAX calculations. For example, although diadinoxanthin and diatoxanthin (DDT) pigments were detected within the HPLC pigment analyses and chromatographically well resolved, they were not included in our CHEMTAX analysis since they may have biased the results (Mackey et al. 1996). Both are involved in the xanthophyll cycle (Brunet et al. 2011), which is highly affected by light and thus potentially causing bias in our experiments on light limitation within certain cells. Mackey et al. (1996) suggested that care should be taken when choosing the pigments used for the CHEMTAX processing, especially for diadinoxanthin and diatoxanthin (DD+DT=DDT) due to interconversions based on the light environment. DD and DT are photoprotective pigments, part of the xanthophyll cycle, where DD is produced and converted to DT in the presence of high light (Brunet et al. 2011). These pigments are frequently found in the light-harvesting complexes of diatoms and haptophytes and prevent photo-inhibition caused by excess light. Therefore, including DDT in the CHEMTAX factorisation would likely have provided unrealistic estimates of diatom and haptophyte contributions.

Figure S3.5 shows two scatter plots produced from the DDT pigment concentration data versus fucoxanthin on the x-axis (Fuco; Table S3.8). The latter is a typical marker pigment for diatoms. Figure S3.6 also shows the ratio of DDT:(Fuco+19-Hex) versus Fv/Fm on the x-axis. DDT concentrations were much lower than fucoxanthin concentrations. In the PFZ, DDT was mostly present in higher concentrations under high light (L2 and L2+Fe) and was correlated to changes in fucoxanthin concentrations (R^2 = 0.81; Figure S3.5a). However, for the AAZ this correlation was not seen, given a much more irregular production of DDT (R^2=0.12; Figure S3.5b). The PFZ community seemed to be able to produce photoprotective pigments like DD and DT more readily. We therefore conclude that DD and DT should not be included in the initial ratio matrix for CHEMTAX processing as it was more likely due to cell acclimation to light rather than changes in group abundance.

8.1.6 Details on the statistical analyses

Kruskal-Wallis tests were used to determine whether there were significant differences between treatments for each variable (POC, chl-a and nutrient concentrations, Fv/Fm and σ_{PSII}) after each incubation. This means that the Kruskal-Wallis test was performed to determine whether at least one treatment differed from any other. A test statistic value was calculated based on the ranked data for each treatment and compared to a critical chi-squared value. The latter was dependent on the degrees of freedom and set probability level. If the calculated test statistic was greater than the critical value, i.e. the Kruskal-Wallis null hypothesis was rejected, it indicates a difference between the samples. In this case, it was followed by a post-hoc Dunn test, a non-parametric alternative to the t-test (Dunn 1964). This test was performed to establish which pairs of tests differed from each other. However, when performing several comparisons (six for each variable and experiments in this case), the probability of type I error increases,

whereby non-significant differences are viewed as significant. The *p* values from the Dunn test were adjusted for multiple comparisons using the Sidak (1967) procedure whereby the adjusted P value was calculated following the equation

$P_{adj} = 1 - (1 - p)^m$.

The P_{adj} value represents the probability that differences between the treatments are due to pure chance rather than meaningful differences. An adjusted *p* value < 0.1 therefore indicates significant differences between treatments, whereas a larger value implies that differences are more likely to be random. However, it is to be noted that the procedure used to correct for multiple comparisons is relatively conservative. Consequently, some of the differences which visually appear significant were found to be non-significant based on the adjusted *p* value. For this reason, both the non-adjusted and adjusted *p* values are reported below.

8.2 Supplemental Tables

Table S3.1. Average pigment concentrations (with standard errors) in µg L- l based on HPLC analysis for the two incubation experiments on this cruise (SANAE54). Exp =Experiment, S54-46 PFZ = experiment conducted at 46°S within the PFZ, S54-65 AAZ = experiment conducted at 65°S within the AAZ. Treatments: Initial = values before start of incubations, L1 = Low light without iron enrichment, L2 = High light, +Fe = with iron enrichment. Resulting CHEMTAX phytoplankton community concentrations are given in table below (Table S3.3) and displayed in Figures 1.4 and S1.4.

Exp	Treat	Chl-c3	Chl-c1c2	Peri	19-But	Fuco	Neo	Pras	Violax	19-Hex	Zea	Chl-b	Chl-a
S54-46 PFZ	Initial	0.0153 ± 0.0020	0.0278 ± 0.0018	0.0000 ± 0.0000	0.0148 ± 0.0010	0.0521 ± 0.0032	0.0000 ± 0.0000	0.0016 ± 0.0008	0.0003 ± 0.0003	0.0575 ± 0.0030	0.0000 ± 0.0000	0.0057 ± 0.0006	**0.1190 ± 0.0059**
	L1	0.0121 ± 0.0005	0.0238 ± 0.0004	0.0000 ± 0.0000	0.0155 ± 0.0012	0.0531 ± 0.0035	0.0013 ± 0.0002	0.0036 ± 0.0003	0.0011 ± 0.0002	0.0395 ± 0.0009	0.0028 ± 0.0009	0.0092 ± 0.0002	**0.1233 ± 0.0013**
	L1 +Fe	0.0146 ± 0.0004	0.0248 ± 0.0016	0.0000 ± 0.0000	0.0165 ± 0.0008	0.0507 ± 0.0025	0.0016 ± 0.0001	0.0041 ± 0.0004	0.0009 ± 0.0001	0.0462 ± 0.0033	0.0019 ± 0.0002	0.0105 ± 0.0007	**0.1427 ± 0.0081**
	L2	0.0236 ± 0.0004	0.0627 ± 0.0013	0.0000 ± 0.0000	0.0394 ± 0.0082	0.1264 ± 0.0076	0.0020 ± 0.0002	0.0052 ± 0.0000	0.0019 ± 0.0003	0.0444 ± 0.0067	0.0028 ± 0.0004	0.0134 ± 0.0007	**0.2510 ± 0.0096**
	L2 +Fe	0.0297 ± 0.0010	0.0643 ± 0.0000	0.0000 ± 0.0000	0.0416 ± 0.0012	0.1461 ± 0.0035	0.0021 ± 0.0001	0.0058 ± 0.0003	0.0018 ± 0.0001	0.0530 ± 0.0035	0.0024 ± 0.0002	0.0109 ± 0.0011	**0.2761 ± 0.0188**
S54-65 AAZ	Initial	0.1633 ± 0.0017	0.3083 ± 0.0045	0.0000 ± 0.0000	0.0143 ± 0.0003	0.6306 ± 0.0116	0.0000 ± 0.0000	0.0070 ± 0.0001	0.0000 ± 0.0000	0.3545 ± 0.0034	0.0000 ± 0.0000	0.0000 ± 0.0000	**0.9620 ± 0.0172**
	L1	0.2207 ± 0.0150	0.6109 ± 0.0419	0.0000 ± 0.0000	0.0186 ± 0.0008	1.2703 ± 0.1119	0.0000 ± 0.0000	0.0000 ± 0.0000	0.0000 ± 0.0000	0.4155 ± 0.0269	0.0000 ± 0.0000	0.0000 ± 0.0000	**1.7648 ± 0.1376**
	L1 +Fe	0.3517 ± 0.0216	1.1304 ± 0.0333	0.0040 ± 0.0040	0.0266 ± 0.0030	2.2922 ± 0.1197	0.0000 ± 0.0000	0.0000 ± 0.0000	0.0000 ± 0.0000	0.4426 ± 0.0632	0.0041 ± 0.0023	0.0000 ± 0.0000	**3.1643 ± 0.1852**
	L2	0.2162 ± 0.0188	0.6941 ± 0.0839	0.0000 ± 0.0000	0.0199 ± 0.0024	1.3529 ± 0.2056	0.0000 ± 0.0000	0.0000 ± 0.0000	0.0000 ± 0.0000	0.4462 ± 0.0419	0.0000 ± 0.0000	0.0000 ± 0.0000	**2.1231 ± 0.3394**
	L2 +Fe	0.3423 ± 0.0226	1.2424 ± 0.0571	0.0039 ± 0.0039	0.0203 ± 0.0022	1.9461 ± 0.1221	0.0000 ± 0.0000	0.0000 ± 0.0000	0.0000 ± 0.0000	0.3582 ± 0.0400	0.0000 ± 0.0000	0.0000 ± 0.0000	**3.0343 ± 0.2390**

Table S3.2. Pigment:Chl-a ratios used in CHEMTAX analysis of pigment data: (a) initial ratios before analysis, optimised ratios for (b) S54-46 and (c) S54-65 after analysis. Abbreviations: Chl, chlorophyll; Peri, peridinin; 19-But, 19'-butanoyloxyfucoxanthin; Fuco, fucoxanthin; Neo, neoxanthin; Pras, prasinoxanthin; Violax, violaxanthin; 19-Hex, 19'-hexanoyloxyfucoxanthin; Zea, zeaxanthin. Data sources for (a): Chl-c1c2, Diatoms and Coccolithophores (Haptophytes-6; Gibberd et al., 2013: G3 and G4), 19-But, Zea and Pelagophytes (Mendes et al., 2015: SAZ), all other values (Wright et al. 2010).

a) **Initial Pigment Ratios**											
Class / Pigment	Chl-c3	Chl-c1c2	Peri	19-But	Fuco	Neo	Pras	Violax	19-Hex	Zea	Chl-b
Cyanobacteria	0	0	0	0	0	0	0	0	0	1.742	0
Prasinophytes	0	0	0	0	0	0.070	0.090	0.049	0	0.042	0.550
Dinoflagellates	0	0.217	0.820	0	0	0	0	0	0	0	0
Phaeocystis-H	0.340	0.137	0	0.153	0.130	0	0	0	0.430	0	0
Phaeocystis-L	0.130	0.184	0	0.153	0.010	0	0	0	1.210	0	0
Coccolithophores	0.133	0.135	0	0.006	0.142	0	0	0	1.092	0	0
Pelagophytes	0.175	0.607	0	1.511	0.213	0	0	0	0	0	0
Chlorophytes	0	0	0	0	0	0.071	0	0.032	0	0.466	0.150
Diatoms	0.067	0.214	0	0	1.078	0	0	0	0	0	0
b) **Final Optimized Pigment Ratios: S54-46**											
Class / Pigment	Chl-c3	Chl-c1c2	Peri	19-But	Fuco	Neo	Pras	Violax	19-Hex	Zea	Chl-b
Cyanobacteria	0	0	0	0	0	0	0	0	0	0.635	0
Prasinophytes	0	0	0	0	0	0.033	0.103	0.028	0	0.015	0.252
Dinoflagellates	0	0.107	0.403	0	0	0	0	0	0	0	0
Phaeocystis-H	0.155	0.063	0	0.070	0.059	0	0	0	0.196	0	0
Phaeocystis-L	0.054	0.076	0	0.063	0.004	0	0	0	0.500	0	0
Coccolithophores	0.049	0.050	0	0.002	0.053	0	0	0	0.406	0	0
Pelagophytes	0.050	0.173	0	0.431	0.061	0	0	0	0	0	0
Chlorophytes	0	0	0	0	0	0.041	0	0.019	0	0.271	0.087
Diatoms	0.008	0.128	0	0	0.415	0	0	0	0	0	0
c) **Final Optimized Pigment Ratios: S54-65**											
Class / Pigment	Chl-c3	Chl-c1c2	Peri	19-But	Fuco	Neo	Pras	Violax	19-Hex	Zea	Chl-b
Cyanobacteria	0	0	0	0	0	0	0	0	0	0.635	0
Prasinophytes	0	0	0	0	0	0.039	0.050	0.027	0	0.023	0.305
Dinoflagellates	0	0.107	0.403	0	0	0	0	0	0	0	0
Phaeocystis-H	0.291	0.052	0	0.023	0.049	0	0	0	0.163	0	0
Phaeocystis-L	0.048	0.068	0	0.057	0.004	0	0	0	0.450	0	0
Coccolithophores	0.059	0.043	0	0.003	0.063	0	0	0	0.482	0	0
Pelagophytes	0.050	0.173	0	0.431	0.061	0	0	0	0	0	0
Chlorophytes	0	0	0	0	0	0.041	0	0.019	0	0.271	0.087
Diatoms	0.008	0.189	0	0	0.370	0	0	0	0	0	0

Table S3.3. Contribution of CHEMTAX phytoplankton groups to Chl-a with averages and standard errors. Values represent the concentration of each phytoplankton group (µg L^{-1} chl-a), averaged per treatment for each experiment (S54-46 and S54-65) with standard error (s.e) between replicates.

Exp	Treatment	Chl-a	Cyanobacteria	Prasinophytes	Dinoflagellates	Phaeocystis-H	Phaeocystis-L	Coccolithophores	Pelagophytes	Chlorophytes	Diatoms
S54-46 PFZ	Initial	0.1190 ± 0.0059	0.0000 ± 0.0000	0.0110 ± 0.0013	0.0000 ± 0.0000	0.0257 ± 0.0056	0.0277 ± 0.0004	0.0004 ± 0.0004	0.0033 ± 0.0001	0.0000 ± 0.0000	0.0508 ± 0.0025
	L1	0.1233 ± 0.0013	0.0007 ± 0.0007	0.0199 ± 0.0007	0.0000 ± 0.0000	0.0187 ± 0.0022	0.0085 ± 0.0026	0.0182 ± 0.0052	0.0069 ± 0.0009	0.0021 ± 0.0013	0.0481 ± 0.0028
	L1 +Fe	0.1427 ± 0.0081	0.0003 ± 0.0003	0.0234 ± 0.0017	0.0000 ± 0.0000	0.0236 ± 0.0011	0.0000 ± 0.0000	0.0399 ± 0.0039	0.0085 ± 0.0006	0.0017 ± 0.0009	0.0454 ± 0.0026
	L2	0.2510 ± 0.0096	0.0000 ± 0.0000	0.0292 ± 0.0014	0.0000 ± 0.0000	0.0437 ± 0.0057	0.0100 ± 0.0012	0.0111 ± 0.0111	0.0208 ± 0.0056	0.0045 ± 0.0009	0.1316 ± 0.0002
	L2 +Fe	0.2761 ± 0.0188	0.0008 ± 0.0002	0.0273 ± 0.0028	0.0000 ± 0.0000	0.0593 ± 0.0042	0.0045 ± 0.0045	0.0220 ± 0.0118	0.0206 ± 0.0010	0.0006 ± 0.0006	0.1410 ± 0.0054
S54-65 AAZ	Initial	0.9620 ± 0.0172	0.0000 ± 0.0000	0.0017 ± 0.0001	0.0000 ± 0.0000	0.1618 ± 0.0023	0.0000 ± 0.0000	0.2016 ± 0.0005	0.0021 ± 0.0001	0.0000 ± 0.0000	0.5947 ± 0.0149
	L1	1.7648 ± 0.1376	0.0000 ± 0.0000	0.0000 ± 0.0000	0.0000 ± 0.0000	0.2230 ± 0.0183	0.0000 ± 0.0000	0.2337 ± 0.0163	0.0027 ± 0.0004	0.0000 ± 0.0000	1.3054 ± 0.1082
	L1 +Fe	3.1643 ± 0.1852	0.0018 ± 0.0009	0.0000 ± 0.0000	0.0051 ± 0.0051	0.3950 ± 0.0286	0.0000 ± 0.0000	0.2142 ± 0.0473	0.0028 ± 0.0015	0.0025 ± 0.0016	2.5430 ± 0.1166
	L2	2.1231 ± 0.3394	0.0000 ± 0.0000	0.0004 ± 0.0003	0.0002 ± 0.0001	0.2230 ± 0.0207	0.0437 ± 0.0098	0.2402 ± 0.0245	0.0000 ± 0.0000	0.0007 ± 0.0004	1.6149 ± 0.2837
	L2 +Fe	3.0343 ± 0.2390	0.0000 ± 0.0000	0.0001 ± 0.0000	0.0052 ± 0.0049	0.4048 ± 0.0319	0.0026 ± 0.0026	0.1503 ± 0.0250	0.0000 ± 0.0000	0.0001 ± 0.0001	2.4713 ± 0.1827

Table S3.4. Specific growth rates (day^{-1}) derived from fluorometer chl-a and POC concentrations as well as the associated chl-a:POC weight ratios before and after incubation for both experiments. The growth rates were derived as the slope of the exponential function of chl-a and POC against time. Negative growth rates imply an apparent loss of biomass over the course of our incubations. The error is the standard error associated with this slope. The asterisks indicate the level of significance of the model; $p < 0.01$ are represented by ***, $p < 0.05$ by ** and $p < 0.1$ by *."n.s" indicates that the p was > 0.1. chl-a:POC weight ratios are shown with the standard error of the mean of the experimental replicates.

Experiment	**Treatment**	**Chl-a growth rate** (d^{-1})	**POC growth rate** (d^{-1})	**Initial Chl-a:POC**	**Final Chl-a:POC**
S54-46 PFZ	L1	0.05 ± 0.02 **	n.s	0.007 ± 0.001	0.007 ± 0.000
	L1 +Fe	n.s	0.03 ± 0.01 **		0.007 ± 0.001
	L2	0.11 ± 0.04 **	0.05 ± 0.02 **		0.009 ± 0.001
	L2 +Fe	0.23 ± 0.03 ***	0.07 ± 0.02 **		0.013 ± 0.001
S54-65 AAZ	L1	0.13 ± 0.01 ***	0.06 ± 0.03 *	0.011 ± 0.001	0.015 ± 0.001
	L1 +Fe	0.23 ± 0.02 ***	0.05 ± 0.01 ***		0.023 ± 0.005
	L2	0.15 ± 0.02 ***	0.19 ± 0.07 **		0.014 ± 0.001
	L2 +Fe	0.26 ± 0.02 ***	0.12 ± 0.01 ***		0.017 ± 0.002

Table S3.5. Average daily changes in chl-a, POC and nutrient (NO_3^-, $Si(OH)_4$, and PO_4^{3-}) concentrations for both experiments (S54-46 and S54-65). The average difference between the concentrations at initial and final time points was divided by the length of the incubation in days. Increases in chl-a and POC concentrations indicate increases in biomass whereas decreases in NO_3^-, $Si(OH)_4$, and PO_4^{3-} concentrations indicate uptake by phytoplankton. The reader is referred to Tables S1.6 and S1.7 for statistically significant differences observed among treatments regarding chl-a concentrations, POC and macronutrient concentrations at the end of the incubations. Values are shown with the standard error of the mean of the experimental replicates.

Experiment	Treatment	Chl-a ($\mu g\ L^{-1}\ d^{-1}$)	POC ($\mu g\ L^{-1}\ d^{-1}$)	NO_3^- ($\mu M\ d^{-1}$)	PO_4^{3-} ($\mu M\ d^{-1}$)	$Si(OH)_4$ ($\mu M\ d^{-1}$)
S54- 46 PFZ	L1	0.02 ± 0.01	1.63 ± 0.55	-1.26 ± 0.46	0.08 ± 0.06	-0.55 ± 0.12
	L1 +Fe	0.02 ± 0.01	1.26 ± 0.94	-1.53 ± 0.79	-0.02 ± 0.08	-0.53 ± 0.11
	L2	0.05 ± 0.03	4.04 ± 0.89	-1.42 ± 0.95	0.15 ± 0.04	-0.39 ± 0.08
	L2 +Fe	0.13 ± 0.01	3.01 ± 0.80	-1.33 ± 0.46	-0.02 ± 0.06	-0.56 ± 0.15
S54-65 AAZ	L1	0.52 ± 0.06	13.12 ± 3.03	-1.64 ± 0.65	-0.08 ± 0.02	-2.39 ± 1.45
	L1 +Fe	1.29 ± 0.08	17.30 ± 8.68	-2.67 ± 0.50	-0.10 ± 0.01	-2.96 ± 1.42
	L2	0.64 ± 0.03	36.65 ± 3.96	-1.67 ± 0.84	-0.07 ± 0.03	-1.98 ± 1.30
	L2 +Fe	1.58 ± 0.08	69.6 ± 14.5	-2.07 ± 0.74	-0.08 ± 0.01	-4.69 ± 1.52

Table S3.6. Results of the Kruskal-Wallis comparisons performed on the data for final termination to verify whether there was a statistically significant difference amongst the various light and iron treatments at the end of the incubations. For example, a P-value of <0.001 indicates that there was a statistically significant difference in that specific variable among the four treatments at the end of the incubation. It does, however, not indicate which treatments differed. Comparisons between specific treatments are given in Table S3.7 for variables, where the Kruskal-Wallis test indicated significant differences (P-value <0.001).

Kruskal-Wallis tests were performed for chl-a, POC and macronutrient concentrations, photochemical efficiency (Fv/Fm) and size of the PSU (σ_{PSII}). The number of degrees of freedom was 3 for all of the experiments. Chi-squared and *p* values for all the tests are shown. P values < 0.01 are represented by ***, $p < 0.05$ by ** and $p < 0.1$ by *."n.s" indicates that the *p* was ≥ 0.1 and that no significant difference was detected.

Experiment	Variable	Critical value (chi-squared)	P value
S54-46	Fv/Fm	6.69	0.08 *
	σ_{PSII}	4.64	0.2 n.s
	[Chl-a]	6.69	0.08 *
	$[NO_2^- + NO_3^-]$	8.19	0.91 n.s
	$[Si(OH)_4]$	1.46	0.69 n.s
	$[PO_4^{3-}]$	5.23	0.16 n.s
	[POC]	5.02	0.17 n.s
S54-65	Fv/Fm	9.36	0.02 **
	σ_{PSII}	5.26	0.15 n.s
	[Chl-a]	9.97	0.02 **
	$[NO_2^- + NO_3^-]$	8.19	0.49 n.s
	$[Si(OH)_4]$	7.73	0.05 **
	$[PO_4^{3-}]$	4.69	0.2 n.s
	[POC]	9.81	0.02 **

Table S3.7. Differences between treatments on the last day of incubation as identified by a post-hoc two-tailed Dunn's test. The post-hoc test was performed following the rejection of the Kruskal-Wallis null hypothesis which indicated that there were significant differences amongst treatments. Results are shown only for those comparisons where the non-adjusted *p* values from the Kruskal-Wallis test were <0.1 (see Table S3.6). Tests were performed for chl-a, POC and macronutrient concentrations, photochemical efficiency (Fv/Fm) and size of the PSU (σ_{PSII}). Adjusted and non-adjusted *p* values are shown. Adjusted $p < 0.1$ indicate statistically significant differences.

Experiment	Variable	Comparisons	P value	Adj. P value
S54-46 PFZ	[Chl-a]	L1 +Fe-L2 +Fe	0.04 **	0.24 n.s
	[Chl-a]	L1 -L2 +Fe	0.02 **	0.10 *
	[Chl-a]	L2 -L2 +Fe	0.09 *	0.48 n.s
	Fv/Fm	L1 +Fe-L2 +Fe	0.02 **	0.10 *
	Fv/Fm	L1 -L2 +Fe	0.09 *	0.48 n.s
	Fv/Fm	L2 -L2 +Fe	0.04 **	0.24 n.s
S54-65 AAZ	[Chl-a]	L1 -L1 +Fe	0.05 **	0.30 n.s
	[Chl-a]	L1 -L2 +Fe	0.00 ***	0.02 **
	[Chl-a]	L2 -L2 +Fe	0.03 **	0.18 n.s
	Fv/Fm	L1 +Fe-L2	0.00 ***	0.01 ***
	[POC]	L1 +Fe-L2 +Fe	0.01 ***	0.08 *
	[POC]	L1 -L2 +Fe	0.00 ***	0.02 **
	$[Si(OH)_4]$	L1 -L2 +Fe	0.05 **	0.27 n.s
	$[Si(OH)_4]$	L2 -L2 +Fe	0.01 ***	0.06 *

Table S3.8. Additional calculated pigment values in µg L^{-1} for specific pigment groupings and ratios for each treatment triplicate of each experiment. Exp =Experiment, S54-46 PFZ = experiment done at 46°S within the PFZ, S54-65 AAZ = experiment done at 65°S within the AAZ. Treatments: Initial = values before start of incubations, L1 = Low light without iron enrichment, L2 = High light and +Fe = with iron enrichment. Phaeo = Phaeophorbide-a (Phorb) + Phaeophytin-a (Phyt), DDT = DD (Diadinoxanthin) + DT (Diatoxanthin), FH = Fucoxanthin (Fuco) + 19'-hexanoyloxyfucoxanthin (Hex). Values are shown with the standard error of the mean of the experimental replicates.

Exp	Treatment	Phaeo	DDT	Fuco+Hex	DDT:FH	Phaeo:Chla	Phorb:Chla	Phyt:Chla	DDT:Chla
S54-46 PFZ	Initial	0.0000 ± 0.0000	0.0082 ± 0.0005	0.1096 ± 0.0054	0.0745 ± 0.0018	0.0000 ± 0.0000	0.0000 ± 0.0000	0.0000 ± 0.0000	0.0686 ± 0.0007
	L1	0.0008 ± 0.0008	0.0081 ± 0.0005	0.0926 ± 0.0030	0.0874 ± 0.0026	0.0066 ± 0.0066	0.0000 ± 0.0000	0.0066 ± 0.0066	0.0657 ± 0.0031
	L1 +Fe	0.0000 ± 0.0000	0.0089 ± 0.0003	0.0969 ± 0.0058	0.0924 ± 0.0023	0.0000 ± 0.0000	0.0000 ± 0.0000	0.0000 ± 0.0000	0.0627 ± 0.0013
	L2	0.0054 ± 0.0012	0.0210 ± 0.0037	0.1708 ± 0.0142	0.1220 ± 0.0114	0.0215 ± 0.0054	0.0000 ± 0.0000	0.0215 ± 0.0054	0.0832 ± 0.0115
	L2 +Fe	0.0060 ± 0.0019	0.0238 ± 0.0003	0.1992 ± 0.0050	0.1199 ± 0.0040	0.0216 ± 0.0066	0.0000 ± 0.0000	0.0216 ± 0.0066	0.0873 ± 0.0070
S54-65 AAZ	Initial	0.0970 ± 0.0074	0.0488 ± 0.0012	0.9851 ± 0.0137	0.0495 ± 0.0010	0.1011 ± 0.0089	0.0772 ± 0.0003	0.0239 ± 0.0090	0.0507 ± 0.0019
	L1	0.1677 ± 0.0314	0.0948 ± 0.0134	1.6858 ± 0.1386	0.0560 ± 0.0060	0.0961 ± 0.0202	0.0664 ± 0.0140	0.0297 ± 0.0062	0.0538 ± 0.0072
	L1 +Fe	0.3751 ± 0.0925	0.1288 ± 0.0290	2.7348 ± 0.1786	0.0461 ± 0.0077	0.1218 ± 0.0359	0.0868 ± 0.0276	0.0350 ± 0.0090	0.0399 ± 0.0069
	L2	0.3143 ± 0.1437	0.1204 ± 0.0460	1.7991 ± 0.2476	0.0646 ± 0.0167	0.1630 ± 0.0937	0.0664 ± 0.0201	0.0966 ± 0.0737	0.0546 ± 0.0129
	L2 +Fe	0.8404 ± 0.1439	0.0644 ± 0.0114	2.3043 ± 0.1621	0.0275 ± 0.0032	0.2864 ± 0.0688	0.1932 ± 0.0160	0.0932 ± 0.0533	0.0209 ± 0.0023

8.3 Supplemental Figures

Figure S3.1. Profiles of the photosynthetic active radiation (PAR; orange) along with temperature (purple) and chl-a concentrations (green) for the upper 200 m at each bioassay station. At each site, the 15 sample GoFlo bottles were all triggered within a few meters during the uplifting of the rosette. Uplifting was slowed down for triggering. The temperature profile was obtained from a Sea-Bird CTD (Sea-Bird Electronics, USA) sensor mounted on the rosette. Note that the temperature values shown in this figure are not calibrated. Chl-a concentration profiles were measured using a fluorometer attached to the rosette and adjusted according to calibration curves derived from discrete bottle measurements. The reader is referred to the main text (Table 3.1) for detailed information on the sample sites. Briefly, S54-46, are located within the PFZ; and S54-65 within the AAZ. **Note that the PAR reflects the snapshot conditions at the time** and date **of sampling**. For instance, S54-46 was sampled during the early afternoon, whereas S54-65 was sampled early in the morning. Thus, the PAR profiles only serve as an indication of light attenuation.

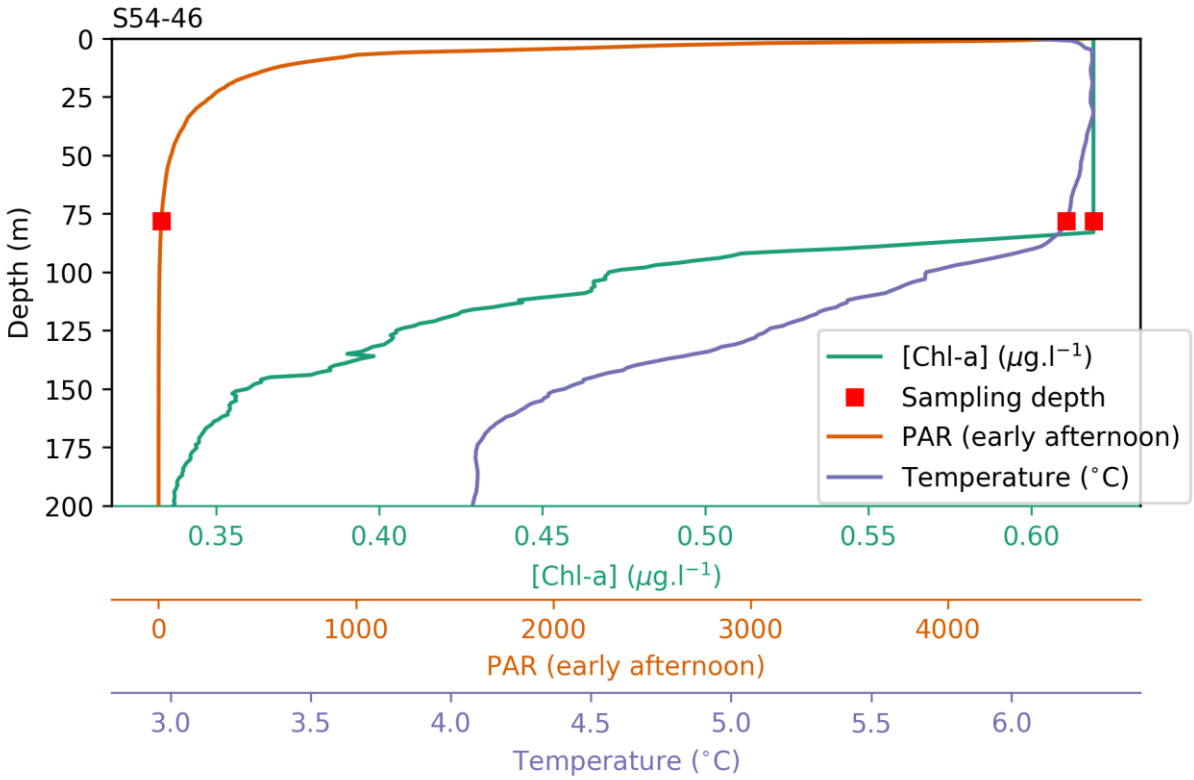

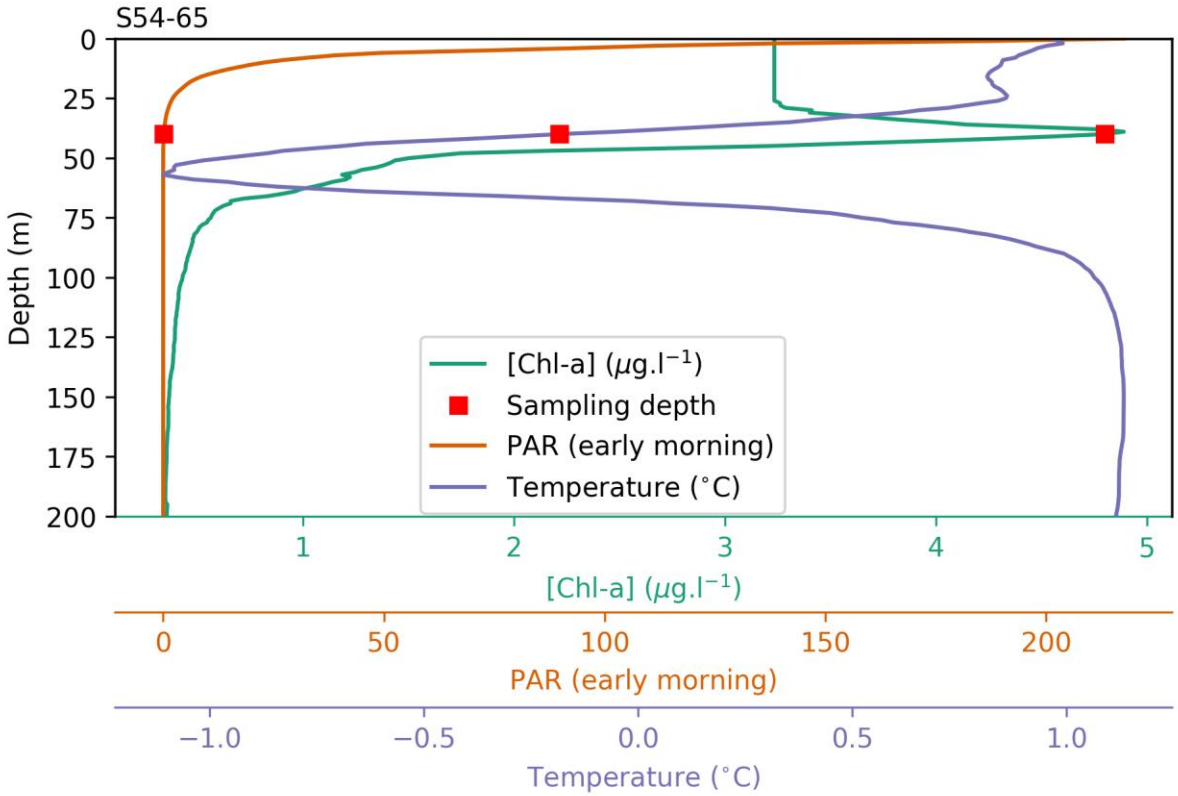

Figure S3.2. Basic incubation scheme that applied to both incubation experiments. Seawater collected with GoFlo bottles was subsampled through a 200 µm mesh into two 50-L acid washed LDPE carboys, homogenised therein and subsequently subsampled into acid washed 2.4-L acid-washed polycarbonate bottles. Three subsamples were dedicated to assessing the initial conditions (T0). The remaining 36 bottles were incubated as triplicates under four treatments, low (in-situ mimicking light conditions; L1), and higher light conditions (L2), with (+Fe) or without (ContFe) artificial iron enrichment. Main growth parameters (chl-a, POC) as well as nutrient uptake were measured at three time points (Terminations T1, T2, and T3). Photophysiology parameters (Fv/Fm, σ_{PSII}) were measured during SANAE 54 every 24 hours in the bottle dedicated for that time point at terminations or the bottle dedicated for next day's termination in between two time points. For example, photophysiology parameters were measured in the bottles dedicated for T1 the day prior to T1 and on T1.

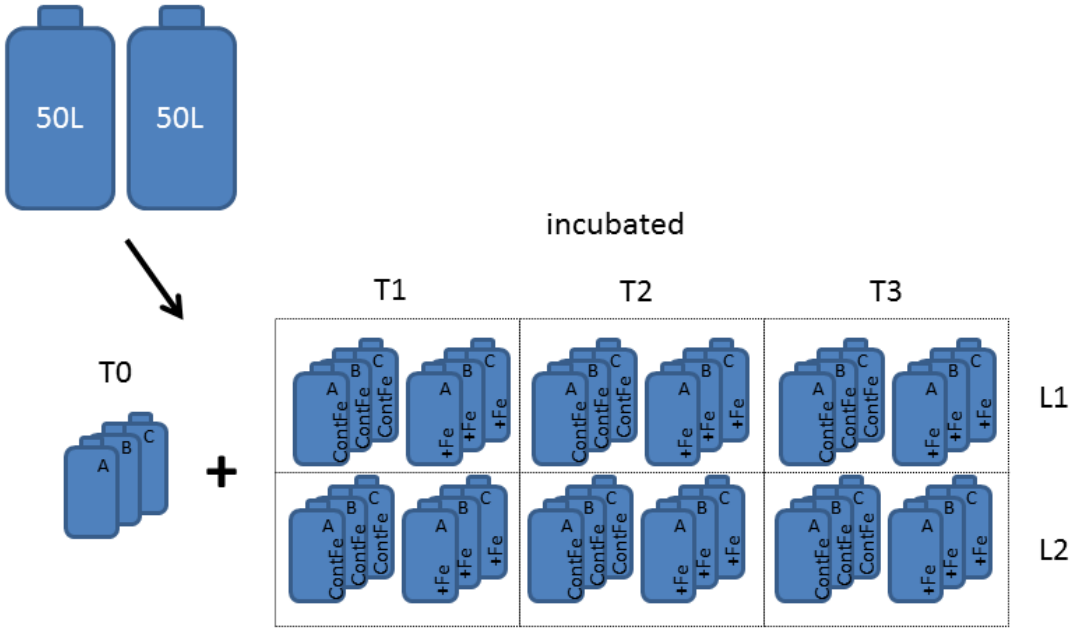

Figure S3.3. Relationship between changes in chl-a and POC combining data from both bioassays: (a) ratio of chl-a specific growth rates versus POC specific growth rates ($r = 0.63$, $p < 0.01$). Growth rates were calculated as the slopes of exponential functions of chl-a and POC against time (Table S3.4). Negative growth rates imply an apparent loss of biomass. The positive correlation indicates agreement between the two measures of growth in most of the treatments, the slope of the chl-a specific growth rates versus POC specific growth rates being larger than 1 indicates that chl-a concentrations generally increased faster than POC concentrations. (b) Average daily changes in chl-a concentration versus average daily changes in POC concentration indicating a positive correlation in chl-a ($r = 0.84$, $p < 0.01$) and POC increases. Graphs were plotted in R using ggplot2 (Wickham 2009; R Core Team 2015). The grey shaded areas around the line indicate the 95% confidence interval calculated by ggplot2.

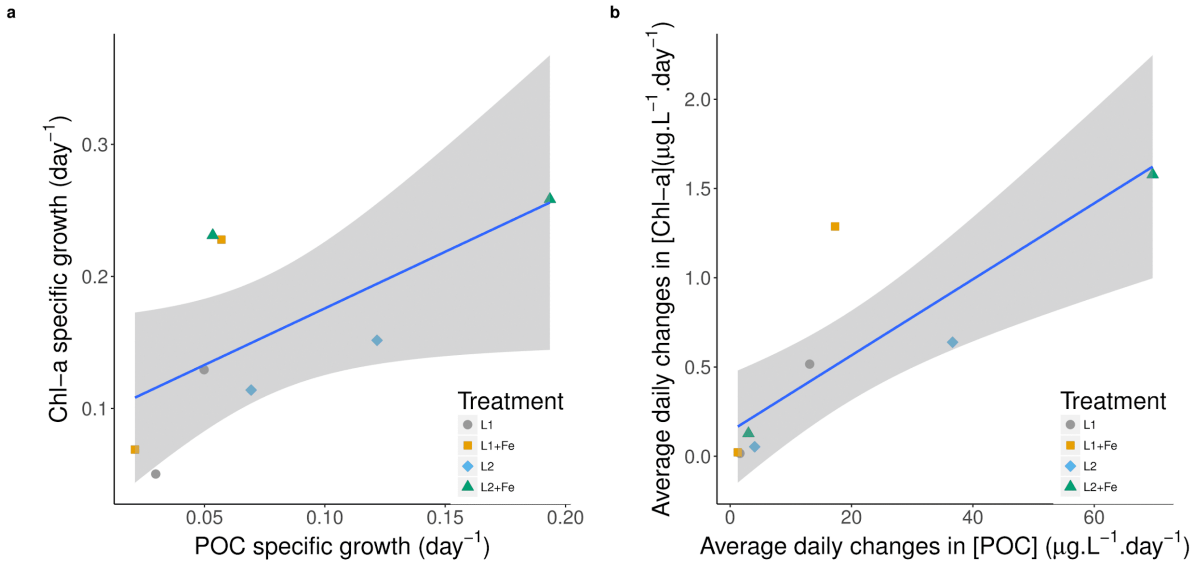

Figure S3.4. Phytoplankton community structure changes in percent group contribution at the end of each treatment for (a) S54-46 and (b) S54-65. Initial = Initial community concentrations with no treatment; L1 = low in-situ light; L2 = High light 10x in situ; +Fe = iron enrichment of 1nM dFe. Graphs were plotted in R using ggplot2 (Wickham 2009). Results in terms of group concentration changes can be found in Figure 3.4 and Table S3.3.

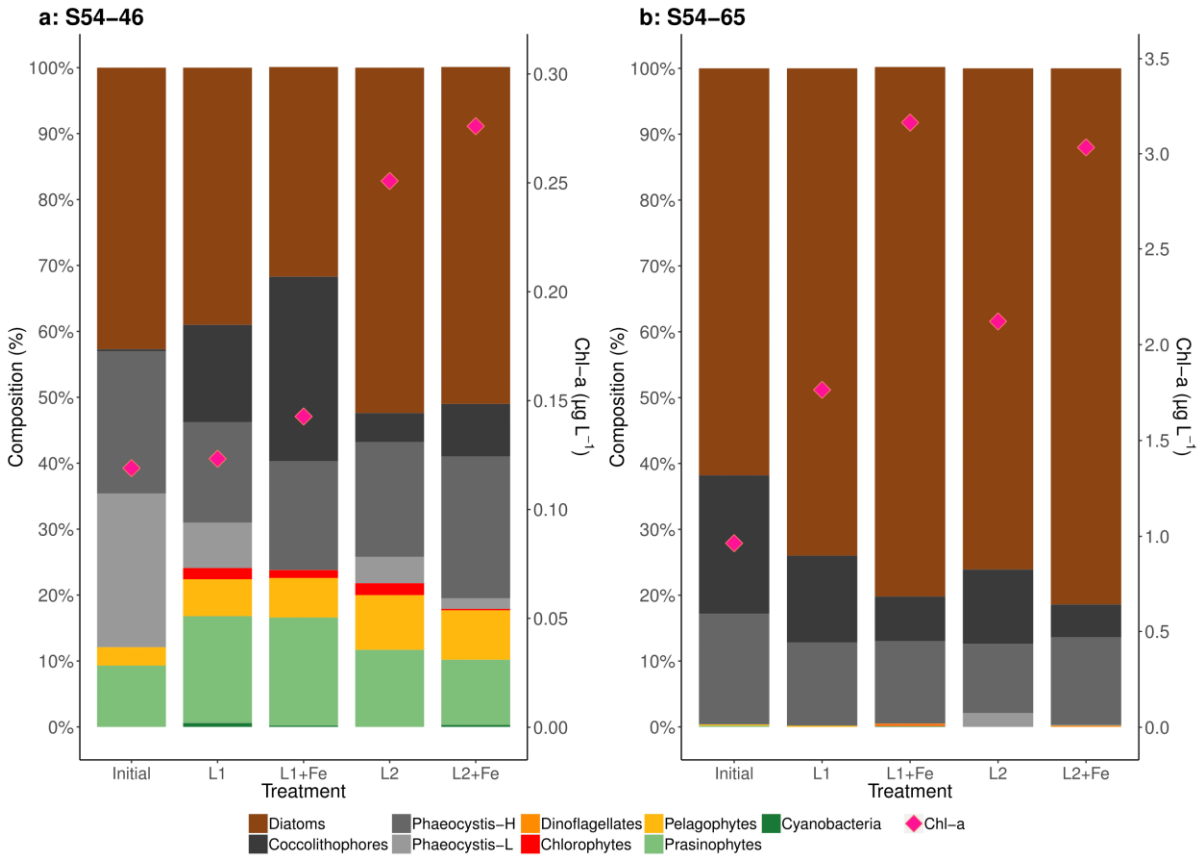

Figure S3.5. Changes in DDT (Diadinoxanthin + Diatoxanthin) against Fucoxanthin concentrations for all treatment triplicates for both experiments: S54-46 (a), and S54-65 (b). Each data point represents HPLC-derived concentration data for each replicate of a treatment or initial condition. Graphs were plotted in R using ggplot2 (Wickham 2009). The blue line is a best fit linear curve through each these individual triplicate points for each experiment. The grey area around the line indicates the 95% confidence interval calculated by ggplot2. The y- and x-axes for DDT and Fucoxanthin are shown on different scales due to the large differences between the two experiments.

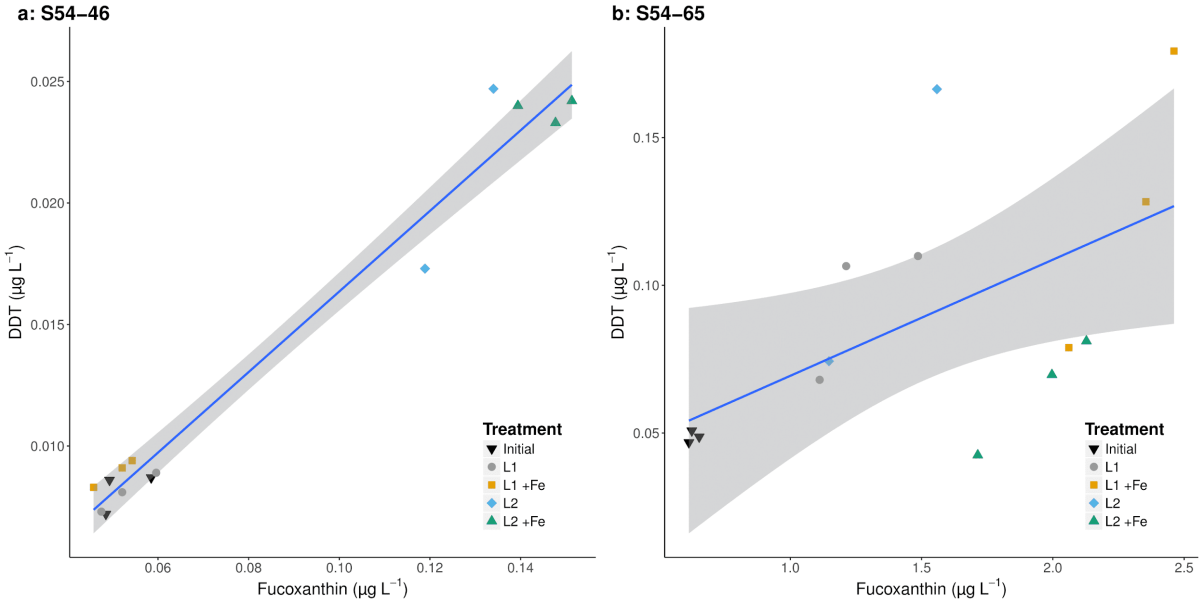

Figure S3.6. Changes in DDT:(Fuco+Hex) against Fv/Fm ratios for all treatment triplicates for both experiments: S54-46 (a), and S54-65 (b) (Table S3.8). Each data point represents HPLC-derived concentration data for a specific triplicate of a treatment or initial condition. Graphs were plotted in R using ggplot2 (Wickham 2009). The blue line is a best fit linear curve through each these individual triplicate points for each experiment. The grey area around the line indicates the 95% confidence interval calculated by ggplot2 (R Core Team 2015). The y- and x-axes for DDT:(Fuco+Hex) and Fv/Fm are shown on different scales due to the large differences between the two experiments.

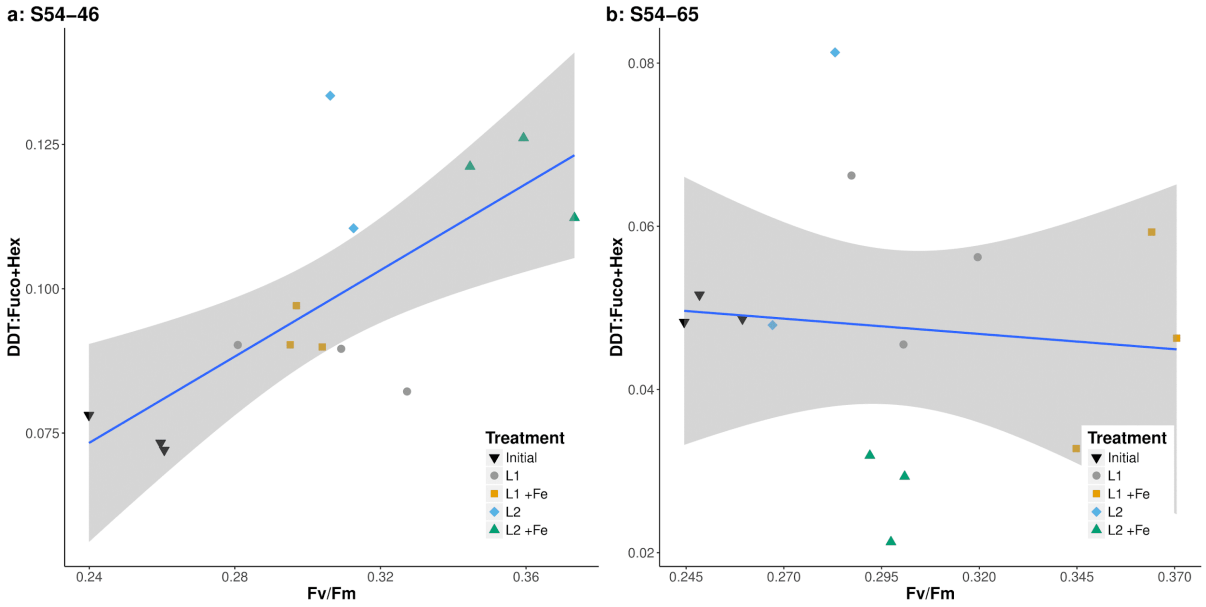

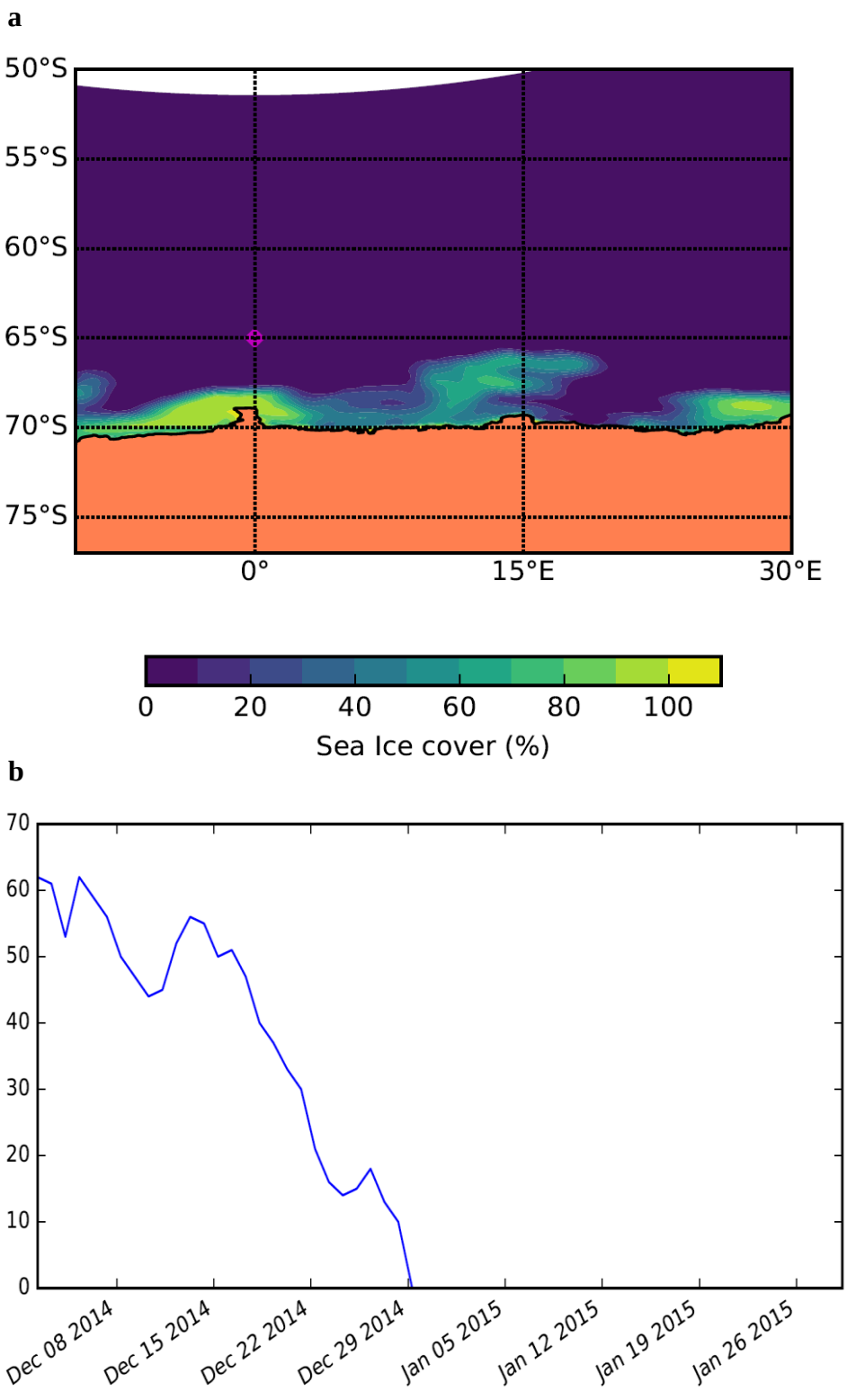

Figure S3.7 Panel a) sea-ice concentrations on 18 January 2015 (S54-65). Panel b) time-series of ice concentrations at the S54-65 site from December 2014 to January 2015 (SANAE54 cruise). Sea-ice concentrations were obtained from satellite imagery (Cavalieri et al. 1996, updated yearly).

Figure S3.8. Data on dissolved iron (dFe) from mid-February until mid-April 2008 along the Good Hope line. (a) A section plot of dFe along the Good Hope line. b) dFe vertical distribution for two stations relevant for our two experiments. Black dots in panel (a) represent Klunder et al. (2011b) sampling stations and depths. All data presented here (panel a and b) are derived from Klunder et al. (2011a) supplementary data set (available at https://doi.pangaea.de/10.1594/PANGAEA.780271). Figures were plotted using Ocean Data View software (Schlitzer 2015).

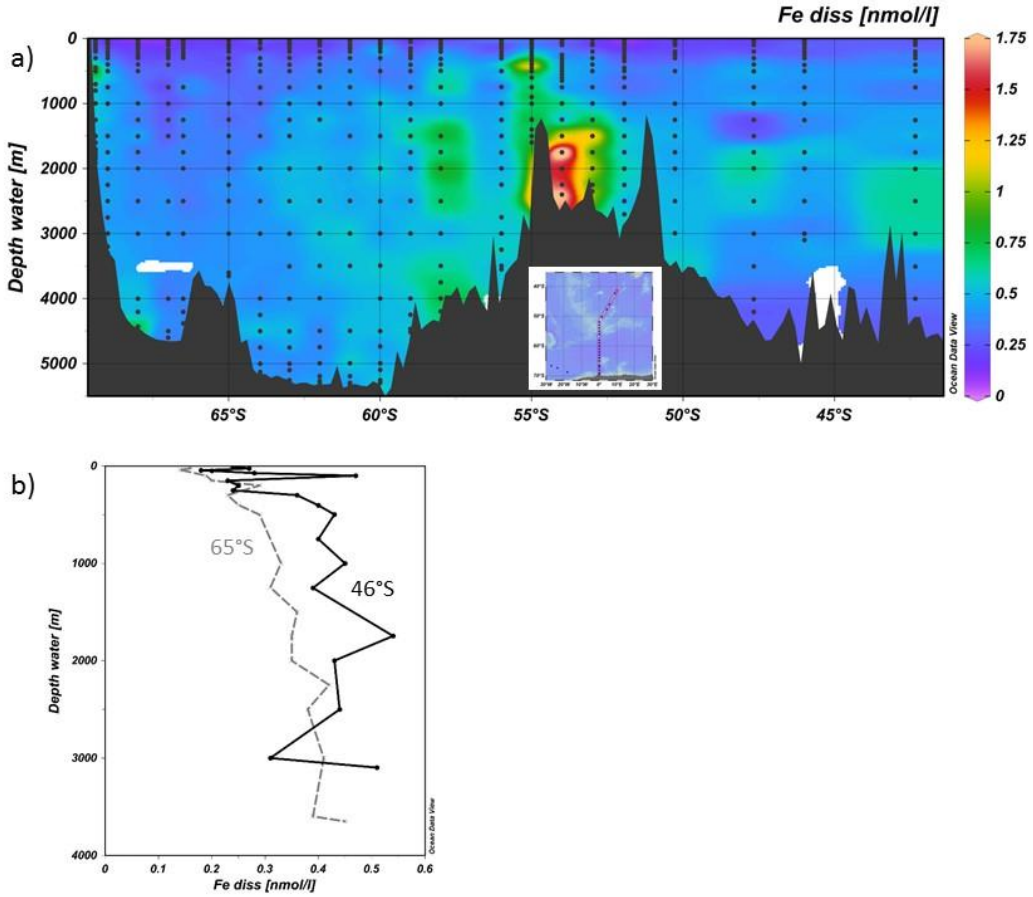

9 Appendix B: Chapter-4 Supplemental Information

Supplemental Information to manuscript

Manuscript in preparation intended for submission to Limnology & Oceanography.

Links between phytoplankton community composition and trace metal distribution in the surface waters of the Atlantic Southern Ocean

Johannes J. Viljoen[1]*, Ian Weir[1]*, Susanne Fietz[1,£], Ryan Cloete[1], Jean Loock[1], Raissa Philibert[1,2], Alakendra N. Roychoudhury[1]

[1]Centre for Trace Metal and Experimental Biogeochemistry, Department of Earth Sciences, University of Stellenbosch, 7600 Stellenbosch, South Africa

[2]Coastal Ocean Research Institute, Vancouver, British Columbia

[*]these authors contributed equally

[£]corresponding author: Department of Earth Sciences, Stellenbosch University, 7600 Stellenbosch, South Africa, sfietz@sun.ac.za, +27218083117

9.1 Supplementary methods

9.1.1 Details regarding the choice of specific pigments and phytoplankton groups in the CHEMTAX processing for S54 cruise Good Hope transect.

The interpretation of HPLC pigment data for the assessment of phytoplankton community composition can be difficult due to pigment markers that are present in several groups. However, with the use of the CHEMTAX v1.95 chemical taxonomy software (Mackey et al. 1996), the HPLC-pigment concentration data sets can be used to calculate the contribution of individual phytoplankton functional groups to total chlorophyll-a (chl-a) (used here as a proxy for biomass). The CHEMTAX phytoplankton community composition estimates are based on the relative abundance of a suite of marker pigments to total chl-a, initial ratios, in water of close proximity to the current study area, determined by previous studies (Wright et al. 2010). Essentially the software makes use of the idea that each group has a characteristic set of accessory pigments, but all phytoplankton groups contains chl-a responsible for the contribution to the total chl-a of a community. The CHEMTAX matrix factorisation is therefore based on the ratios between at least two, often various accessory pigments and chl-a per group (Mackey et al. 1996; Wright et al. 2010). These ratios are loaded into the program along with the pigment concentrations determined by HPLC analysis where after it goes through a suite of iterations and provides an estimate of the group contribution to the total chl-a. For the results of the CHEMTAX software to be reliable and as accurate as possible, knowledge on the phytoplankton communities present in the study area is needed in the form of pigment ratios per phytoplankton group (Schlüter et al. 2011). Below we briefly describe the set-up of the CHEMTAX software (choices of groups and their accessory pigments) to process the respective pigment data for the identification of phytoplankton functional groups and determination of their relative abundances for each surface sample taken. We also provide additional explanations on less typical selections of groups and "marker" pigments.

Choice of groups: The main phytoplankton groups to be included into the initial ratio matrix that were used by the CHEMTAX processing were selected based on literature data published for the Atlantic Southern Ocean and nearby regions (Wright et al. 2010; Gibberd et al. 2013; Mendes et al. 2015). Ten phytoplankton groups were chosen: cyanobacteria, prasinophytes, dinoflagellates, cryptophytes, *Phaeocystis*-H (High iron-acclimated state of *Phaeocystis antarctica*), *Phaeocystis*-L (Low iron-acclimated state of *P. antarctica*), coccolithophores (haptophytes-6), pelagophytes (pelago-1), chlorophytes and diatoms. *Phaeocystis*-H and -L here refers exclusively to *P. antarctica* (Wright et al. 2010) but was separated into functional forms acclimated to low and high iron due to the ability of *P. antarctica* to adjust their pigment ratios to various ambient iron concentration and conditions, iron enriched vs. iron depleted conditions (DiTullio et al. 2007). Although it would be the ideal, no separate bins were created according to depth or regional differences as with different zones. This was due to the limitation of samples and HPLC data as that only represents surface communities. Therefore, all HPLC pigment data was set to be processed within one run. The optimised ratios after the CHEMTAX analyses can be found in Table S4.3. Below we provide further details regarding the choice of specific pigments for the CHEMTAX.

Choice of pigments: The following pigments were included in our analysis: Chl-c3; Chl-c1c2; peridinin (Peri); 19'-butanoyloxyfucoxanthin (19-But); fucoxanthin (Fuco); neoxanthin (Neo); prasinoxanthin (Pras); 19'-hexanoyloxyfucoxanthin (19-Hex); alloxanthin (Allox); zeaxanthin

(Zea); Chl-b (Table S4.2). From the detected pigments, these pigments were selected as two or more of them together are indicative of the identified phytoplankton groups in certain ranges of ratios versus chl-a. Since the published optimised ratios from Wright et al. (2010) for the Southern Ocean do not contain zeaxanthin values and no other literature was found that reports zeaxanthin ratios for phytoplankton studies that include pelagophytes and coccolithophores in the same initial pigment ratio set, ratios for the Indian SAZ from Mendes et al. (2015) were used in our study. Some pigments known to be prominent and suitable marker pigments in other oceanic regions, such as lutein, for example, were below detection limit in our Atlantic Southern Ocean study. In contrast to Viljoen et al. (2018), Allox was detected and was included as it was an indication of the presence of the cryptophyte group. However, to ensure that the number of pigments used for the CHEMTAX analyses is higher than the number of phytoplankton groups (i.e. ten; Mackey et al. 1996), we added the pigment pair chl-c1c2 to the suite of marker pigments used in our CHEMTAX processing. This chl-c1c2 ratio is a combined signal of the chl-c1 and chl-c2 pigments, which could not be separated by the HPLC system used. The chl-c1c2 was included as it was the only pigment left within our HPLC-pigment data set that is not drastically influenced by degradation or photo-acclimation (Appendix A -Supplemental information of Viljoen et al. 2018; section 1.1.5). The CHEMTAX software does not allow the number of phytoplankton groups to be equal or more than the number of pigments used in the calculations. To adhere to this, diatoms were grouped as total diatoms to reduce the number of phytoplankton and due to the need of both chl-c3 and chl-c1 separate from chl-c2 to distinguish two separate group of diatoms with the use of pigments (Wright et al. 2010).

Pelagophytes (pelago-1), which are not commonly reported in Atlantic Southern Ocean CHEMTAX studies (Gibberd et al. 2013), was included as their presence in our samples was supported by the presence of their dominant marker pigment 19'-butanoyloxyfucoxanthin (19-But; Schlüter et al. 2011). This proved valuable, since the CHEMTAX results showed that they were present in noticeable contributions within a reasonable amount of our samples, especially in the PFZ and AAZ. For all 19-But ratios, the latest and geographically, closest available ratios optimised for the Indian SAZ was used (Mendes et al. 2015).

9.2 Supplemental Tables

Table S4.1. Averages and ranges of macronutrient concentrations (A) and ratios (B) in the four distinguished water masses across the Atlantic sector of the Southern Ocean measured during the first (December), third (January) and fourth (February) leg of voyage SANAE54 (see Figure 4.1 for cruise map). Avg. – average. Nutrient concentration surface profiles are shown in Figure 4.3, while nutrient ratios along the transect are shown in Supplementary Figure S4.1.

A)	Zone	H_4SiO_4 (µM)		NO_3^- (µM)		PO_4^{2-} (µM)	
		Range	Avg.	Range	Avg.	Range	Avg.
	STZ (34 - 40.4°S)	(0.2-3.8)	1.5	(1.3-7.9)	1.3	(0.00-0.46)	0.2
	SAZ (40.41 - 44°S)	(0.3-10.1)	1.7	(2.7-40.2)	24	(0.36-1.57)	0.9
Dec	PFZ (44.1 - 50.4°S)	(0.3-10.1)	2.1	(20.7-40.2)	30	(0.42-1.57)	1.0
	AAZ (50.4 - 55.4°S)	(4.5-66.8)	24	(10.5-40.1)	30	(0.6-2.9)	1.5
	WG (55.4-70°S)	(37.5-87)	56	(6.8-36.6)	14	0.57-3.3)	1.7
	STZ (34 - 40.4°S)	N.D.	N.D.	N.D.	N.D.	N.D.	N.D.
	SAZ (40.41 - 44°S)	N.D.	N.D.	N.D.	N.D.	N.D.	N.D.
Jan	PFZ (44.1 - 50.4°S)	(0.7-6.7)	2.7	(5.9-28)	16	(0.03-2.02)	1.1
	AAZ (50.4 - 55.4°S)	(3.6-19.8)	12	(14.3-24)	18	(0.95-1.77)	1.3
	WG (55.4-70°S)	(28.2-84.3)	53	(11.8-25.9)	19	(0.66-2.4)	1.4
	STZ (34 - 40.4°S)	(0-1.7)	0.6	(0.2-0.7)	0.4	(0-0.25)	0.1
	SAZ (40.41 - 44°S)	(0.6-4.3)	0.9	(0.3-8.8)	4.5	(0.06-0.63)	0.4
Feb	PFZ (44.1 - 50.4°S)	(0.6-4.3)	2.2	(4.9-13.4)	9.5	(0.57-1.6)	1.0
	AAZ (50.4 - 55.4°S)	(2.8-98)	24	(12.7-22.1)	17	(0.66-2.4)	1.3
	WG (55.4-70°S)	(18.7-57.1)	41	(6.9-34.4)	13	(0.34-1.86)	1.0

B)	Zone	Si/P (µmol:µmol)		Si/N (µmol:µmol)		N/P (µmol:µmol)	
		Range	Avg.	Range	Avg.	Range	Avg.
	STZ (34 - 40.4°S)	(0-53)	11	(0.03-3.89)	1.8	(0-31.3)	7.8
	SAZ (40.41 - 44°S)	(0.6-3.3)	1.8	(0.03-0.76)	0.2	94.4-52)	18
Dec	PFZ (44.1 - 50.4°S)	(0.2-8.1)	1.9	(0.01-0.37)	0.1	(16.2-94.9)	35
	AAZ (50.4 - 55.4°S)	(1.7-51)	20	(0.2-4.7)	1.1	(6.3-69)	26
	WG (55.4-70°S)	(21.4-78.5)	37	(2-7.05)	4.2	(3.9-31)	9.5
	STZ (34 - 40.4°S)	N.D.	N.D.	N.D.	N.D.	N.D.	N.D.
	SAZ (40.41 - 44°S)	N.D.	N.D.	N.D.	N.D.	N.D.	N.D.
Jan	PFZ (44.1 - 50.4°S)	(0.5-6.9)	2.5	(0.04-0.44)	0.2	(6.8-32.4)	15
	AAZ (50.4 - 55.4°S)	(3-14.9)	8.7	(0.2-1.01)	0.7	(8-25.4)	14
	WG (55.4-70°S)	(17.7-127)	43	(1.35-6.31)	3.0	(9.5-26)	15
	STZ (34 - 40.4°S)	(0-32.4)	8.8	0.1-4.13	1.8	(0-10)	3.7
	SAZ (40.41 - 44°S)	(0.4-33)	5.0	0.04-3.36	0.8	(1.8-16.3)	11
Feb	PFZ (44.1 - 50.4°S)	(0.9-4.4)	2.2	0.12-0.35	0.2	(5.1-18.9)	9.7
	AAZ (50.4 - 55.4°S)	(2.1-64.3)	19	(0.2-5.03)	1.4	(6.2-23.3)	14
	WG (55.4-70°S)	(20.1-88.3)	45	(1.66-4.06)	3.2	(6.6-38.9)	15

Table S4.2. Pigment concentrations in µg L^{-1} based on HPLC analysis for the Good Hope transect on this cruise (SANAE54). Resulting CHEMTAX phytoplankton community concentrations are given in table below (Table S4.4) and displayed in Figure 4.3 and S2.1.

Latitude (N)	Longitude (E)	Date	Month	Chl-c3	Chl-c1c2	Peri	But	Fuco	Neo	Pras	Hex	Allox	Zea	Chl-b	Chl-a
-36.4249	**13.166**	12/6/2014	Dec	0.0000	0.0000	0.0000	0.0000	0.0000	0.0000	0.0000	0.0051	0.0000	0.0144	0.0000	**0.0303**
-39.0427	**11.4504**	12/7/2014	Dec	0.0000	0.0115	0.0058	0.0060	0.0126	0.0000	0.0000	0.0286	0.0000	0.0039	0.0075	**0.0962**
-41.7949	**8.6075**	2/14/2015	Feb	0.0000	0.0046	0.0000	0.0044	0.0096	0.0000	0.0000	0.0218	0.0000	0.0000	0.0000	**0.0480**
-44.4375	**7.1044**	12/9/2014	Dec	0.0046	0.0095	0.0000	0.0068	0.0183	0.0000	0.0000	0.0175	0.0000	0.0024	0.0000	**0.0742**
-44.6305	**6.2283**	2/13/2015	Feb	0.0050	0.0083	0.0041	0.0060	0.0130	0.0000	0.0021	0.0309	0.0000	0.0000	0.0000	**0.0840**
-46.0015	**7.3337**	1/12/2015	Jan	0.0089	0.0225	0.0093	0.0121	0.0816	0.0000	0.0000	0.0803	0.0000	0.0000	0.0000	**0.1828**
-49.1514	**2.4357**	12/10/2014	Dec	0.0196	0.0299	0.0114	0.0365	0.0335	0.0000	0.0000	0.0436	0.0000	0.0032	0.0109	**0.1826**
-49.1984	**2.137**	2/12/2015	Feb	0.0066	0.0146	0.0000	0.0027	0.0307	0.0000	0.0000	0.0208	0.0000	0.0000	0.0000	**0.1000**
-50.1477	**2.429**	1/14/2015	Jan	0.0000	0.0041	0.0000	0.0081	0.0177	0.0000	0.0028	0.0225	0.0000	0.0000	0.0052	**0.0725**
-52.1328	**-0.002**	12/11/2014	Dec	0.0079	0.0166	0.0000	0.0072	0.0443	0.0000	0.0000	0.0184	0.0000	0.0000	0.0071	**0.1190**
-52.8469	**1.541**	2/11/2015	Feb	0.0000	0.0122	0.0053	0.0000	0.0290	0.0000	0.0000	0.0075	0.0031	0.0000	0.0000	**0.0971**
-53.5562	**2.429**	1/14/2015	Jan	0.0204	0.0452	0.0518	0.0134	0.1492	0.0000	0.0000	0.0293	0.0000	0.0000	0.0083	**0.2861**
-54.6081	**2.828**	12/12/2014	Dec	0.0065	0.0151	0.0085	0.0046	0.0338	0.0000	0.0000	0.0130	0.0011	0.0000	0.0000	**0.1002**
-57.5542	**-1.7895**	1/1/2015	Jan	0.0087	0.0325	0.0000	0.0014	0.1018	0.0000	0.0000	0.0121	0.0000	0.0033	0.0000	**0.2079**
-58.3048	**-0.0017**	12/13/2014	Dec	0.0148	0.0404	0.0080	0.0083	0.1025	0.0000	0.0000	0.0265	0.0000	0.0000	0.0000	**0.2253**
-59.722	**-0.0027**	1/16/2015	Jan	0.0091	0.0188	0.0000	0.0067	0.0698	0.0000	0.0000	0.0272	0.0000	0.0000	0.0000	**0.1421**
-62.1655	**-3.069**	12/31/2014	Dec	0.0097	0.0289	0.0000	0.0026	0.0579	0.0000	0.0000	0.0543	0.0000	0.0039	0.0082	**0.1929**
-62.823	**-0.4718**	12/14/2014	Dec	0.0160	0.0456	0.0043	0.0056	0.1087	0.0000	0.0000	0.0300	0.0000	0.0000	0.0000	**0.2339**
-65.0015	**0.6542**	1/18/2015	Jan	0.0263	0.0650	0.0077	0.0054	0.1479	0.0000	0.0000	0.0582	0.0000	0.0000	0.0000	**0.2765**
-66.6125	**-1.4187**	12/15/2014	Dec	0.0000	0.0029	0.0000	0.0016	0.0150	0.0000	0.0000	0.0045	0.0000	0.0000	0.0000	**0.0437**
-67.638	**-0.0045**	1/19/2015	Jan	0.0567	0.1397	0.0075	0.0133	0.2211	0.0000	0.0000	0.2652	0.0000	0.0000	0.0000	**0.5704**
-69.792	**-1.9392**	1/20/2015	Jan	0.0192	0.0705	0.0039	0.0055	0.1833	0.0000	0.0000	0.0418	0.0000	0.0000	0.0000	**0.3773**
-70.034	**-2.6444**	12/16/2014	Dec	0.0080	0.0254	0.0000	0.0045	0.0965	0.0000	0.0000	0.0851	0.0000	0.0000	0.0000	**0.2597**
-70.09	**-1.5887**	1/23/2015	Jan	0.0035	0.0129	0.0000	0.0027	0.0410	0.0000	0.0024	0.0085	0.0015	0.0000	0.0128	**0.1140**

Table S4.3. Pigment:Chl-a ratios used in CHEMTAX analysis of pigment data: (a) initial ratios before analysis and b) final optimised ratios after analysis. Abbreviations: Chl, chlorophyll; Peri, peridinin; 19-But, 19'-butanoyloxyfucoxanthin; Fuco, fucoxanthin; Neo, neoxanthin; Pras, prasinoxanthin; 19-Hex, 19'-hexanoyloxyfucoxanthin; Allox, alloxanthin; Zea, zeaxanthin. Data sources for (a): Chl-c1c2, Diatoms and Coccolithophores (Haptophytes-6; Gibberd et al., 2013: G3 and G4), 19-But, Zea and Pelagophytes (Mendes et al., 2015: SAZ), all other values (Wright et al. 2010).

a) Initial Pigment Ratios

Class / Pigment	Chl-c3	Chl-c1c2	Peri	19-But	Fuco	Neo	Pras	19-Hex	Allox	Zea	Chl-b
Cyanobacteria	0	0	0	0	0	0	0	0	0	1.742	0
Prasinophytes	0	0	0	0	0	0.07	0.09	0	0	0.042	0.55
Dinoflagellates	0	0.217	0.82	0	0	0	0	0	0	0	0
Cryptophytes	0	0.127	0	0	0	0	0	0	0.21	0	0
Phaeocystis-H	0.34	0.137	0	0.153	0.13	0	0	0.43	0	0	0
Phaeocystis-L	0.13	0.184	0	0.153	0.01	0	0	1.21	0	0	0
Coccolithophores	0.133	0.135	0	0.006	0.142	0	0	1.092	0	0	0
Pelagophytes	0.175	0.607	0	1.511	0.213	0	0	0	0	0	0
Chlorophytes	0	0	0	0	0	0.071	0	0	0	0.594	0.15
Diatoms	0.067	0.214	0	0	1.078	0	0	0	0	0	0

b) Final Optimized Pigment Ratios

Class / Pigment	Chl-c3	Chl-c1c2	Peri	19-But	Fuco	Neo	Pras	19-Hex	Allox	Zea	Chl-b
Cyanobacteria	0	0	0	0	0	0	0	0	0	0.635	0
Prasinophytes	0	0	0	0	0	0.031	0.052	0	0	0.024	0.317
Dinoflagellates	0	0.107	0.403	0	0	0	0	0	0	0	0
Cryptophytes	0	0.095	0	0	0	0	0	0	0.157	0	0
Phaeocystis-H	0.155	0.063	0	0.070	0.059	0	0	0.196	0	0	0
Phaeocystis-L	0.016	0.054	0	0.047	0.003	0	0	0.375	0	0	0
Coccolithophores	0.053	0.054	0	0.002	0.057	0	0	0.435	0	0	0
Pelagophytes	0.050	0.173	0	0.431	0.061	0	0	0	0	0	0
Chlorophytes	0	0	0	0	0	0.039	0	0	0	0.327	0.083
Diatoms	0.009	0.083	0	0	0.315	0	0	0	0	0	0

Table S4.4. Contribution of CHEMTAX phytoplankton groups to Chl-a. Values represent the concentration of each phytoplankton group (µg L^{-1} chl-a), per sample.

Latitude (N)	Longitude (E)	Date	Month	Chl-a	Cyanobacteria	Prasinophytes	Dinoflagellates	Cryptophytes	Phaeocystis-H	Phaeocystis-L	Coccolithophores	Pelagophytes	Chlorophytes	Diatoms
-36.4249	**13.166**	12/6/2014	Dec	**0.0303**	0.0108	0.0000	0.0000	0.0005	0.0000	0.0036	0.0037	0.0000	0.0008	0.0109
-39.0427	**11.4504**	12/7/2014	Dec	**0.0962**	0.0020	0.0140	0.0076	0.0004	0.0000	0.0411	0.0000	0.0016	0.0000	0.0295
-41.7949	**8.6075**	2/14/2015	Feb	**0.0480**	0.0000	0.0000	0.0000	0.0001	0.0000	0.0304	0.0000	0.0011	0.0000	0.0164
-44.4375	**7.1044**	12/9/2014	Dec	**0.0742**	0.0014	0.0000	0.0000	0.0002	0.0094	0.0206	0.0000	0.0026	0.0003	0.0397
-44.6305	**6.2283**	2/13/2015	Feb	**0.0840**	0.0000	0.0007	0.0053	0.0002	0.0103	0.0390	0.0000	0.0007	0.0000	0.0278
-46.0015	**7.3337**	1/12/2015	Jan	**0.1828**	0.0000	0.0000	0.0102	0.0000	0.0000	0.0386	0.0386	0.0047	0.0000	0.0907
-49.1514	**2.4357**	12/10/2014	Dec	**0.1826**	0.0014	0.0197	0.0143	0.0001	0.0442	0.0351	0.0000	0.0181	0.0000	0.0496
-49.1984	**2.137**	2/12/2015	Feb	**0.1000**	0.0000	0.0000	0.0000	0.0005	0.0129	0.0099	0.0089	0.0000	0.0000	0.0677
-50.1477	**2.429**	1/14/2015	Jan	**0.0725**	0.0000	0.0104	0.0000	0.0000	0.0000	0.0316	0.0000	0.0035	0.0000	0.0270
-52.1328	**-0.002**	12/11/2014	Dec	**0.1190**	0.0000	0.0126	0.0000	0.0000	0.0137	0.0003	0.0115	0.0034	0.0000	0.0775
-52.8469	**1.541**	2/11/2015	Feb	**0.0971**	0.0000	0.0001	0.0069	0.0162	0.0000	0.0055	0.0021	0.0000	0.0001	0.0662
-53.5562	**2.429**	1/14/2015	Jan	**0.2861**	0.0000	0.0125	0.0556	0.0000	0.0400	0.0000	0.0047	0.0037	0.0000	0.1696
-54.6081	**2.828**	12/12/2014	Dec	**0.1002**	0.0000	0.0000	0.0104	0.0053	0.0148	0.0083	0.0004	0.0010	0.0000	0.0599
-57.5542	**-1.7895**	1/1/2015	Jan	**0.2079**	0.0019	0.0000	0.0000	0.0001	0.0121	0.0000	0.0068	0.0000	0.0000	0.1871
-58.3048	**-0.0017**	12/13/2014	Dec	**0.2253**	0.0000	0.0000	0.0095	0.0000	0.0274	0.0000	0.0122	0.0025	0.0000	0.1736
-59.722	**-0.0027**	1/16/2015	Jan	**0.1421**	0.0000	0.0000	0.0000	0.0000	0.0119	0.0000	0.0192	0.0030	0.0000	0.1080
-62.1655	**-3.069**	12/31/2014	Dec	**0.1929**	0.0019	0.0147	0.0001	0.0006	0.0074	0.0150	0.0383	0.0000	0.0000	0.1148
-62.823	**-0.4718**	12/14/2014	Dec	**0.2339**	0.0000	0.0000	0.0050	0.0001	0.0299	0.0000	0.0139	0.0005	0.0000	0.1844
-65.0015	**0.6542**	1/18/2015	Jan	**0.2765**	0.0000	0.0000	0.0082	0.0000	0.0397	0.0000	0.0305	0.0000	0.0000	0.1981
-66.6125	**-1.4187**	12/15/2014	Dec	**0.0437**	0.0000	0.0001	0.0000	0.0002	0.0000	0.0078	0.0000	0.0007	0.0001	0.0349
-67.638	**-0.0045**	1/19/2015	Jan	**0.5704**	0.0000	0.0000	0.0085	0.0003	0.0566	0.0000	0.1956	0.0019	0.0000	0.3076
-69.792	**-1.9392**	1/20/2015	Jan	**0.3773**	0.0000	0.0000	0.0046	0.0002	0.0283	0.0000	0.0249	0.0007	0.0000	0.3186
-70.034	**-2.6444**	12/16/2014	Dec	**0.2597**	0.0000	0.0001	0.0000	0.0000	0.0000	0.0514	0.0423	0.0000	0.0001	0.1658
-70.09	**-1.5887**	1/23/2015	Jan	**0.1140**	0.0000	0.0231	0.0000	0.0071	0.0038	0.0000	0.0062	0.0014	0.0000	0.0724

Table S4.5. Additional pigment concentrations in µg L^{-1} not used in the group estimations, for specific pigment groupings and ratios sample. Phaeo = Phaeophorbide-a (Phorb) + Phaeophytin-a (Phyt), DDT = DD (Diadinoxanthin) + DT (Diatoxanthin), FH = Fucoxanthin (Fuco) + 19'-hexanoyloxyfucoxanthin (Hex).

Latitude (N)	Longitude (E)	Date	Month	Chl-a	Phorb	Diadino	Diato	Phyt	Phaeo	DDT	Fuco+Hex	DDT:FH	DDT:Chla	Phaeo:Chla
-36.4249	**13.166**	12/6/2014	Dec	**0.0303**	0.0000	0.0000	0.0000	0.0000	0.0000	0.0000	0.0051	0.0000	0.0000	0.0000
-39.0427	**11.4504**	12/7/2014	Dec	**0.0962**	0.0000	0.0048	0.0000	0.0000	0.0000	0.0048	0.0412	0.1165	0.0499	0.0000
-41.7949	**8.6075**	2/14/2015	Feb	**0.0480**	0.0000	0.0021	0.0000	0.0000	0.0000	0.0021	0.0314	0.0669	0.0438	0.0000
-44.4375	**7.1044**	12/9/2014	Dec	**0.0742**	0.0000	0.0040	0.0016	0.0000	0.0000	0.0056	0.0358	0.1564	0.0755	0.0000
-44.6305	**6.2283**	2/13/2015	Feb	**0.0840**	0.0000	0.0042	0.0000	0.0000	0.0000	0.0042	0.0439	0.0957	0.0500	0.0000
-46.0015	**7.3337**	1/12/2015	Jan	**0.1828**	0.0000	0.0144	0.0000	0.0000	0.0000	0.0144	0.1619	0.0889	0.0788	0.0000
-49.1514	**2.4357**	12/10/2014	Dec	**0.1826**	0.0000	0.0097	0.0038	0.0000	0.0000	0.0135	0.0771	0.1751	0.0739	0.0000
-49.1984	**2.137**	2/12/2015	Feb	**0.1000**	0.0000	0.0050	0.0000	0.0000	0.0000	0.0050	0.0515	0.0971	0.0500	0.0000
-50.1477	**2.429**	1/14/2015	Jan	**0.0725**	0.0000	0.0039	0.0000	0.0000	0.0000	0.0039	0.0402	0.0970	0.0538	0.0000
-52.1328	**-0.002**	12/11/2014	Dec	**0.1190**	0.0000	0.0061	0.0000	0.0000	0.0000	0.0061	0.0627	0.0973	0.0513	0.0000
-52.8469	**1.541**	2/11/2015	Feb	**0.0971**	0.0000	0.0037	0.0000	0.0000	0.0000	0.0037	0.0365	0.1014	0.0381	0.0000
-53.5562	**2.429**	1/14/2015	Jan	**0.2861**	0.0144	0.0179	0.0000	0.0051	0.0195	0.0179	0.1785	0.1003	0.0626	0.0682
-54.6081	**2.828**	12/12/2014	Dec	**0.1002**	0.0000	0.0036	0.0015	0.0000	0.0000	0.0051	0.0468	0.1090	0.0509	0.0000
-57.5542	**-1.7895**	1/1/2015	Jan	**0.2079**	0.0301	0.0147	0.0089	0.0000	0.0301	0.0236	0.1139	0.2072	0.1135	0.1448
-58.3048	**-0.0017**	12/13/2014	Dec	**0.2253**	0.0129	0.0092	0.0046	0.0000	0.0129	0.0138	0.1290	0.1070	0.0613	0.0573
-59.722	**-0.0027**	1/16/2015	Jan	**0.1421**	0.0000	0.0098	0.0000	0.0000	0.0000	0.0098	0.0970	0.1010	0.0690	0.0000
-62.1655	**-3.069**	12/31/2014	Dec	**0.1929**	0.0000	0.0100	0.0043	0.0000	0.0000	0.0143	0.1122	0.1275	0.0741	0.0000
-62.823	**-0.4718**	12/14/2014	Dec	**0.2339**	0.0229	0.0166	0.0033	0.0000	0.0229	0.0199	0.1387	0.1435	0.0851	0.0979
-65.0015	**0.6542**	1/18/2015	Jan	**0.2765**	0.0500	0.0202	0.0031	0.0042	0.0542	0.0233	0.2061	0.1131	0.0843	0.1960
-66.6125	**-1.4187**	12/15/2014	Dec	**0.0437**	0.0000	0.0035	0.0000	0.0000	0.0000	0.0035	0.0195	0.1795	0.0801	0.0000
-67.638	**-0.0045**	1/19/2015	Jan	**0.5704**	0.0157	0.0445	0.0000	0.0000	0.0157	0.0445	0.4863	0.0915	0.0780	0.0275
-69.792	**-1.9392**	1/20/2015	Jan	**0.3773**	0.0130	0.0196	0.0000	0.0080	0.0210	0.0196	0.2251	0.0871	0.0519	0.0557
-70.034	**-2.6444**	12/16/2014	Dec	**0.2597**	0.0000	0.0148	0.0029	0.0000	0.0000	0.0177	0.1816	0.0975	0.0682	0.0000
-70.09	**-1.5887**	1/23/2015	Jan	**0.1140**	0.0062	0.0034	0.0000	0.0000	0.0062	0.0034	0.0495	0.0687	0.0298	0.0544

9.3 Supplemental Figures

Figure S4.1. Macronutrient ratios A) N/P, B) Si:N and C) Si:P and D) phytoplankton community composition along the transect.

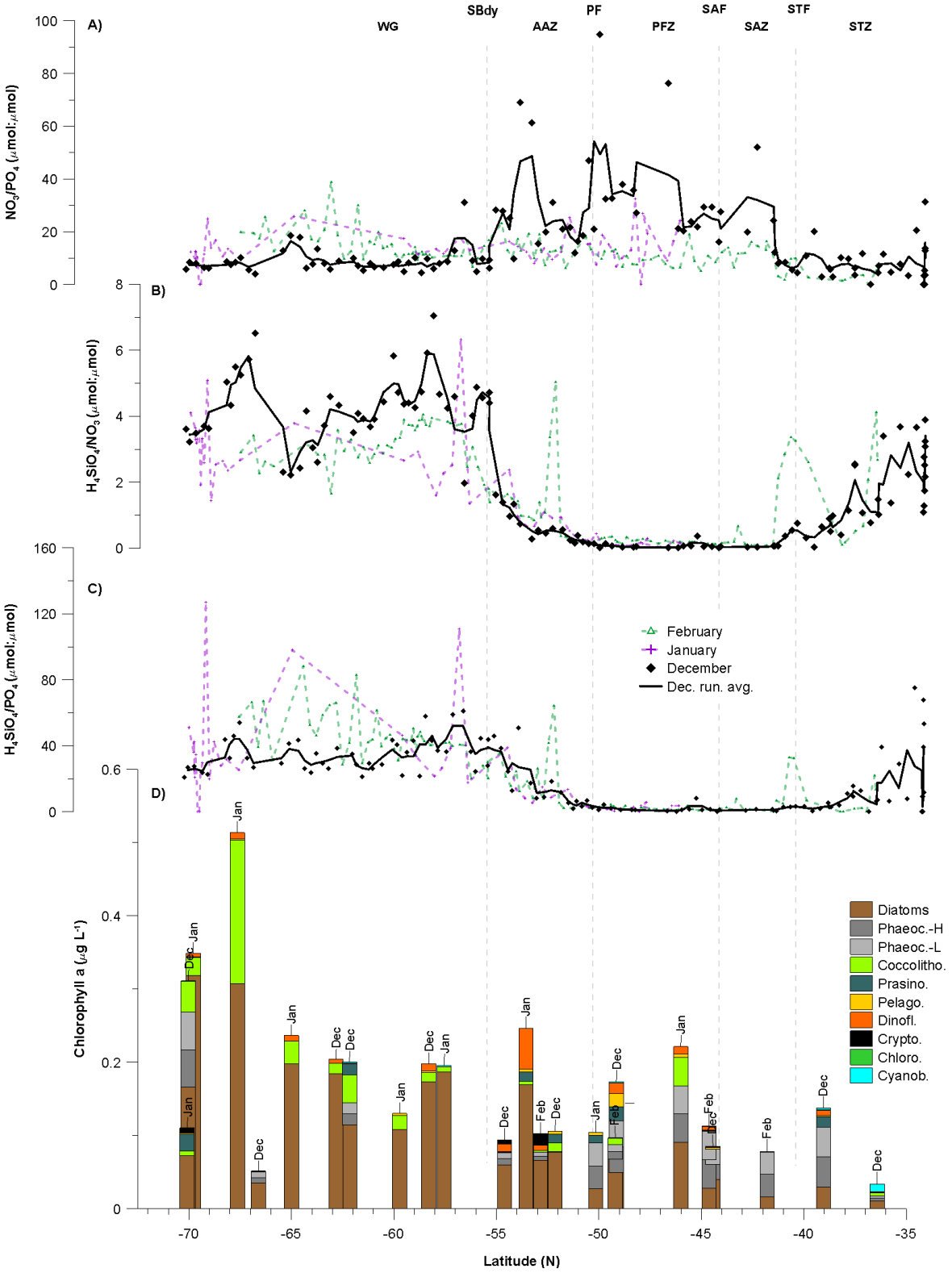

Figure S4.2. Principal component analysis (PCA) for dissolved trace metal and phytoplankton composition. A) PCA loading plot of trace metal distribution, where component 1 explains 41% and component 2 35% of the variance. A third component accounts for 22% of the variance. B) PCA loading plot of phytoplankton groups, where component 1 explains 26% and component 2 19.5% of the variance.

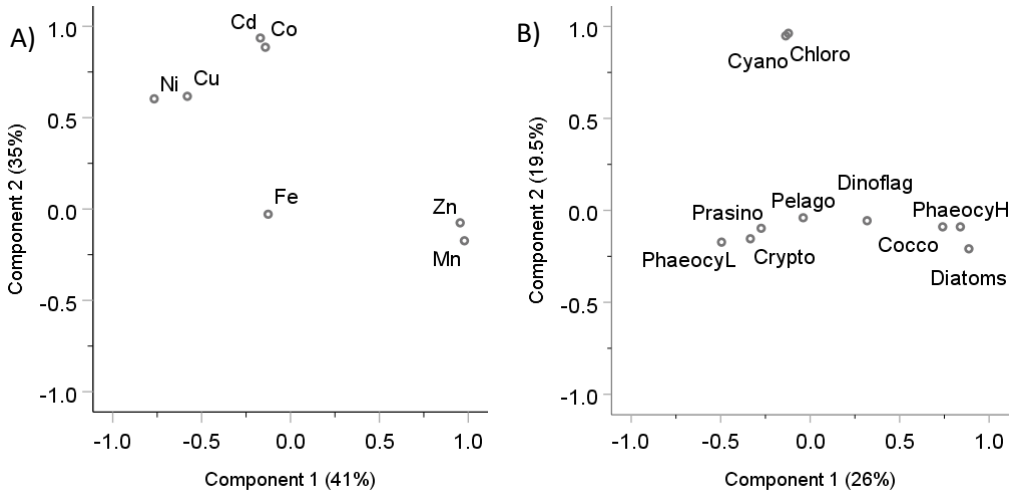

Figure S4.3. Transect profiles of pigments indicative of degradation and photo-acclimation. A) Phaeopigments (Pheophorbide a and Pheophytin a) concentrations, and ratio of phaeopigment (sum of phaeophorbide plus phaeophytin) versus chl-a (Phaeo:chla); B) Sum of diadinoxanthin and diatoxanthin concentrations (DDT), and ratio of DDT versus sum of Fucoxanthin + 19'-hexanoyloxyfucoxanthin, (DDT:FH).

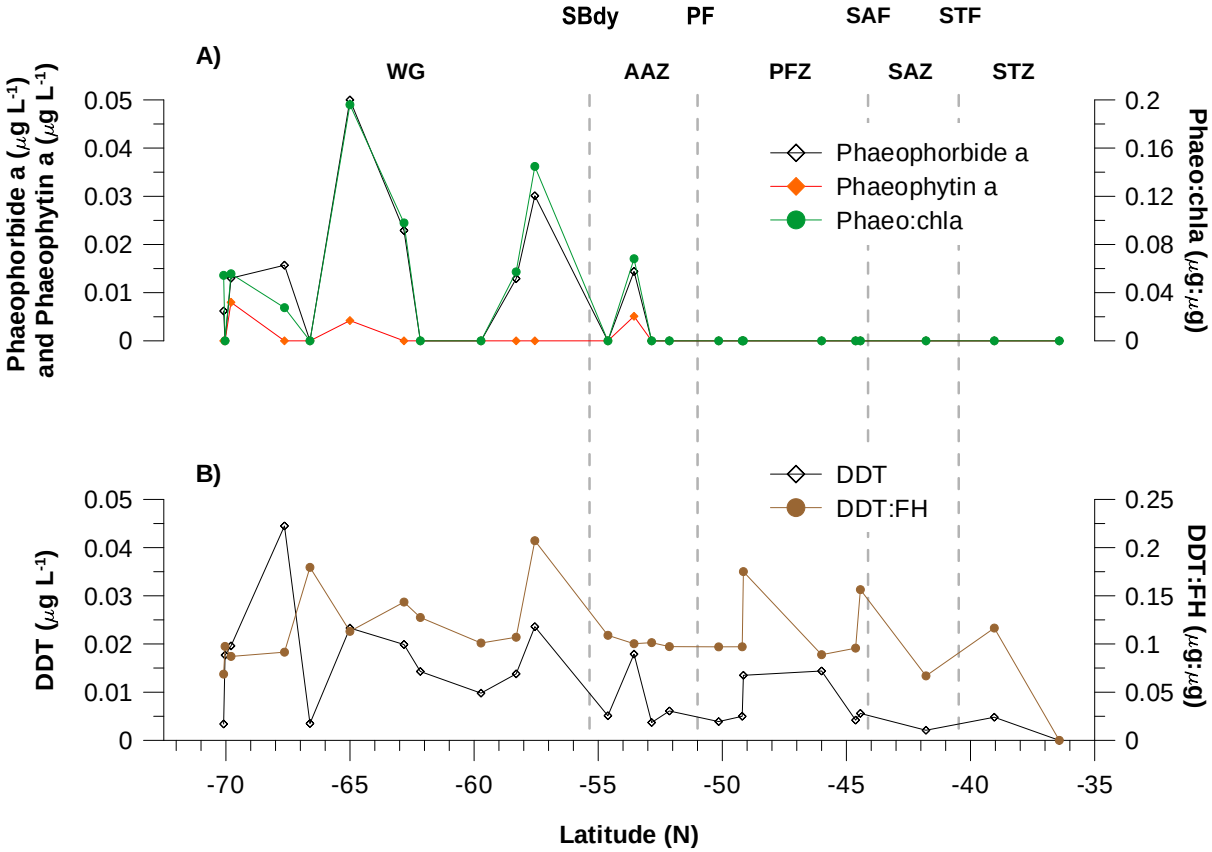

Figure S4.4. (Next page). Trends in diatom (A, B) and *Phaeocystis antarctica* (C,D) distribution along Good Hope Line transect. The trends in contribution and in group-specific chl-a are estimated based on the marker pigments composition using CHEMTAX matrix factorisation software (Mackey et al. 1996; Wright et al. 2010). (A) diatom contribution to total chl-a, B) chl-a derived from diatoms, C) *Phaeocystis* contribution to total chl-a, D) chl-a derived from *Phaeocystis*, which can be distinguished into forms acclimated to high iron concentrations and forms acclimated to low iron concentrations (Wright et al. 2010). The coefficient of determination for diatom contribution (%) is $R^2 = 0.49$.

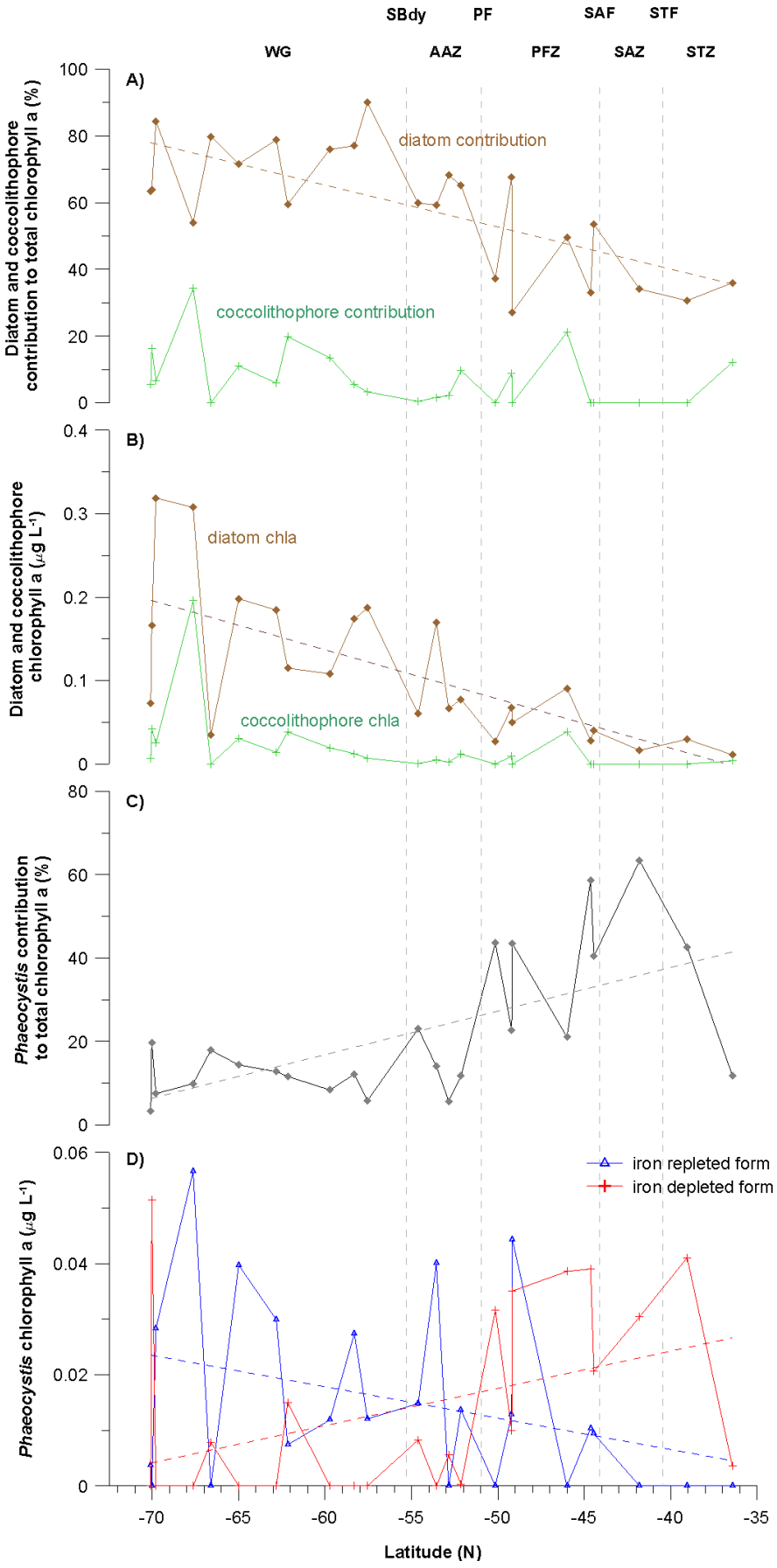

10 Appendix C: Chapter-5 Supplemental Information

Supplemental Information to manuscript

Manuscript in preparation intended for publication in Polar Biology

How representative are surface and chla-max communities: can we use only one or do we need both to understand phytoplankton dynamics in the Southern Ocean?

Johannes J. Viljoen and Susanne Fietz

Centre for Trace Metal and Experimental Biogeochemistry, Department of Earth Sciences, University of Stellenbosch, 7600 Stellenbosch, South Africa

10.1 Supplemental Tables

Table S5.1. Pigment concentrations in µg L^{-1} for specific pigment groupings for both depths and stations at 46 °S: 46S-Surface, 46S-FlMax and 65 °S: 65S-Surface, 65S-FlMax. Phaeo = Phaeophorbide-a (Phorb) + Phaeophytin-a (Phyt), DDT = Diadinoxanthin + Diatoxanthin, Fuco+Hex = Fucoxanthin + 19'-hexanoyloxyfucoxanthin.

Community	Chl-c3	Chl-c1c2	Peri	Phorb	But	Fuco	Pras	Violax	Hex	Diadino	Diato	Chl-b	Chl-a	Phyt	Phaeo	DDT	Fuco+Hex
46S-Surface	0.0089	0.0225	0.0093	0.0000	0.0121	0.0816	0.0000	0.0000	0.0803	0.0144	0.0000	0.0000	**0.1828**	0.0000	0.0000	0.0144	0.1619
46S-FlMax	0.0153	0.0278	0.0000	0.0000	0.0148	0.0521	0.0016	0.0003	0.0575	0.0082	0.0000	0.0057	**0.1190**	0.0000	0.0000	0.0082	0.1096
65S-Surface	0.0263	0.0650	0.0077	0.0500	0.0054	0.1479	0.0000	0.0000	0.0582	0.0202	0.0031	0.0000	**0.2765**	0.0042	0.0542	0.0233	0.2061
65S-FlMax	0.1633	0.3083	0.0000	0.0743	0.0143	0.6306	0.0070	0.0000	0.3545	0.0488	0.0000	0.0000	**0.9620**	0.0228	0.0970	0.0488	0.9851

Table S5.2. Contribution of CHEMTAX phytoplankton groups to chl-a for both depths and stations at 46 °S: 46S-Surface, 46S-FlMax and 65 °S: 65S-Surface, 65S-FlMax. Values in A) represent the concentration of each phytoplankton group (µg L^{-1} chl-a) and B) the percentage contribution of each group to the total community chl-a concentration.

A) Concentration:

Community	Chl-a	Prasinophytes	Dinoflagellates	Phaeocystis-H	Phaeocystis-L	Coccolithophores	Pelagophytes	Diatoms
46S-Surface	0.18280	0.00000	0.01024	0.00000	0.03857	0.03861	0.00466	0.09072
46S-FlMax	0.11897	0.01103	0.00000	0.02566	0.02770	0.00041	0.00334	0.05083
65S-Surface	0.27650	0.00000	0.00818	0.03973	0.00000	0.03053	0.00000	0.19805
65S-FlMax	0.96197	0.00172	0.00000	0.16184	0.00000	0.20159	0.00212	0.59469

B) Percentages:

Community	Chl-a	Prasinophytes	Dinoflagellates	Phaeocystis-H	Phaeocystis-L	Coccolithophores	Pelagophytes	Diatoms
46S-Surface	0.18280	0.00	5.60	0.00	21.10	21.12	2.55	49.63
46S-FlMax	0.11897	9.27	0.00	21.57	23.28	0.35	2.81	42.73
65S-Surface	0.27650	0.00	2.96	14.37	0.00	11.04	0.00	71.63
65S-FlMax	0.96197	0.18	0.00	16.82	0.00	20.96	0.22	61.82

10.2 Supplemental Figures

Figure S5.1. Macronutrient concentrations (µM) depth profiles for both stations at 46 °S: (a) S54-46 and 65 °S: (b) S54-65. Nitrate (NO_3^-) in yellow and Silicic Acid (H_4SiO_4) in blue.